Sirindhorn International Institute of Technology
Thammasat University

Thesis ME-Ph.D.-2008-01

CFD AND EXPERIMENTAL ANALYSIS OF AN R141b EJECTOR USED IN A JET REFRIGERATOR

Thanarath Sriveerakul

CFD AND EXPERIMENTAL ANALYSIS OF AN R141b EJECTOR USED IN A JET REFRIGERATOR

A Thesis Presented

By

Thanarath Sriveerakul

Doctor of Philosophy
Mechanical Engineering Program
Sirindhorn International Institute of Technology
Thammasat University
August 2008

CFD AND EXPERIMENTAL ANALYSIS OF AN R141b EJECTOR USED IN A JET REFRIGERATOR

A Thesis Presented

By

Thanarath Sriveerakul

Submitted to
Sirindhorn International Institute of Technology,
Thammasat University
In partial fulfillment of the requirement for the degree of

DOCTOR OF PHILOSOPHY IN ENGINEERING

Approved as to style and content by Thesis Committee:

Chair and Advisor	______________________ Assoc. Prof. Dr. Satha Aphornratana
Member	______________________ Assoc. Prof. Dr. Bundit Limmeechokchai
Member	______________________ Asst. Prof. Dr. Lalita Tantimuratha
Member	______________________ Asst. Prof. Dr. Kulachate Pianthong

August 2008

Acknowledgement

Firstly, I would like to gratefully acknowledge my advisor, Assoc.Prof.Dr. Satha Aphornratana. Without his generous guidance and encouragement, the completion of this research would not be possible.

I would like to acknowledge the members of the thesis examination committee, Assoc.Prof.Dr. Bundit Limmeechokchai, Asst.Prof.Dr. Lalita Tantimuratha and Asst.Prof.Dr. Kulachate Pianthong, for their valuable technical advice. I wish to also acknowledge Prof.Dr. Masud Behnia for his comments as the external examiner of this research.

Thanks to the Sirindhorn International Institute of Technology (SIIT) for giving an opportunity to undertake the Ph.D. course. I also wish to acknowledge the financial support from Thailand Research Fund and the Royal Golden Jubilee Program, Government of Thailand for the academic sponsorship. My acknowledgement gratefully extends to the Faculty of Engineering, Ubon Ratchathani University for the contribution of the CFD software (Fluent 6.0).

Grateful appreciation goes to Dr. Kanjanapon Chunnanond, Mr. Raksit Thistipatanapong and Mr. Passakorn Srisastra for their valuable research experiences, technical advice and contributions to this research. Also thanks to Mr. Somrerk Sutthichai and all other technicians for their technical assistance.

Finally, I am deeply grateful to my beloved mum, dad and sister and to my wife and her parents for their enormous support, understanding and endless encouragement in many difficult situations.

Abstract

Most of previous analysis had assumed the flow in ejectors as a simple one-dimensional compressible flow. Such the flow omits the existence of shocks in the flow which is normally induced by the primary fluid entering the ejector at very high speed and hence cannot be used to represent the real flow phenomena inside the ejector. The aims of this study are to investigate the use of CFD in predicting performance of an R141b ejector used in refrigeration application and to reveal the complications of the flow characteristics reflected to the performance of the ejector. The performances of the ejector were evaluated in term of the entrainment ratio (Rm), and the critical back pressure (P_C). In order to obtain the accurate models, the CFD results were validated with the experimental values. In this study, an experimental R141b ejector refrigerator with the test ejector was built. The test ejector was designed to be easily fitted with different pieces so that the investigation on the effect of geometries would be allowed. It was found that the predicted performances of the simulated models were agreed well with the experimental values. Average errors of the predicted entrainment ratio and the critical back pressure were 9% and 2%, respectively.

After the validations were satisfied, the changes in the flow phenomena inside the R141b ejector, when its operating conditions and geometries were varied, could be analyzed. Using the applications provided by the CFD software, the flow structure of the modeled ejectors could be created graphically, and the phenomena inside the flow passage were explored. Introducing a new parameter, primary flow state (the state of the primary flow immediately after leaving the primary nozzle), which is a combined parameter of the ejector's operating conditions, it was discovered that when the ejector operated with various primary flow states, this parameter had a major impact reflected to the flow and the mixing process in the ejector.

In addition to the effects of operating conditions, the effects of geometry's variations including the primary nozzle throat diameter, the mixing camber inlet diameter, the throat length, and the primary nozzle exit position (NXP) were also investigated. The investigation on the effect of the ejector's geometries on the flow characteristics and the performance of the ejector were made. The simulation results show that the performances of the ejector varied when there was a change in the geometries. However, the change in the performance when the geometries were changed also depended on the primary flow state. At the different primary flow states, the change in the ejector's geometries could affect the change in the flow in different ways.

To be concluded, the CFD was found to be not only a sufficient tool in predicting ejector performance, it also provides a better understanding of the flow and mixing processes within the ejector. Significant phenomena of the flow in the ejector, such as choke flow, mixing behavior, jet core effect and the presence of oblique shock, which cannot be investigated in the one-dimensional analyses, were explored using useful functions available in the CFD.

Table of Contents

Table of Contents (Cont')

List of Figures

List of Figures (Cont')

List of Tables

Nomenclature

COP	Coefficient of performance	
$\dot{Q}$	Heat load or Cooling load	kJ/s
Rm	Entrainment ratio	
$\dot{m}$	Mass flow rate	kg/s
Pr	Pressure ratio	
P	Pressure	kPa
M	Mach number	
C	Speed of sound in a gas	m/s
U	Gas flow velocity	m/s
T	Temperature	K or $^{\circ}$C
R	Gas constant	kg/kmol.K
D	Diameter	m
Y	Diameter of the primary nozzle's exit	m
Z	Diameter at the entrance of the mixing chamber	m
l	Throat length	m
NXP	Nozzle exit position (the distance between the nozzle exit plane and the mixing chamber inlet plane)	m
η	Friction loss efficiency	
k	Ratio of specific heats or isentropic index of a gas	
V	velocity of fluid	m/s
h	Enthalpy	kJ/kg.K
A	Cross sectional area	m^2
F	Applied force	N

Greek Letters

ρ	Density of fluid	kg/m^3

Subscripts

evap	Evaporator
generator	Vapour-generator
p	The primary fluid
s	The secondary fluid
b	Diffuser's exit
c	Condenser
op	Operating condition
th	Primary nozzle's throat

Nomenclature (Cont')

n	Primary nozzle
m	Mixing chamber
d	Diffuser
i	Inlet
e	Exit
0	Stagnation point
1	Primary nozzle throat position
2	Primary nozzle's exit position
3	Secondary flow choking position
4	Ejector's throat inlet position
5 and 6	Shocking position in the throat based on 1-D assumption
7	Ejector's throat outlet position
max	Maximum
e	Evaporator
c	Condenser

CHAPTER I

INTRODUCTION

1.1 Motivation and Background

At present, the world energy consumption is increased steadily. Use of refrigeration and air conditioning application is one of the most heavy energy usages and also produces significant environmental hazard. Many inventions have been proposed to reduce the energy use of the typical refrigeration and air conditioning systems. For the vapour compression refrigeration cycle (Figure 1.1a), the most widely used air conditioning system; a mechanical compressor is a part that consumes more energy, mostly in the form of electrical energy, than other parts of the system. If this mechanical compressor is replaced with other devices such as an ejector (thermo-compressor), the system would become less dependent on electricity.

An ejector refrigeration system or Jet refrigeration system can be considered as one of the most suitable refrigeration systems for the present energy and environment situations. It utilizes a low temperature thermal energy (100-200°C) from inexpensive or even free sources such as industrial waste heat or a solar collector.

The first ejector refrigeration system was invented by Maurice Leblanc in 1910 [1]. Early in the 1930's, it was used widely for air conditioning of large buildings. Figure 1.1b shows a schematic diagram of the ejector refrigeration cycle. In the system, a vapour-generator, an ejector, and a pump are used to replace the role of the mechanical compressor of a conventional vapour compression refrigeration system. As heat is added to the vapour-generator, a high pressure and temperature refrigerant vapour is evolved and used as a primary fluid for the ejector. The ejector draws a low pressure refrigerant from the evaporator as its secondary fluid. This causes the refrigerant to evaporate at low pressure and produce a useful refrigeration effect. The ejector discharges its exhaust to the condenser where it is liquefied by rejection heat to ambient. Part of the liquid condensate refrigerant is pumped back to the vapour-generator whilst the remainder is returned to the evaporator via an expansion valve. The operating condition of the vapour-generator, evaporator and condenser of an ejector refrigeration cycle are determined by heat source, refrigerated purpose and local climate, respectively.

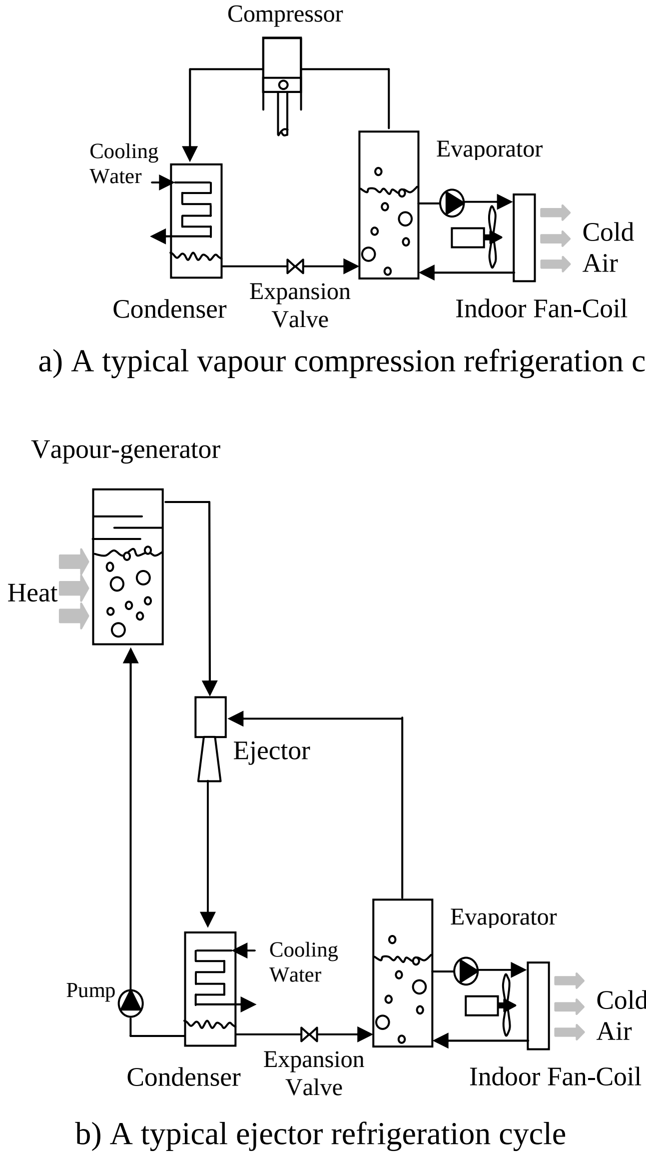

a) A typical vapour compression refrigeration cycle

b) A typical ejector refrigeration cycle

Figure 1.1 Typical vapour compression and ejector refrigeration cycle.

The input required for the pump is typically less than 1 percent of the heat supplied to the vapour-generator, thus the Coefficient of Performance (COP) [2] may be estimated as:

$$\mathrm{COP} = \frac{\text{refrigeration effect at the evaporator}}{\text{heat input at the vapour} - \text{generator}} = \frac{\dot{Q}_{\mathrm{evap}}}{\dot{Q}_{\mathrm{generator}}} \tag{1.1}$$

The major disadvantage of the ejector refrigeration cycle is its relatively low Coefficient of Performance (COP), compared to other types of refrigeration cycles. However, in most industrial processes, some heat is rejected to the surrounding as waste. If this waste heat can be further used in the ejector refrigeration to produce refrigeration effects, more efficient energy use is the result.

From a summary of the important works in the literature of ejector refrigeration systems, an ejector can be considered as the most important part in the system. The performance of an ejector refrigeration system is directly related to the performance of the utilized ejector. Basically, an ejector is designed so that the supersonic high-pressure fluid exiting from the vapour-generator entrains the lower pressure fluid from an evaporator to produce the refrigeration effect. These two fluids mix and return their kinetic energy to pressure energy at the diffuser end and settle at a pressure between the two incoming pressures. It can be said that a high performance ejector is an ejector that could entrain the maximum amount of entrained lower pressure fluid at the highest possible discharged pressure. The design and the performance study of ejectors have been of interest for a considerable time. Perhaps one of the reasons for this interest is the complexity of the flow phenomena in the ejectors. The refrigerant flow in the ejector is complex, since it involves the speed of the flow ranging from low speed to supersonic speed. In order to design and develop a high performance ejector, a clear understanding of the flow and mixing inside the ejector is first needed. Although a number of investigations have been carried out covering both experimental and theoretical aspects in the field of ejectors and their refrigeration cycles, there are still some areas where experimental data are insufficient and where CFD techniques are rarely applied.

1.2 Objective of the Study

The aim of this study is to investigate the use of CFD in predicting performance of an R141b ejector used in refrigeration applications and to reveal the complication of the flow and the mixing process within the R141b ejector. With the built-up R141b experimental ejector refrigerator, the validation of the CFD results was satisfied. It was able to analyze the flow phenomena inside the ejector when its operating conditions and geometries were varied. Using the applications provided by the CFD software, the flow structure of the modeled ejectors could be created graphically, and the phenomena inside the flow passage were explored.

1.3 Organization of the Thesis

This thesis is composed of 9 chapters. The literature review on past researches and the basic backgrounds in the field of ejector and its application in refrigeration are described in Chapter II. In Chapter III, the information based on the constructions of a current R141b ejector refrigerator is provided. Furthermore, details of the constructed ejectors' components are also explained. In Chapter IV, the criterions of creating calculation domain and grid elements, including the concept of setting up the CFD simulation models of the R141 ejector, are described. In Chapter V, the validations of the calculated models with the experimental data are presented. At the end of the chapter, it was concluded that the CFD method shows the proficiency in predicting the accurate ejector performance over other ejector performance prediction models, both the entrainment ratio and the critical back pressure. Due to successful achievement of the validation process in Chapter V, the detailed analyses of contours of Mach number and the static pressure distribution along the ejector's centerline obtained from the CFD package, simultaneously, introduce the concepts explaining the flow structures and the mixing processes of the R141b ejector in Chapter VI. Also the significant differences between the flow structures of the R141b ejector and the steam ejector are also discussed. In Chapter VII and Chapter VIII, the influences of various operating conditions and various ejector's geometries on the ejector performance are proposed. At the study of each parameter, not only the effect of the parameter on ejector performance, but the changes of flow structure inside the ejector are also proposed. In the last chapter of this thesis, Chapter IX, there are the conclusions and the recommendations for future study.

CHAPTER II

LITERATURE REVIEW

As mentioned in the introduction, ejectors and their applications in refrigeration system have been researched and developed continuously over the decades. This chapter provides a literature review of the ejectors background and past researches on improvement to the performance of the ejectors, highlighting their application in refrigeration systems.

2.1 Background of Ejector

An ejector was first invented by Sir Charles Parsons around 1901 for removing air from the condenser of a steam engine [23]. Over the decades, ejectors have been applied for many industrial applications. For example, it was used as a thermo-compressor, a desuperheater and a vacuum generator. It was also used as a jet-conveyer in particulate solid transportation. For refrigeration purposes, an ejector was used to replace the role of a conventional mechanical-drive compressor with addition of a vapour-generator which provides thermal energy.

A typical ejector is composed of two major components, a primary nozzle and a mixing chamber. The design theory of ejectors can be classified into two theories based on the shapes of the mixing chamber, *"constant-pressure mixing ejector"* and *"constant-area mixing ejector"*. A *"constant-area mixing ejector"* is an ejector whose primary nozzle exit is placed within the constant-area section of the mixing chamber (Figure 2.1a) [24~26]. For a *"constant-pressure mixing ejector"* (Figure 2.1b), an ejector which has its nozzle exit position placed in a convergent chamber upstream of the constant-area section [27], the static pressure through the mixing process was assumed to be constant. Both types of ejector have been extensively tested experimentally and theoretically [24~27]. It was found that the constant-pressure mixing ejector had a better performance than the constant-area one. Therefore, after that, almost all studies have been focused on the constant-pressure mixing ejector.

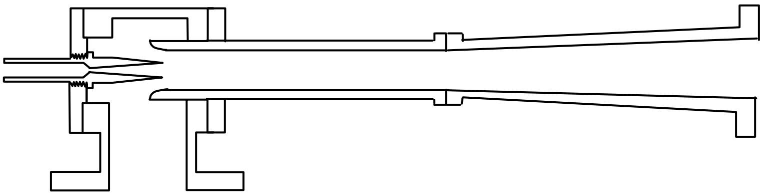

a) “Constant-Area Mixing” Ejector

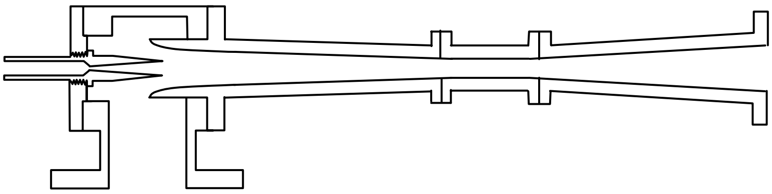

b) “Constant-Pressure Mixing” Ejector

Figure 2.1. Configurations of typical ejectors.

Conventional ejectors were designed and analyzed base on one-dimensional analysis. The design method based on one-dimensional analysis for compressible-gas flow in ejector using the models of stream mixing at constant pressure was first proposed by Keenan and Neumann [27]which was later become a classical theory. The analysis was based on the ideal gas assumption combined with the principles of mass, momentum, and energy conservation. Eames et al. [28] proposed a set of the 1-D equation in designing the ejector based on Keenan and Neumann’s theory [27]. The loss coefficient at the primary nozzle, the mixing chamber and the diffuser were accounted. The mixing of the two streams is able to start at any point from the exit of the nozzle plane to the exit of the constant area section. The equation of pressure ratio across the normal shock was expressed. Discussion on choke at the entrained flow was not given. Huang et al. [29] developed the 1-D analysis based on Manday and Bagster's theory [30] with assumption that no mixing occurs before choking at the hypothetical throat. The mixing of the two streams begins at some point inside the constant area section. The equation of pressure ratio across the shock expressed by Huang et al. [30] is derived from the mixing section to the exit of the constant area section. His results show only a small error in the values of entrainment ratio compared to the experiment results. The one-dimensional analysis, however, can be used to predict the performance when the ejector is operated at its design condition (at critical back pressure) only. Moreover, effects of the ejector's geometries were not included.

The flow phenomena in ejectors are very complicated, and thus, cannot be explained easily. In the past, therefore, the analyses of the ejector were usually done based on one dimensional (1-D) analysis. A schematic view of a typical steam ejector based on one-dimensional theory [31] is shown in Figure 2.2. As the high pressure steam, known as "a primary fluid", expands and accelerates through the primary nozzle (1), it fans out with supersonic speed to create a very low pressure region at the nozzle exit plane (2′) and subsequently in the mixing chamber (2″). This means "a secondary fluid" can be entrained into the mixing chamber. The primary fluid's expanded wave was thought to flow and form a converging duct without mixing with the secondary fluid. At some cross-section along this duct, the speed of the secondary fluid rises to sonic value (3) and chokes [30]. Then the mixing process begins after the secondary flow chokes. This mixing causes the primary flow to be retarded whilst secondary flow is accelerated. By the end of the mixing chamber, the two streams are completely mixed and the static pressure was assumed to remain constant until it reaches the throat section (4). Due to a high pressure region downstream of the mixing chamber's throat, a normal shock of essentially zero thickness is induced (5-6). This shock causes a major compression effect and a sudden drop in the flow speed from supersonic to subsonic. A further compression of the flow is achieved (7) as it is brought to stagnation through a subsonic diffuser until it reaches a desired discharged pressure (b).

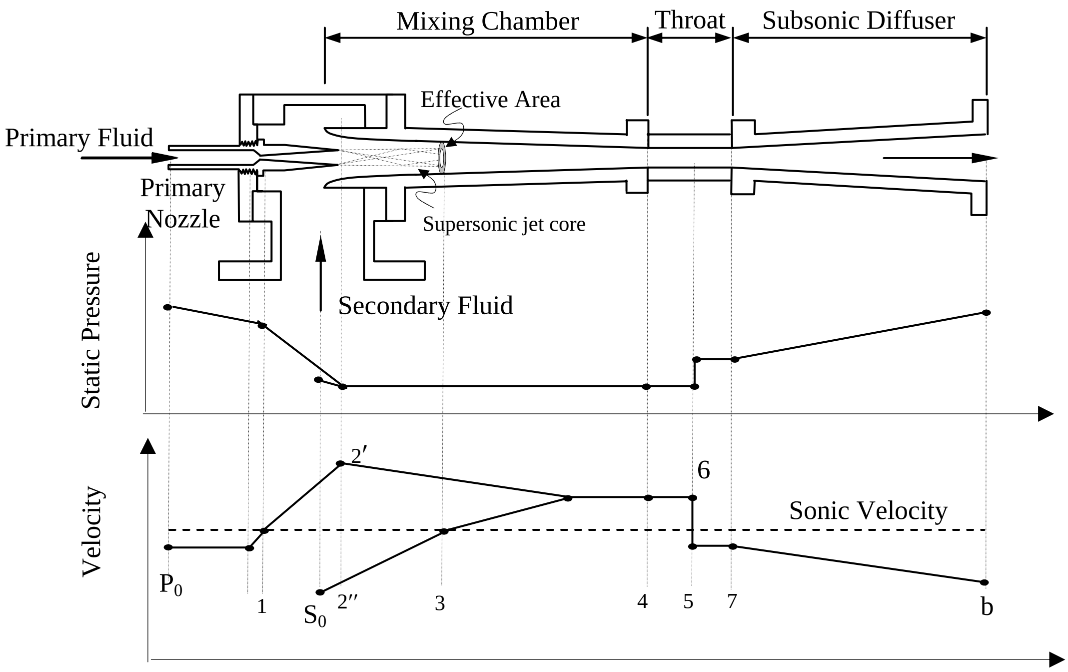

Figure 2.2 Variation of stream pressure and velocity as a function of location along a steam ejector [31].

Matsuo et al. [32] study the flow in a rectangular supersonic ejector using the schlieren photograph technique. An example of schlieren photographs taken in a rectangular supersonic ejector is reproduced in Figure 2.3. In contrast to the 1-D analysis, the major compression effect of the flow in the ejector was found to be caused by a bifurcated shock plus a series of repeated shocks (pseudo shock followed by shock train) instead of a single normal shock. It was also concluded that the pseudo-shock occurs in the deceleration process of the flow in the ejector (downstream of the ejector's throat).

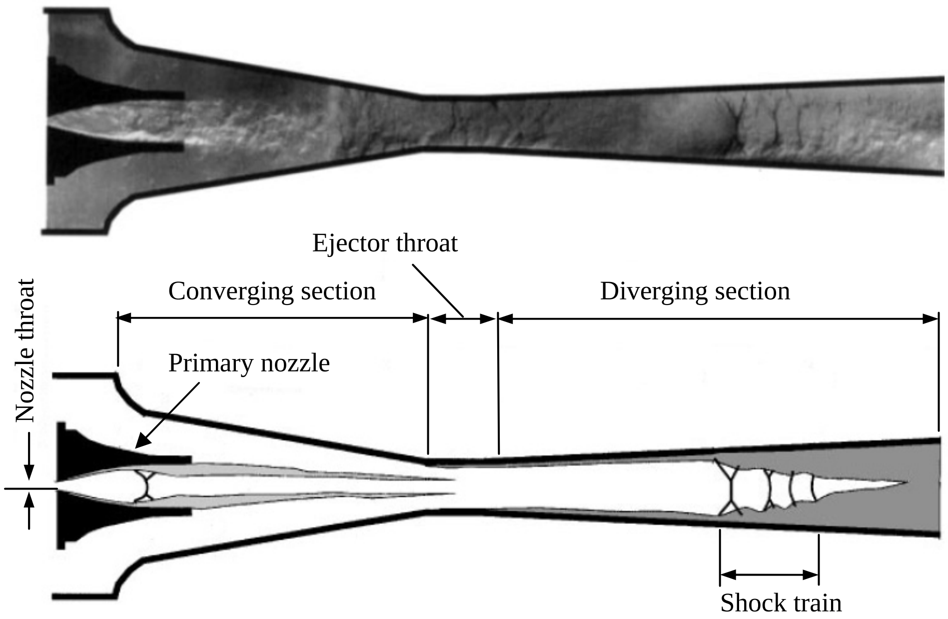

Figure 2.3 An example of Schlieren photograph of flow in an air ejector (Source: Matsuo et al. [32]).

The difference in pressure jump across the pseudo-shock to that obtained from the normal shock was discussed using Figure 2.4, an illustration of the shock train (a series of repeated shocks) and the corresponding static pressure distributions at the wall and at the centerline of the constant-area duct, based on experimental data provided by Tamaki et al., [33]. As shown in this figure, if only a single normal shock occurs, the pressure across the shock jumps suddenly. With existence of a series of repeated shocks, pressure at downstream of the shocks increases continuously at the wall, but fluctuates at the centerline of the duct till the shocks disappear.

With rapid development in computer technology and numerical solution method, some researchers attempted to apply Computational Fluid Dynamics (CFD) in modeling the flow within ejectors [26 and 34~40]. Early of the 90S, the CFD technique was applied to analyze the mixing behavior only for some specific parts of the ejector [34~36]. The use of CFD to study the flow processes in a whole ejector assembly was still incomplete.

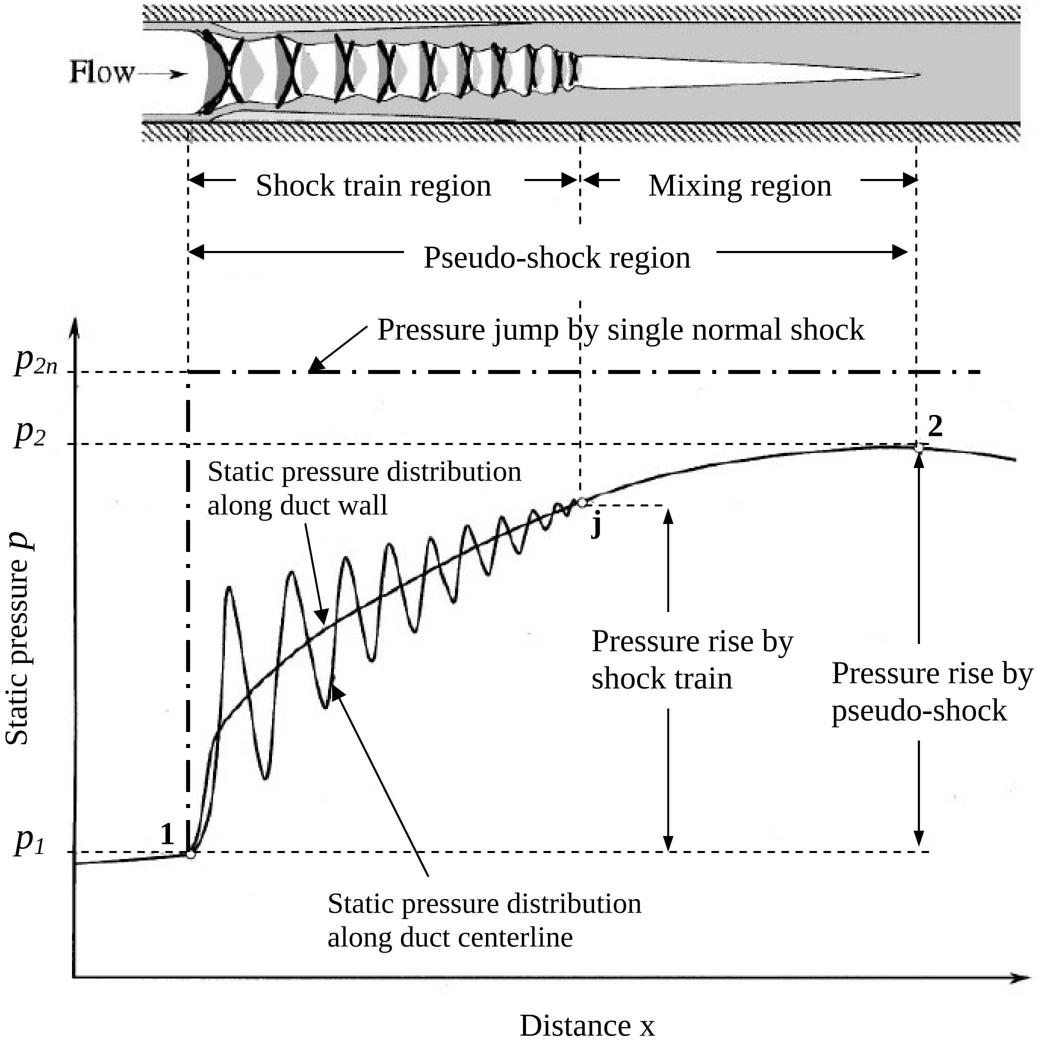

Figure 2.4 Static pressure distribution along duct centerline and wall surface in constant-area duct [33].

In 1996, Riffat et al. [37] employed the CFD method to analyze the performance of ejectors when operating with various types of working fluids and with various shapes of primary nozzles. The three dimensional ejector was modeled and meshed with a grid size of around 37,000 elements. The fluid was assumed as incompressible fluid to avoid convergence difficulty with compressible fluid. This contradicts to the fact that high speed fluid is compressible. Moreover, using the incompressible flow assumption, the effects of shock associated with supersonic were discounted.

Riffat and Omer [38] used the 2 dimensional CFD results to obtain the optimum shape of the methanol driven ejector with the coefficient of performance (COP) between 0.2 and 0.4. The results show that higher entrainment ratio would be obtained by positioning the primary nozzle exit at least 0.21 the length of the mixing chamber. Unfortunately, the calculated results were not validated through any experimental data.

Rusly et al. [26] analyzed the flow through an ejector using CFD technique. The method of simulation is different from others since the real gas model was used instead of the ideal gas model and the geometry of the ejector was chosen as the 2-dimensional constant area-mixing ejector. The results indicate the presence of oblique shock in the constant area section. The CFD's results were validated with experimental data provided by others. Most of the previous studies including the above CFD studies have generally focused on the prediction of the maximum performance and the flow when the discharge pressure of the ejectors were lower than the critical back pressure.

Sriveerakul et al. [39 and 40] reported the use of CFD to simulate the flow within a constant pressure mixing-steam ejector along with validation data from experiments. Using helpful functions available in the CFD package, the flow characteristics within the steam ejector were explained and also the performances of the steam ejector, when its operating conditions and geometries were varied, were predicted. It was shown that CFD predictions could satisfactorily predict the entrainment ratio and the critical back pressure under the choked flow mode, but provided large error in the prediction under the unchoked flow mode.

Pianthong et al. [41] simulated a flow within a steam ejector using a 2-dimensional axisymmetric model and a 3-dimensional model. The results obtained from both models were almost the same. However, due to the larger number of grid elements of the 3-

dimensional model than that of the 2-dimensional axisymmetric model, the more computational time to obtain a converged solution was required.

2.2 Performance Characteristics of the Ejector

For refrigeration applications, the most two significant parameters used to describe the performance of an ejector are *"an entrainment ratio"* and *"a pressure lift ratio"* [42]:

$$\text{entrainment ratio, } Rm = \frac{\text{mass of secondary flow}}{\text{mass of primary flow}} = \frac{\dot{m}_s}{\dot{m}_p} \tag{2.1}$$

$$\text{pressure ratio, } Pr = \frac{\text{static pressure at diffuser exit}}{\text{static pressure secondary flow}} = \frac{P_b}{P_s} \tag{2.2}$$

The entrainment ratio relates to the energy efficiency of a refrigeration cycle, the COP, while the pressure ratio limits a temperature at which the mixed stream can be rejected [1]. Therefore, there is no doubt that an ejector, which operates at the given operating conditions with the highest entrainment ratio and maintains the highest possible discharged pressure, is the most desirable ejector.

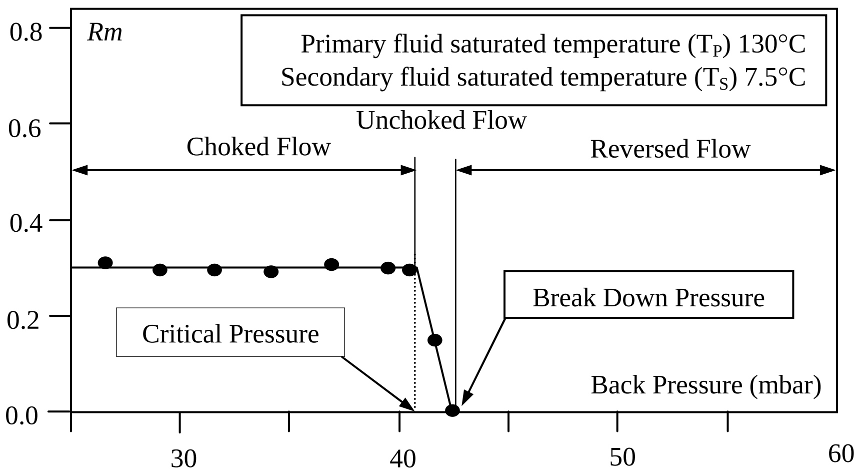

Figure 2.5 Performance characteristics of a steam ejector based on experimental data provided by Eames and Aphornratana [2].

Experimental investigations of ejectors and their application in refrigeration have been conducted. Those provided similar results in term of performance characteristic curves of ejectors [1, 2, 28, 39, 40, and 43~46]. Consider a typical performance curve of a steam ejector for the specified primary and secondary flow pressures as shown in Figure 2.5. There are three operating regions distinguished by the critical back pressure and the breakdown back pressure: the choked flow, the unchoked flow, and the reversed flow of secondary fluid. In the "choked flow" region, where the back pressures are below the "critical value", the secondary flow choking in the mixing chamber causes the ejector to entrain the same amount of secondary fluid. This causes the entrainment ratio to remain constant all over this region. This essential character is called "constant-capacity characteristic" of an ejector. In this "choked flow" region, a transverse shock, which creates a compression effect, was thought to appear in either the throat or diffuser section. The location of the shock process varies with the back pressure. If the back pressure is increased, the shock will move upstream into the ejector throat without disturbing the mixing process.

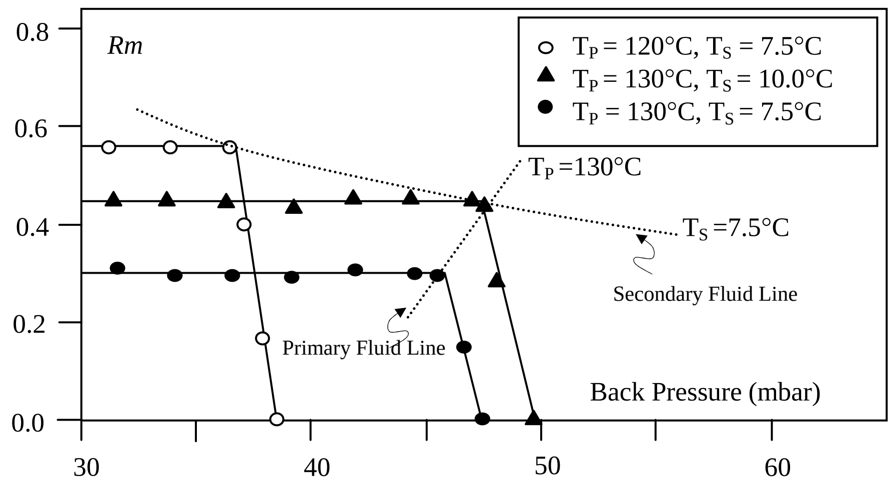

Figure 2.6 Effect of operating pressures on performance of a steam jet refrigerator based on experimental data provided by Eames and Aphornratana [2].

In the “unchoked flow” region, where the back pressures are in excess of the critical value, there is no secondary flow choking. The entrained secondary fluid varies and the entrainment ratio begins to drop rapidly. The transverse shock was believed to move upstream into the mixing chamber and disturb the mixing between primary and secondary fluid. Further increase in the back pressure to the point called “break down” pressure (“reversed flow” region) causes the flow to reverse back to the secondary flow inlet and the ejector finally malfunctions.

Figure 2.6 shows the effect of operating pressures on the performance of a steam ejector based on experimental data provided by Eames and Aphornratana [2]. A decrease in the primary fluid saturated pressure causes the primary fluid mass flow to reduce. As the flow area in the mixing chamber is fixed, an increase in the secondary flow results. This causes the entrainment ratio of the ejector to rise. However, this causes the momentum of the mixed flow to drop. Thus, the critical pressure is reduced. On the other hand, an increase in the secondary fluid pressure, which is the ejector’s upstream pressure, will increase the critical pressure. This also increases the mass flow through the mixing chamber, which results in an increase of entrainment ratio.

Many past studies [3, 24, 27, 31, 39~40 and 46~47] show that, not only operating conditions, but ejector geometries also affect the ejector performance. The experimental studies of the effect of primary nozzle throat size and ejector geometry on system performance were conducted [47]. The influence of using a small primary nozzle throat diameter was similar to that of decreasing primary fluid pressure, whilst the influence of the primary nozzle exit diameter was not significant.

2.3 Conclusions

From the literature survey, the ejectors have significant impact on the performance of the jet refrigeration system. Even though the ejector was invented more than a century ago, very few of them focused on improving the performance of the ejector, especially, in the field of refrigeration application. Most researches were found to emphasize their objectives in improving the overall performance of the system only.

Since the complexity of the flow behavior and the mixing process within the ejectors, the use of 1-D assumption only may not be adequate to improve in the design of the ejector. Some past researches have been made to analyze the flow and the mixing process in the ejector in order to understand them clearly. Unfortunately, the very high-speed fluid flow, the shock behavior and the interaction between the primary and its surrounding fluid were not simple to experimentally investigate. There were very few studies made to reveal the flow characteristics in ejectors by various methods, i.e., the flow visualization, and the CFD (Computational Fluid Dynamics). However, their analytical results were not completed and some of them were out of experimental ranges and some were unable to be applied for the refrigeration applications.

To be concluded, a clear understanding of the performance characteristics, the nature of flow structure and the mixing process within an ejector is needed to improve the performance of an ejector, and thus, increase the COP of the jet refrigeration system. In this study, CFD software will be used to model the R141b ejector at various geometries and operating conditions. At specified operating conditions and geometries, the performance of the ejector can be predicted. Thanks to the advantage of the CFD software, the flow and mixing process within the ejectors can be explored graphically and numerically using the post function available within the software.

CHAPTER III

EXPERIMENTAL APPARATUS

To validate the CFD results of the flow phenomena in the R141b ejector and to ensure the optimized model for further CFD simulation, a small experimental ejector refrigeration system was constructed. The system was designed to measure the desired parameters, mainly the performance of an installed ejector in term of its entrainment ratio and the static pressure profile along the wall of the R141b ejector. This section proposes the design and the construction of the experimental refrigerator.

3.1 Refrigerant Selection

It was advised that favorable substance to be selected as a refrigerant flowing through any ejectors should be inflammable, chemically stable, and available. In order to minimize the input energy to the system, its latent heat of evaporation should be as high as possible. The compressibility factor should be nearly the value of 1, so that the ideal gas assumption would be reasonably applied in designing an ejector. Past study [4] showed that the performance of an ejector was increased when molecular weight of the refrigerant was high. Many attempts have been made by using various kind of halocarbon refrigerant such as R11 [5], R12 [6], R113 [7], R123 [8] R134a [9], and R141b [10]. It was found that when using the halocarbon refrigerants, the systems were able to be operated at higher condenser temperatures than that was found in the steam jet refrigerator. The use of R11, R12 and R113 were prohibited and the productions of them are reduced and will finally be eliminated due to their ozone depletion. R123 and R141b are both the replacements of R11 and R113. The ozone depletion potential is 0.02 for R123 and 0.15 for R141b. Even though R141b has a lower molecular weight than that of R123, its boiling point is higher (32°C). The benefit of using the higher boiling point liquid (as high as the room temperature) is that the maintenance and the operation of the system would be easier and cheaper. For example, if the room temperature is below 32°C, when maintenance is needed or there is leakage in the system, there will be only a small chance that R141b will evaporate to the atmosphere and need makeup. This study concentrated only on the use of R141b, since it satisfied the above criteria and was available in the local market at lower cost and higher boiling point than R123. Physical properties of the R141b and R123 are listed in Table 3.1. Although there is a production of R245fa, the new replacement of R11, R123, R141b and R123 and the more environmental friendly, it was not available to the local market at the time of experiment.

Table 3.1 Physical property table for R123 [49] and R141b [50]

Physical properties:	R141b	R123	Unit
Molecular weight	116.95	152.9	
Boiling point under $1.013x10^5$ Pa	32.05	27.85	°C
Density of liquid at 25°C	1.227	1.458	g/cm^3
Vapor pressure at 25°C	79	96	kPa
Critical temperature	204.15	183.7	°C
Critical pressure	$4.25x10^3$	$3.67\ x10^3$	kPa
Critical density	0.430	0.549	g/cm^3
Latent heat of vaporization at boiling point	223.0	171.0	kJ/kg
Solubility in water at 25°C	0.509	0.39	% by weight
Specific heat of liquid at 25°C	1.16	0.985	kJ/kg. °C

3.2 Design Concept of the Experimental R141b Ejector Refrigerator

To investigate the flow phenomena and the influences of interested parameters which were thought to affect the performance of an R141b ejector, an experimental ejector refrigeration system was designed as shown in Figure 3.1. The major components of the system were the vapour-generator vessel, the evaporator vessel, the condenser, the receiver tank, the pumping system, and the ejector. The vapour-generator was designed to be able to generate the primary fluid up to 150^{o}C. Two electric immersion heaters were used as simulated heat source and cooling load at the vapour-generator and the evaporator, respectively. The condenser was a plated-heat exchanger type. A liquid refrigerant in the receiver tank was returned back to the vapour-generator and the evaporator via a hydraulic diaphragm pump.

3.3 Construction and Components

Figure 3.1 shows the construction of the experimental R141b ejector refrigerator. All vessels were fabricated from stainless steel 304. Fittings and valves were made from brass. Copper and polyethylene tubes were used as connection lines where the temperature was above and below 50^{o}C, respectively. In the same manner with connection lines, temperature was the criterion of the sealing material selection. Viton A O-rings and Teflon gaskets were used as sealing material of the vapour-generator, where operating temperature exceeds 100^{o}C. For the rest, of which temperature were below 100^{o}C, NBR rubber was selected as the sealing material.

3.3.1 The Vapour-generator

The vessel of the vapour-generator was fabricated from a 6-inch, 120 cm long, schedule 40s, 304 stainless steel pipes with flanges welded at the top and the bottom. A 8 kW immersible electric heater (Figure 3.2) was placed at the lower part of the vessel to generate the primary fluid up to 150^{o}C. Power of the heater was controlled by means of a digital thermostat. At the upper end, three baffles were welded to the vessel to prevent

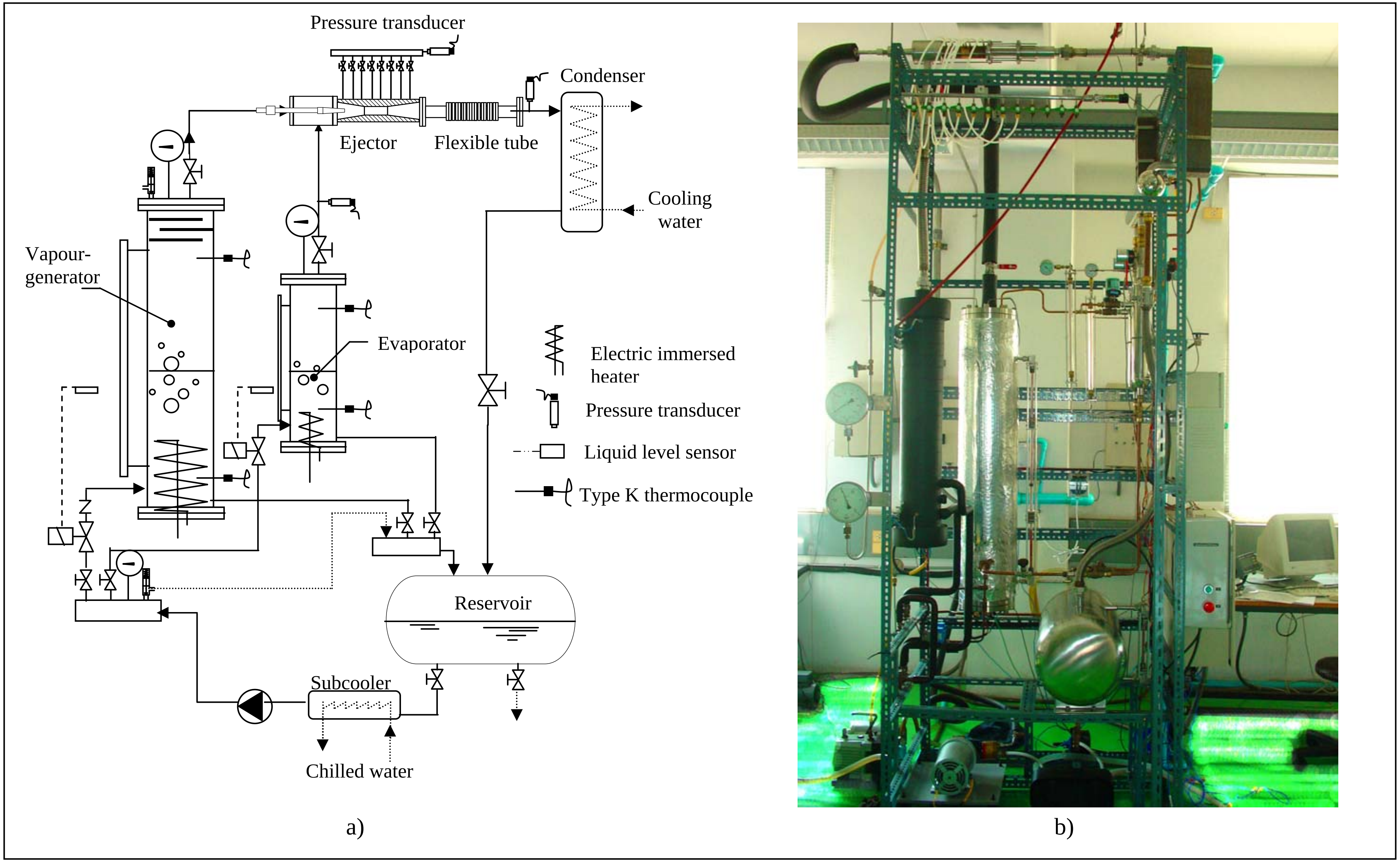

Figure 3.1 The experimental R141b ejector refrigerator.

liquid droplets being carried over with refrigerant vapour to the ejector. The vapour-generator was well insulated by a 40 mm thickness of glass fiber wool with aluminum foil backing to prevent the thermal loss from the machine. The level of liquid in the vessel can be observed via the attached sight glass.

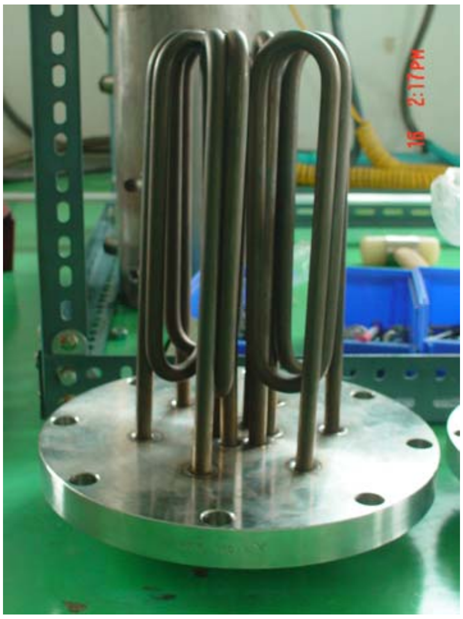

Figure 3.2 The immersible electric heater.

3.3.2 The Evaporator

The evaporator design was similar to the generator. The evaporator shell was fabricated from a 4-inch, 80 cm long, schedule 10s, 304 stainless steel pipe. Similar to that shown in Figure 3.2, a 3 kW immersible electric heater was installed to generate the system cooling load. To prevent the unwanted heat gain from the surrounding, the evaporator was well insulated, by a 30 mm thickness of neoprene foam rubber, from an unexpected heat gain from the environment. The liquid level in the vessel could be observed via the attached sight glass.

3.3.3 The Condenser

A water-cooled plate-type heat exchanger was used as a condenser. The entrance and the exit of the condenser were connected to the other parts of the system using 1-inch, stainless flexible tubes. In addition, an extendable-pipe was connected between the ejector's end and the flexible tube to allow sizing changes of the ejector (Figure 3.3). The liquefied refrigerant was collected in the reservoir tank before it was returned back to the vapour-generator and the evaporator via a pumping system.

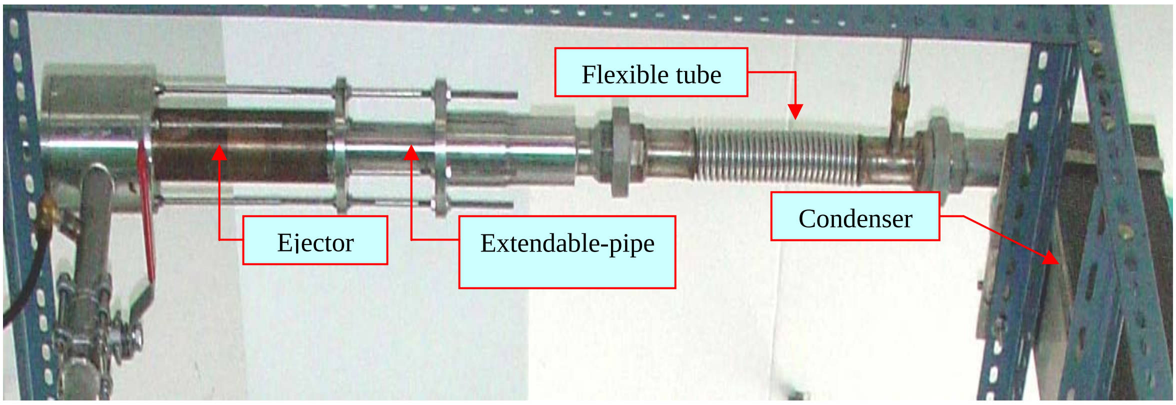

Figure 3.3 Connection of the ejector in the experimental refrigerator.

3.3.4 The Pumping System

Pumping of halocarbon refrigerants such as R11, R123, or R141b is no easy task with commercially available hardware. For example, when R141b is used as the refrigerant, the major difference between R141b and steam-water is their heat of vaporization. At 100°C, for water, the heat of vaporization is around 2,257 kJ/kg compared with 182.8 kJ/kg for R141b. This causes the feeding rate of the vapour-generator for a R141b system to be more than ten times greater than that of the vapour-generator for a steam water system. Due to the large differential pressure across the pump, a positive displacement type pump (gear pump, diaphragm pump, or piston pump) must be used. Both diaphragm pumps and piston pumps are always equipped with a check-valve at the inlet, which will significantly result in pressure drop in the suction-line. Since the liquid refrigerant at the pump inlet is always in saturated condition or slightly sub-cooled, a reduction in pressure, caused by the inlet check-valve, will cause the liquid refrigerant to evaporate and results in cavitations problem. For a gear pump, there is no inlet check valve; therefore, the pressure drop at the inlet is minimal. However, because halocarbon refrigerants, such as R141b, have extremely low lubrication characteristics, this soon will cause the moving parts and mechanical seal to wear away. Therefore, the commercially available pumping system for a jet refrigeration cycle using R141b is more critical than that for a steam-water system.

In this system, a mechanical diaphragm pump (Hydra-Cell Model: F20) as shown in Figure 3.4 was used to circulate liquid refrigerant from the reservoir tank to the vapour-generator and evaporator vessel. This pump was driven by a variable-speed 1 hp electric motor. The hydraulic diaphragm pump is a positive displacement pump which is able to supply maximum flow rate at 4.0 l/min and pressure up to 70 bar. For system protection, a pop-off safety relief valve was installed in the discharge line to bypass the exceed pressure refrigerant back into the receiver tank. Inlet and outlet valves of the pump were stainless steel. The diaphragm and all sealing materials of the pump were selected as Neoprene, the elastomer material resistive to R141b.

As stated previously, in the suction line the refrigerant is always at the saturated phase, so the slightest heat addition or pressure loss causes the cavitations to occur within the pump. This could lead to failure of the valve spring or retainer and diaphragm of the pump. In addition, a subcooler was placed at the inlet line of the diaphragm pump, between the reservoir tank and the pump (Figure 3.4). This subcooler is a small plated heat exchanger which is used to cool the refrigerant down by chilled water obtained from a laboratory’s water chiller.

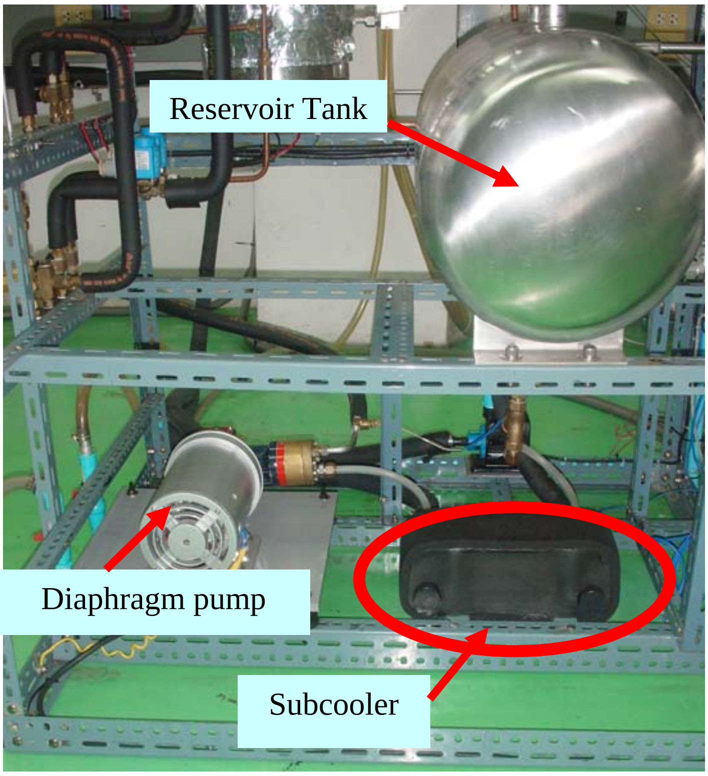

Figure 3.4 The pumping system with the subcooler.

3.4 Instrumentation and Control

In this experimental R141b ejector refrigerator, the operating conditions of each vessel could be controlled separately using the data acquisition system, connected to a personal computer. Parameters to be measured and controlled while the system was operated were temperature, pressure and mass flow rate of the refrigerant.

Type K thermocouples with uncertainties of ± 0.5°C were used to detect the temperature change of the interested position as shown in Figure 3.1. The detected signal of each probe was connected to the compensator and signal amplifier circuit. All probes were carefully calibrated using a precision glass thermometer. Pressures were detected by the absolute pressure transducers. At the evaporator and the pressure manifold, the ranges of the attached transducers were the same at 0-2.0 bar absolute, while the range of the one at the condenser was 0-3.0 bar absolute. All pressure transducers with uncertainties of ±

0.25% were calibrated using a double stage liquid ring vacuum pump and a standard mercury barometer for absolute zero and atmospheric pressure values, respectively.

The operating conditions of the vapour-generator and the evaporator were controlled by applying the ON/OFF logic to the respective heaters. Concerning the condenser, the operating pressure was controlled by adjusting appropriate volume flow rate of cooling water via a flow control valve and an on-off valve in the cooling water circuits. This allowed the system to maintain the operating condition of the condenser at the desired back pressure.

Liquid level in each vessel could be observed by using attached sight glasses. During each test run, the mass flow rates of the refrigerant could be determined by measuring the decreased level of the working fluid, during the certain interval of elapsed time in a steady operation, via the attached sight glasses. This allowed the evaluation of ejector entrainment ratio at the particular operating condition. In addition, for the system to operate continuously, the liquid in the reservoir tank was fed back to the vapour-generator and the evaporator via the pumping system. The liquid level in the evaporator and the vapour-generator were maintained using a variable speed motor drive controller. Electrical power inputs to the heaters (both generator and evaporator) were measured using a digital (Watt-Hour) power analyzer.

3.5 The Ejector

The design of an ejector used in this experiment, the R141b ejector, was based on the one-dimensional analysis of the compressible gas flow through the nozzle and diffuser as described in Appendix A. The following sectional drawing in Figure 3.5 shows the details of the ejector’s internal geometry and the connections to other components in the system. The ejector used in the experiment was designed to deliver suction mass of 0.3 kg/min at

0.351 bar abs (5°C saturation temperature) when the primary motive flow rate was 0.96 kg/min at 6.771 bar abs (100°C saturation temperature) and the discharge pressure was 1.33 bar abs. (40°C saturation temperature). The material used for ejector parts was brass. The internal geometry of the ejector was machined employing the EDM technique. A photograph of the ejector used in the experiment is shown in Figure 3.6.

To investigate the flowing and the mixing characteristics at each operating condition, the static pressure was tapped and measured along the vertical axis of the ejector. Polyethylene with 6mm. outer diameter was used as the tapping lines. They were connected to the 8-way pressure manifold and the static pressures were detected by an absolute pressure transducer (0-2.0 bar absolute).

Since geometry of the ejector was one of interested parameters and the recommended dimensions from ESDU [48] were given in the range of numbers, there were 3 primary nozzles, 3 mixing chambers and 3 throats constructed with various sizes. Each of them was designed to be easily fitted and interchanged with others as will be described in the following section. Please note that, the diffuser was thought to have very small influence on ejector performance. Therefore, the studying of effect of the diffuser geometries was omitted and every test was done with only one diffuser.

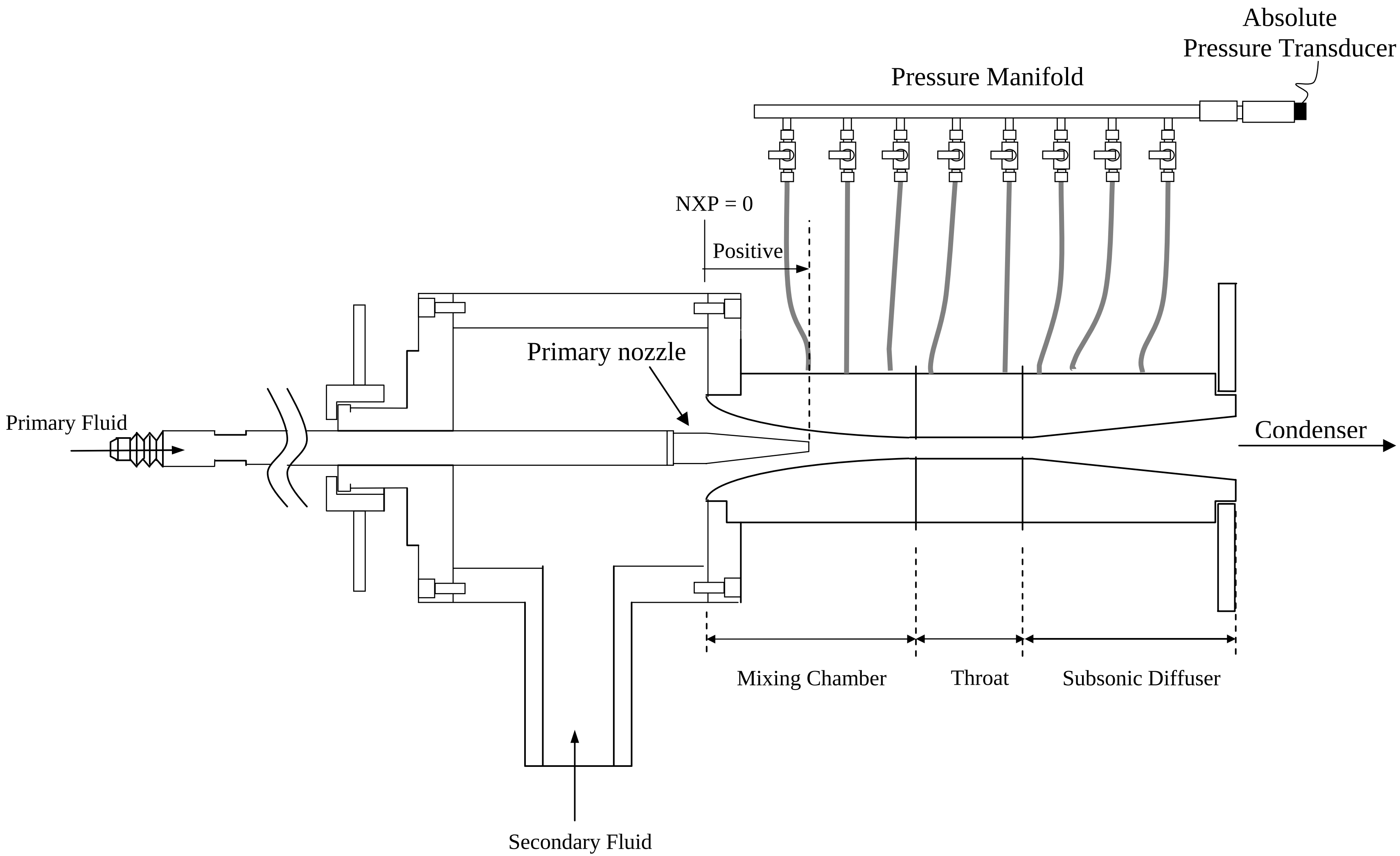

Figure 3.5 Schematic Diagram of Experimental R141b Ejector.

Figure 3.6 Photograph of an ejector used in the expeiment.

3.5.1 The Primary Nozzle

The 3 primary nozzles were constructed with a diameter of 2.5, 2.8 and 3.2 mm at the throat. Nozzle inlets were circular and the exit portions had an included angle of 10°. The ratio of the nozzles throat's diameters to their exit diameter was kept as constant. The nozzle was mounted on the threaded shaft which allowed the axial position of the nozzle in a mixing chamber to be adjusted. The significant geometries of the experiment nozzle are described in Table 3.1. A photograph of the constructed nozzle No.1 is shown in Figure 3.7.

Figure 3.7 Photograph of the primary nozzle.

3.5.2 The Mixing Chamber

There were 3 mixing chambers constructed with 3 different inlet diameters. These allow the investigation of the effect of the mixing chamber's inlet diameters on the ejector performance. Two of them were converging ducts (constant pressure type), while the other one was straight duct (constant area type). For a constant pressure type, the entry sections of the mixing tubes were bell mounted. Other significant dimensions are illustrated in Table 3.2.

3.5.3 The Throat

Four pieces of ejector throat were constructed with the length varying from 2 to 5 times its diameter (8 mm). The cross-sectional area of these throats was constant throughout the conduit. The significant dimensions are described in Table 3.2.

3.5.4 The Subsonic Diffuser

As described previously, only 1 diffuser was constructed. The diffuser has its inlet and exit inside diameters of 8 and 22 mm, respectively. Its cross-sectional area was gradually increased along the length of 77 mm. The detailed dimension of its internal geometry is shown in Table 3.2.

Table 3.2 Ejector's geometry.

Primary Nozzle Geometries			Mixing Chamber Inlet Diameter		Throat Length		
	D_{th}	Y		Z		*l*	
Nozzle No.	mm	mm	Mixing Chamber No.	mm	Throat No.	mm	Times of Diameter
1	2.8	6.3	1	36	1	16	2d
2	2.5	5.4	2	12	3	32	4d
3	3.2	7.2	3	48	4	40	5d

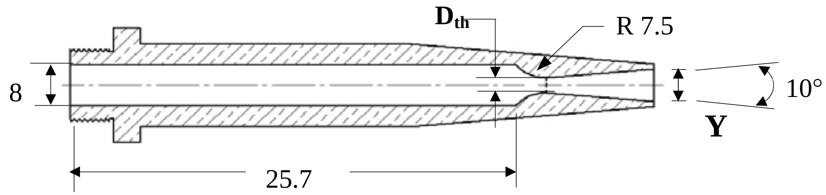

a) Primary nozzle

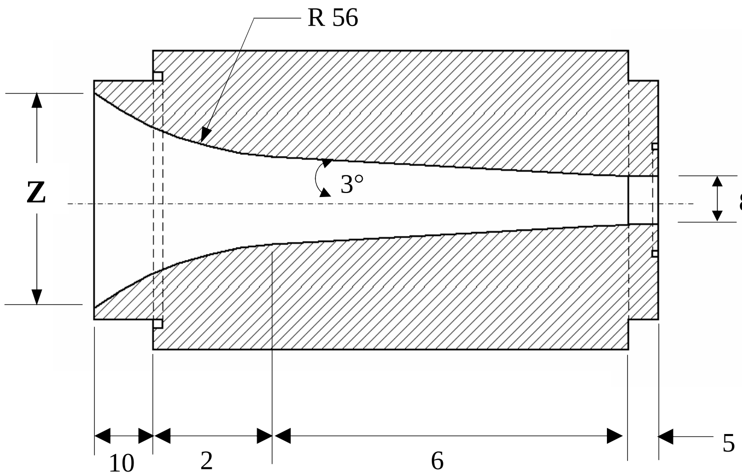

b) Mixing chamber

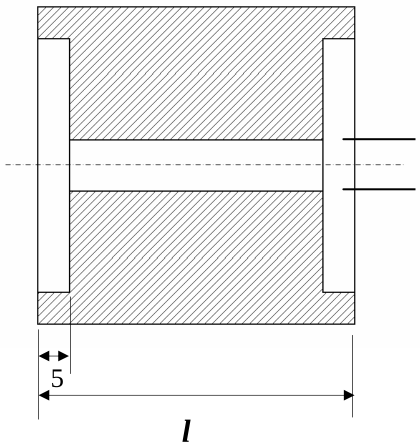

c) Throat

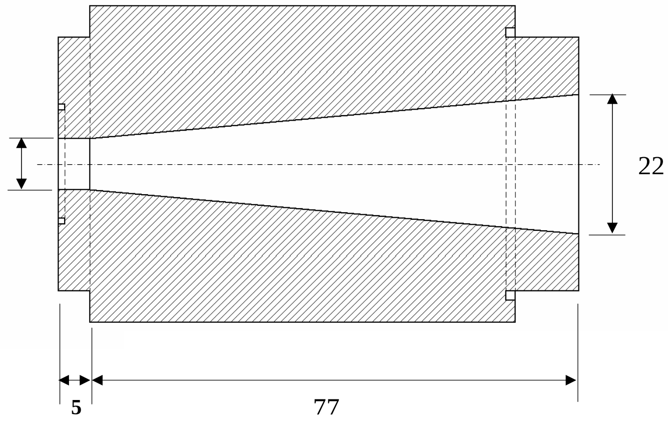

d) Diffuser

3.6 Test Procedures

To start a test, the vapour-generator's heater should be switched on to raise the refrigerant temperature to the desired temperature. The next step was to turn the water pump on. The condenser water valve that was closed could now be opened to allow water to flow through the condenser. After the refrigerant temperature reached its set point on the digital controller key pad, the R141b vapor was released from the top of the vapour-generator to enter the primary nozzle of the ejector by opening the valve at the top of the vapour-generator manually. After the temperature in the vapour-generator was steady, by opening the valve at the top of the evaporator vessel, the secondary flow could be entrained to the ejector and mixed with the primary flow. The refrigerant temperature in the evaporator was also dropped; hence, it was be able to produce a refrigeration effect. To reach the desired evaporator temperature, the evaporator heater was then turned on.

In order to make the system operate continuously, the refrigerant level in the vapour-generator could be maintained by switching on the hydraulic diaphragm pump to feed the refrigerant from the receiver tank via the subcooler back to the vapour-generator and the evaporator. It is recommended that this pump, which is equipped with a speed controller, be set to operate at around 18 Hz at the beginning and then the motor speed could be increased slowly if a higher pressure is required. During the test run, the motor speed and the vapour-generator temperature were responsible for the condition of the primary flow and they could be controlled quite independently without causing too much disruption to the system operation. After the temperature of the refrigerant in the vapour-generator and the evaporator were steady, the primary and secondary mass flow could then be measured as described previously.

3.7 Conclusions

This chapter illustrates the information of the design and construction of the experimental R141b ejector refrigerator. Reasons for choosing R141b as a circulated refrigerant in the system were given. The operating conditions of the constructed test rig were fully automated controlled by a personal computer and data acquisition system. This allows the investigation on the performance characteristics of the ejector. The detailed geometries of the fabricated ejector were described. At the end, the test procedure of the experimental refrigerator was brief. The experimental results based on this experimental refrigerator are provided in Appendix B. The results of the ejector's performance will later be used to validate the CFD results in Chapter V.

CHAPTER IV

COMPUTATIONAL FLUID DYNAMICS (CFD): MODEL SETUP

Currently, the CFD technique is widely used in many applications. Engineers and researchers use CFD to design, analyze, and simulate fluid flows in interested devices such as turbo machinery, wind tunnels, and aerodynamics applications. Although, there are numbers of ready commercial CFD software and codes being available for use, in order to obtain good results and analysis in fluid dynamics problems good knowledge in the physics of the problem and basic understanding of numerical methods is required. Moreover, validation of the CFD results with real experiments should also be performed so that the results are creditable.

For this study, the finite volume method in a commercial CFD package (FLUENT 6.0) is used to simulate the flow and predict the performance of the R141b ejector. This chapter provides the informative description of the theory and assumptions used for the simulation. Basic information on setting up the calculated model and the mesh generation method are also presented.

4.1 Introduction to Computational Fluid Dynamics (CFD)

Computational Fluid Dynamics is a branch of fluid mechanics employing numerical methods and algorithms to solve and analyze the systems involving fluid flows. If the problems or systems are complex, computers may be required in order to compute a numerical solution. Generally, the algorithm of the CFD is composed of pre-processing step, solver step and post-processing step. Pre-Processing is a process that uses a post-processor in identifying the system geometry (physical boundaries) and the system volume inside the physical boundaries is divided into a number of discrete cells (mesh). All necessary information on fluid properties at the boundaries is defined. The simulation step (Solver Step) is the step of solving all equations of a specified problem numerically and iteratively. Fluid Dynamics problems always involve numbers of partial derivative equations of the Navier-Stokes equation in the conservative form of energy, mass and momentum. Some of the discretization methods being used for solving those equations are finite volume method (FVM), finite element method (FEM) and finite difference method. Finite Volume Method, the classical and the most used in commercial CFD codes, employs the control-volume-based technique to convert all governing equations into an algebraic form that can be solved numerically. This control volume technique consists of integrating the governing equations about each control volume, yielding discrete equations that conserve each quantity on a control-volume basis. Post-Processing is a process in which a post-processor program is used to view, present, and analyzes the results. The resulting solution can be plotted and presented graphically.

As mentioned previously, fluid dynamics problems might be complex and the partial derivative equations could be composed of many terms. Hence the finite volume method for commercial CFD codes needs good algorithms of equation solving steps. Basically, there are 2 solution methods, the segregated and the coupled solver. The segregated solver is the solution algorithm in which, the governing equations are solved sequentially. Several iterations of the sequential solution are continued until the convergence criteria are satisfied. Whereas, the coupled solver performs its solving step by solving the governing equations of mass, momentum, and energy simultaneously (i.e., coupled together). To reach a converged solution, several iterations of the coupled solutions must be performed.

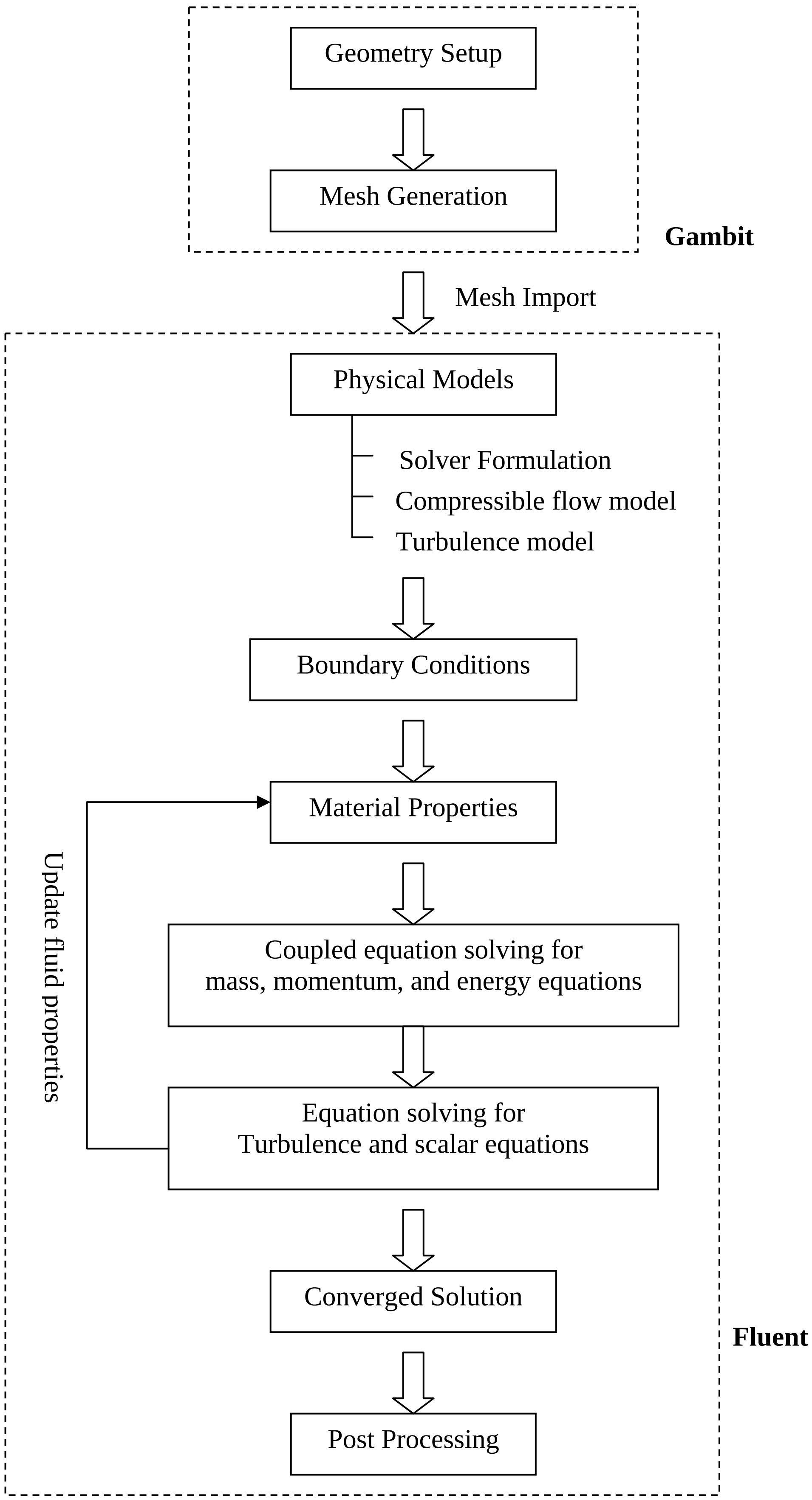

Figure 4.1 Flow chart of the CFD procedure for modeling the R141b ejector.

4.2 CFD Technical Data for the Current Study

The problem under investigation here involved the supersonic flow inside the flow passage of the experimental R141b ejector. Working conditions of the model were set at the same ranges as was done in the experiments. In order to simulate this particular situation, Gambit 2.1 and FLUENT 6.0 were used as the pre-processor to generate grid network (mesh) and the CFD solver, respectively. The procedure of using the Gambit 2.1 and FLUENT 6.0 for this analysis is shown in Figure 4.1.

4.2.1 Modeling Assumptions

These following assumptions are made in order to perform the CFD analysis for an ejector:

- The flow is assumed to be steady and two-dimensional compressible flow.
- The flows at all inlets are accelerated from their stagnation points.
- The flow is turbulence.
- The property of working fluid is set as an ideal gas.
- Wall boundary condition of the ejector was set as adiabatic wall and was assumed to be stationary and non-slipped surface.

4.2.2 Geometry setup

As proposed, Gambit version 2.1 was used as a preprocessor to create the calculation domain of the models. The geometries of the calculation domain of the modeled ejectors were taken from those which were used in the experiment. For example, Figure 4.2 a) presents an ejector model that used primary nozzle No.1, throat No.1 and mixing chamber No.1. Their significant dimensions have already been described in Chapter 3. The models were created in a two dimension (2-D) domain. The 2-D domains of the ejector were created in a rectangular coordinate x-y. Since, in the Fluent step, the axisymmetric model was applied to the simulation, the geometry was dimensioned only above the x-axis as shown in Figure 4.2 b). The two-dimensional axisymmetric model had axial symmetrical domain about the x-axis. The advantage of using the two-dimensional axisymmetric model was that the three-dimensional effect (3-D) was taken into account in the simulation.

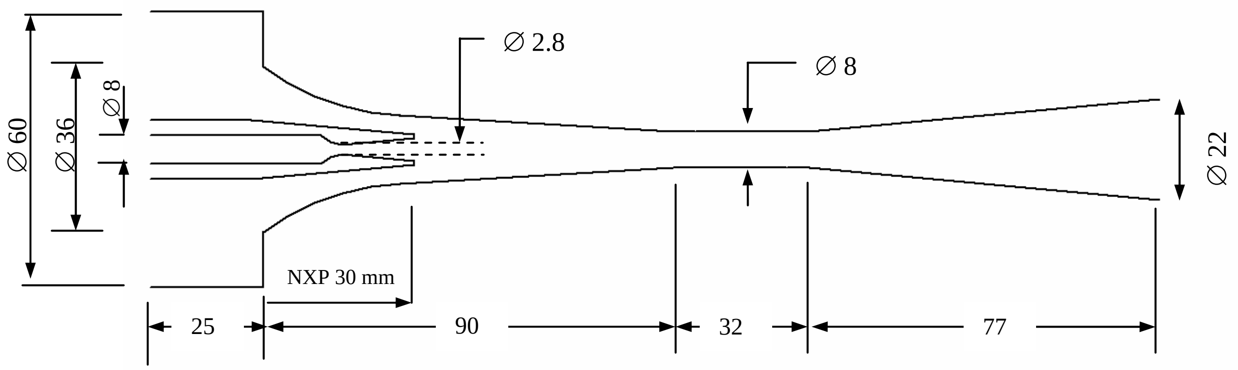

a) Full shape of the geometry with dimensions (Units in millimeters).

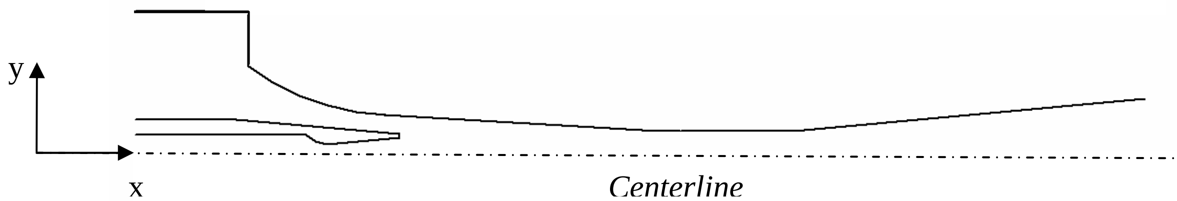

b) Axisymmetric geometry in Gambit 2.1.

Figure 4.2 Geometry setup for the R141b ejector.

4.2.3 Meshing the model

The grid network models were meshed using a mesh function in Gambit 2.1 and then were transferred to FLUENT. Grid structures of the models were meshed using the normal quadrilateral grid. Since concentration of the grid density is critical to the stability and the convergence of the simulation, the grid network models were focused and dense on the areas where the large gradient in fluid properties and the significant flow phenomena were expected. For example, the grid was dense at the place where the primary fluid and the secondary fluid were mixed and where the shock phenomenon was likely to occur. In the nature of the flow through an ejector where shock and turbulence are common, the near wall boundary layer needs to be meshed at the boundary layer. Grid structure for the 2-dimensional ejector model corresponding to the geometry model in Figure 4.2 is shown in Figure 4.3. The mesh was made of 43,000 structured quadrilateral elements. To investigate the effects of geometry on the flow of the R141b ejector, the number of grid elements was changed when the computational models were changed corresponding to the change in geometrical experimental investigation. To ensure the stability of the simulated solutions with grid independence, a grid refinement (increasing grid numbers to around 80,000) was performed. After refining the grid elements, the solutions of the models with the order of 40,000 elements and 80,000 elements were found no different. Thus, considering the mesh resolutions, the numbers of grid elements of all models were set high enough (in the order of 40,000 elements) to capture all the flow features inside the ejector.

4.2.4 Solver Formulation

FLUENT [51] provides three optional solver formulations: segregated, coupled-implicit, and coupled-explicit. Before any case of the simulation could be performed, one of the solver formulations should be assigned to the calculation model. The segregated solver is the default solver set in FLUENT. It can be applied to many practical flows. However, the solver used in this study was selected as a coupled-implicit solution. This solver is suitable for a case of high speed compressible flow. In the calculation process, the coupled-implicit solver couples the flow and energy equations; hence, the faster converging solution results. The disadvantage of using the couple solver is that it requires about 2 times the memory resources of the segregated solver. The couple-explicit solver may be considered if less memory is required. However, it consumes more computational time to reach a converged solution.

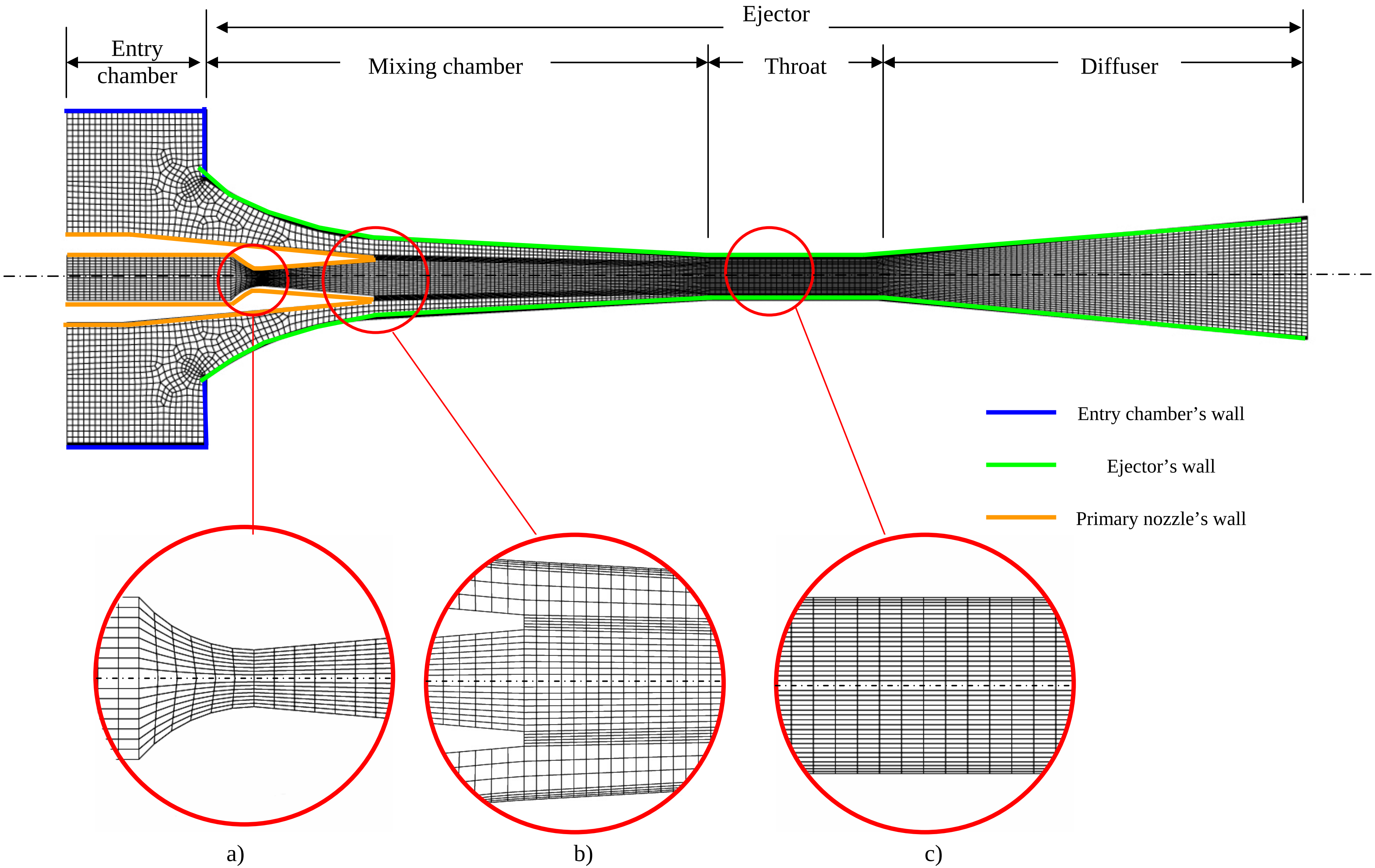

Figure 4.3 Calculation domain and grid structure of the R141b ejector CFD model.

4.2.5 Compressible Flows Model

Compressible flows can be classified by the flow velocity of a gas (U) over the speed of sound in the gas (C), which are combined to a single parameter called Mach number, M.

$$M = \frac{U}{C} \tag{4.1}$$

Since compressibility effects become important for transonic flow and supersonic flow, the compressible flows model should be applied to the calculation. Especially for supersonic flow, the flow may contain shocks and expansion fans which can impact the flow pattern significantly.

In FLUENT, it is not necessary to set up any special cases to handle the compressible flow assumptions. FLUENT solves the continuity and momentum equations by incorporating the flow speed and its related static pressures and temperature given in the boundary setup procedure.

4.2.6 Turbulence model

Due to the high speed flow in the ejector channel, the flow model is set as realizable k-epsilon model which is one of the turbulence models provided in FLUENT. The realizable k-epsilon model satisfies certain mathematical constraints on the Reynolds stresses, consistent with the physics of turbulent flows in which both the standard k-epsilon model and the RNG k-epsilon model are not applicable. For the case of the flow in ejectors, the realizable k-epsilon model provides the spreading rate of round jets more accurately and suitably for flows under strong adverse pressure gradients as expected to occur for the flow in ejectors.

4.2.7 Wall functions

Turbulent flow behaviors at the region close to the wall are always exclusive to the CFD solver. Accurate representation of the flow in the near-wall region determines successful predictions of wall-bounded turbulent flows. Two different near-wall flow representations or wall functions are provided in FLUENT [51], standard wall function and non-equilibrium wall function. The standard wall function gives reasonably accurate predictions for the majority of high-Reynolds-number, wall-bounded flow. The non-equilibrium wall function further extends the applicability of the wall function approach by including the effects of pressure gradient and strong non-equilibrium. However, the wall function approach becomes less reliable when the flow conditions depart too much from the ideal conditions underlying the wall function, for example, a low Reynolds number flow, boundary layer separation flows, buoyancy-driven flows. In such cases, the enhanced wall treatment provided in FLUENT is required to account for accurate mesh resolution and the near wall modeling approach.

To ensure the completeness of the standard wall treatment to the successful results of the R141b ejector, previous results from the study of Chunnanond [47] were manipulated to account for the effect of three different near-wall approaches. As seen from Figure 4.4, the results of static pressure distributions obtained from the model using the non-equilibrium wall function provided the worst agreement with the experimental values. The CFD’s result using the enhanced wall treatment assumption provides the closest results of static pressure in the diffuser region compared to the experimental values. However, using the enhanced wall treatment approach consumes much more computational time than others. Even though, the standard wall function provides a larger error in calculated pressure in the diffuser part compared to the enhanced wall treatment, upstream of the diffuser the results are similar to those obtained using the enhanced wall function. Moreover, the standard wall treatment consumes much less computational time compared to the other wall approaches.

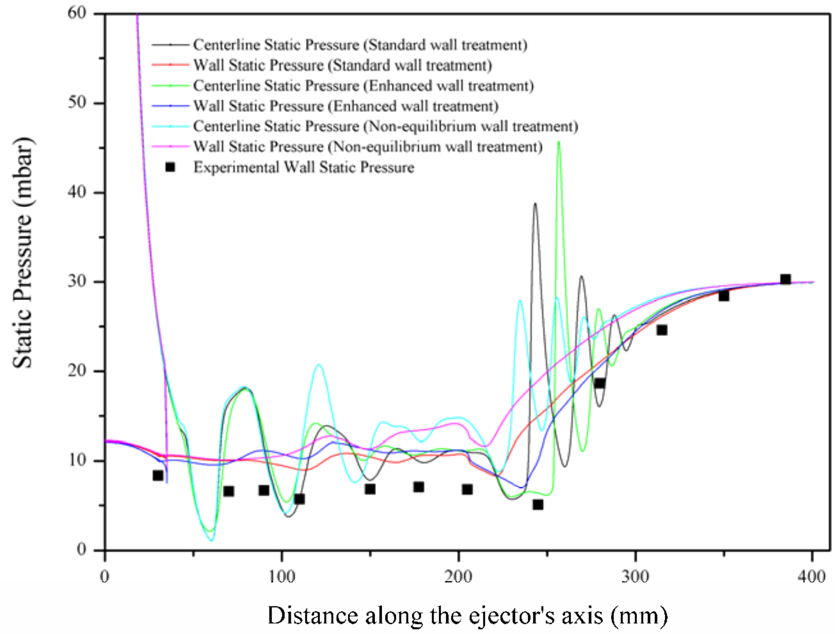

a) At T_P = 130 ^oC, T_S = 10 ^oC and P_b = 30 mbar.

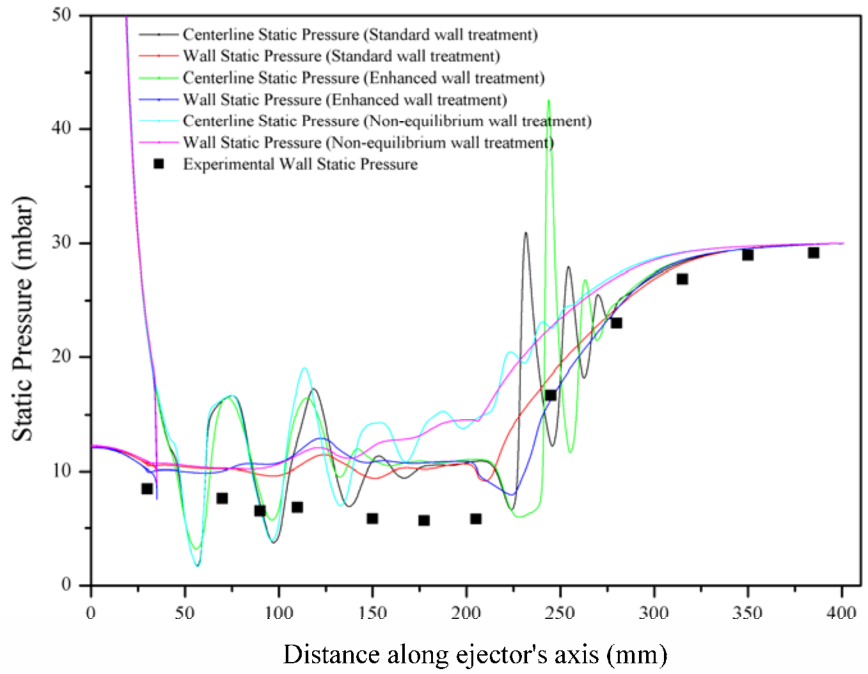

b) At T_P = 120 ^oC, T_S = 10 ^oC and P_b = 30 mbar.

Figure 4.4 Static pressure profiles for different wall treatment assumptions for a steam ejector (manipulated from data provided by Chunnanond [47]).

It was also reported by Sriveerakul et al. [39~40] that the simulation results of a steam ejector using the standard wall function provide accurate results compared to the experimental values. Therefore, in this study, the standard wall function was selected to use in setting up the simulated models.

4.2.8 Boundary conditions

By ignoring the heat transfer in the calculation, the wall was simply set to be non-conducting (adiabatic) wall. Pressure inlet and pressure outlet conditions were applied to the entrances and exit of the models. Two pressure inlet conditions were set for the primary fluid inlet (the vapour-generator saturated condition) and the secondary fluid inlet (the evaporator saturated condition). A pressure outlet boundary condition was set for the discharge of the ejector (the condenser condition).These conditions were varied with the same ranges as were conducted in the experiments. The values of each boundary were assigned as the saturation properties (temperature and pressure) of each operating state. Since the velocity of the flow entering and leaving the domain was thought to be relatively small compared with the supersonic speed during the flow process of the ejector, there was no difference between an input of the stagnation pressure and static pressure.

In fact, the arrangement of the ejector in the system could be either in horizontal or vertical setting, with no significant difference from each other due to a very high speed fluid flow in the flow channel. However, if heat transfer needs to be considered, the difference in horizontal and vertical flow may not be neglected.

4.2.9 Working fluid properties

The working fluid properties of the R141b in the models were treated using the assumption of an ideal gas. Even though the ideal gas relation seemed to be an unrealistic assumption to the model, for ejector applications where the operating pressure is relatively low, it was proved by some researchers [26] that it provided similar results to a real gas model. The properties of R141b vapour, as provided in FLUENT database, are shown in Table 4.1. Note that, the density of the working fluid is evaluated using the ideal gas relation as part of the calculation as it progresses. Other properties are defined as constant throughout the simulation.

Table 4.1 Fluid properties of selected refrigerant R141b.

Property	Physical property data
	R141b
Replaces	R11
Chemical formula	$CCl_2F\text{-}CH_3$
Molecular weight	117.0
Boiling point at 1 atm (°C)	32.05
Liquid density at 25°C (kg/m^3)	1234

For a compressible flow, the ideal gas law is expressed in the following equation.

$$\rho = \frac{P_{op} + P}{RT} \tag{4.1}$$

Where P is the local relative (or gauge) pressure predicted by FLUENT and P_{op} is defined as the operating pressure which was absolute zero for this study.

4.3 Convergence Criteria

The CFD simulation of the ejector model was considered as converged and its data was ready to be proceeded when the following 2 converging criteria were satisfied. Firstly, it had to be shown that the calculated mass fluxes of every face in the model were stable. In addition, to conserve the mass, the summation of mass fluxes that entered the domain should be equal to that which left the domain. Secondly, every type of the calculation residual must be reduced lower than the specified value (in this case, less than 10^{-6}).

4.4 Results

After the CFD solution of each simulation was considered as converged, three significant types of the solution data could be presented which were:

- The entrainment ratio of the ejector
- The X-Y plot of static pressure distribution along the ejector wall and along the centerline of the ejector
- The contours of Mach number inside the ejector

The entrainment ratio (Rm) of the ejector by this simulation approach is simply evaluated from the ratio of the sum of mass flux entering the mixing chamber inlet's face to the sum of mass flux entering the primary nozzle inlet's face, both of which can be directly determined in FLUENT.

Please note that the simulated entrainment ratio and the static pressure profile along the ejector wall were the 2 most significant parameters in validating the CFD results with the experimental results. If the comparison showed the similarity between the results from both approaches, then the correctness of the simulated CFD model was verified. Thus, other related solution data obtained from the CFD, such as the static pressure profile along the centerline of the ejector and the contours of Mach number or the plot of the Mach number could be fairly used to explain and represent the flow inside the ejector.

4.5 Conclusions

In this chapter, the background of the CFD technique was presented. The criteria of creating the calculation domain, grid elements, and the information of the CFD ejector model setup (fluid properties, solver selection, turbulence model and boundaries conditions), including the convergence criteria and types of solution data to be considered were provided and summarized as shown in Table 4.2.

Before the analyses of the simulated results were made, some of them had to be validated through the reliable data from the experiments. In the next chapter, the validation process of the simulated results with the experiment results measured from the constructed R141b ejector refrigerator is presented. After the correctness of the model was guaranteed, then other calculated information obtained from the CFD models could be used to represent the flow phenomena and the mixing behaviors in the R141b ejector, as will be discussed in Chapter VI, VII and VIII.

Table 4.2 Setup information of the CFD model.

Criteria of numerical model	**Selected criteria**
1. Domain	Axisymmetric domain
2. Boundary conditions	
Inlet boundary condition	Pressure inlet condition
Outlet boundary condition	Pressure outlet condition
3. Meshing information	43,000 structured quadrilateral elements
4. Solver formulation	Coupled-implicit solution
5. Turbulence model	Realizable k-epsilon model
6. Working fluid	R141b (CCl_2F-CH_3)
7. Wall-treatment method	Standard wall function
8. Convergence criteria	Calculation residual less than 10^{-6}

CHAPTER V

VALIDATION OF CFD RESULTS

In this chapter, the CFD results of the R141b ejector model were validated with the experimental data. The boundary conditions of the simulated model were set as was done in the experiment. The primary fluid inlet conditions of the model were set to the saturated conditions corresponding to the vapour-generator temperature ranges from 90°C to 120°C. While, the secondary fluid inlet conditions were set to the saturated conditions corresponding to the evaporator temperature ranges from 0°C to 10°C. The downstream conditions of the ejector were varied from 0.7 bar to 1.8 bar corresponding to the condenser temperatures of around 25°C to 50°C. The validation process was performed by validating the CFD results of primary fluid mass flow rates, the entrainment ratios and the wall static pressure distributions of the R141b ejector model with the actual values.

5.1 Validation of the Primary Fluid Mass Flow Rate

Table 5.1 and Figure 5.1 compare the predictions of the primary fluid's flow rates through the primary nozzles by CFD with the experimental results when the primary fluid temperature was ranged from 90°C to 120°C. The primary flow rates predicted by CFD for both nozzles' throat diameter of 2.8 and 2.5 mm. were mostly over predicted compared to the measurement values. The average error of only 1.86 % was found for the predicted mass flow rate through the 2.8 mm. nozzle throat diameter; whereas a higher average error of only 5% was found for the nozzle whose throat diameter was 2.5 mm. This validation of the primary mass flow rate, hence, guarantees the accuracy of the results of the flow through the primary nozzle.

Table 5.1 Validation of calculated primary mass flow rate with the experimental values.

	Primary mass flow rate, $\dot{m}_p$ (kg/s)					
T_P (°C)	Nozzle throat diameter= 2.8 mm			Nozzle throat diameter= 2.5 mm		
	CFD	Experiment	Error (%)	CFD	Experiment	Error (%)
90	0.0130	0.0129	0.9302	0.0103	0.0107	-3.8380
95	0.0145	0.0145	0.0144	0.0116	0.0113	2.3200
100	0.0162	0.0160	0.8739	0.0128	0.0123	4.7209
105	0.0179	0.0174	2.6965	0.0142	0.0133	6.6213
110	0.0198	0.0192	3.0729	0.0157	0.0147	7.1042
115	0.0218	0.0211	3.3175	0.0173	0.0159	8.8523
120	0.0240	0.0235	2.1277	0.0190	0.0177	7.6785
Average Error (%)			1.862			4.780

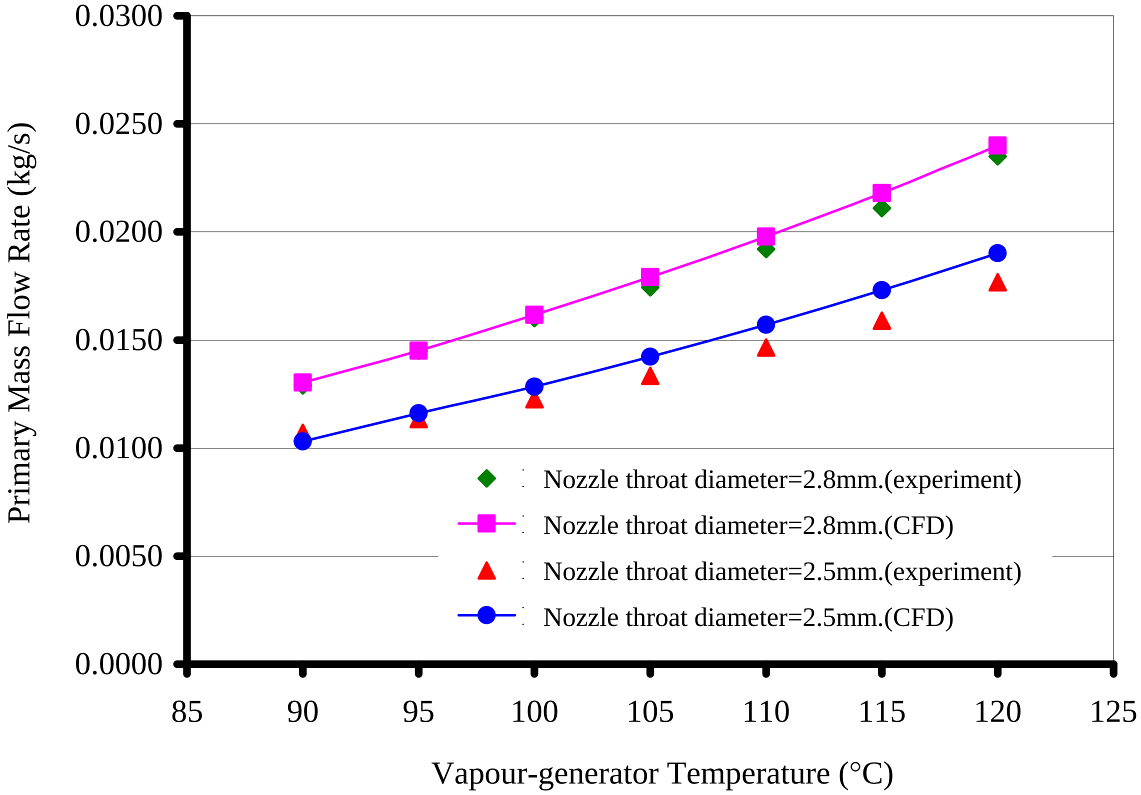

Figure 5.1 Comparison between CFD and experimental results of the primary mass flow rate.

5.2 Validation of the Wall Static Pressure Distributions

This section presents the validation of the calculated wall static pressure distributions with the experimental values. As described in Chapter III, the static pressures along the wall of the ejector were measured using the 8-port pressure manifold connected to an absolute pressure transducer (0-2.0 bar absolute). Each port of the pressure manifold was connected to the tapping hole drilled at the wall of the ejector, using polyethylene tube with 4mm. outer diameter. The measured static pressure distributions along the wall of the experimental R141b ejector were used as the reference data for validating with one from the simulated solutions.

Figure 5.2 to 5.7 illustrate the comparison between the static pressure distributions at the wall from the two different approaches, the experimental versus the simulated results. The comparisons of the calculated and the measured wall static pressure distribution at various downstream and upstream operating conditions are presented in Figure 5.2 and Figure 5.3, respectively. Also, the comparisons when the ejector was operated at various geometries are presented in Figure 5.4 to Figure 5.7.

The distributions of the predicted static pressure at the wall in Figure 5.2 to Figure 5.7 were mostly found to be offset lower than the one from the experiments, especially at the throat section. One possible reason for this error may come from the difficulty of calibrating the absolute pressure transducer at very low range near the absolute zero level. Another possible cause was thought to occur by an unexpected surface-roughness or mis-alignment in the primary nozzle and the ejector.

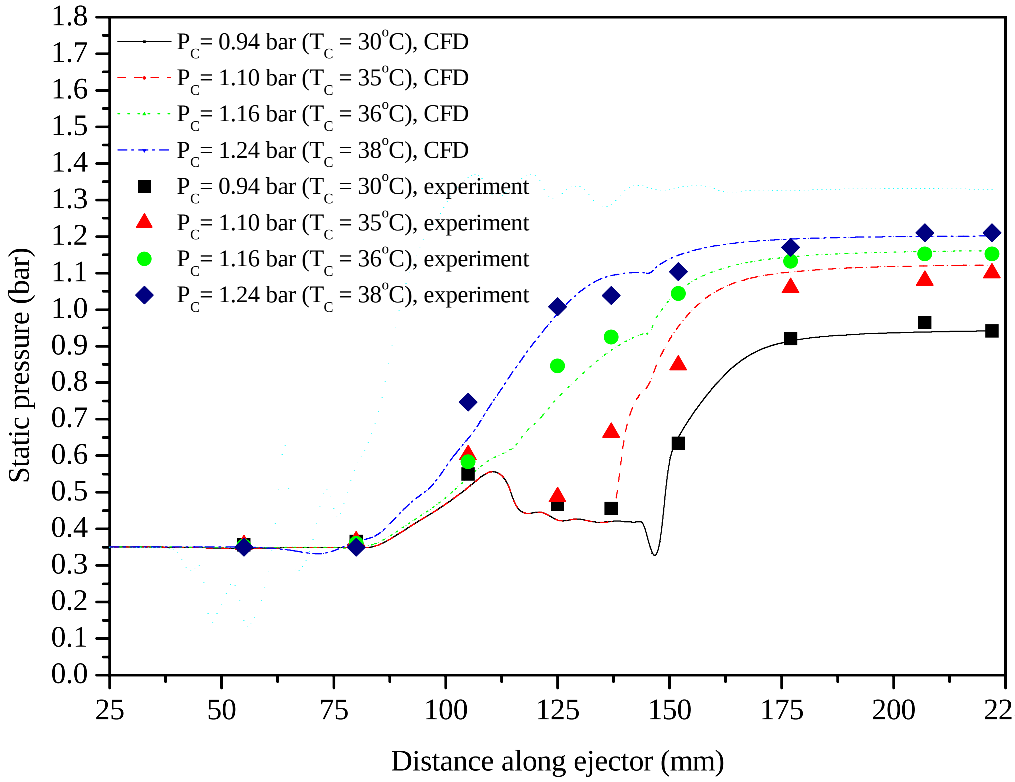

Figure 5.2 Static pressure profile along the ejector at T_P = 100°C, T_S = 5°C and at various condenser pressures, effect of downstream pressure.

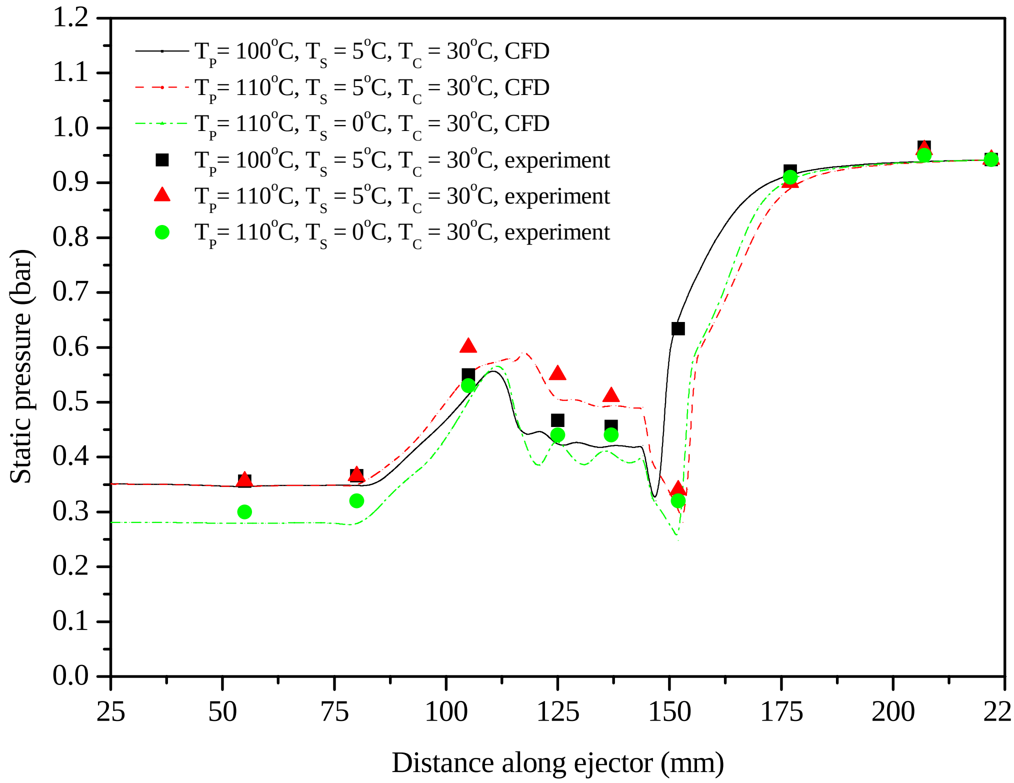

Figure 5.3 Static pressure profile along the ejector at T_C =30°C (P_C =0.94 bar), effect of primary and secondary fluid pressure.

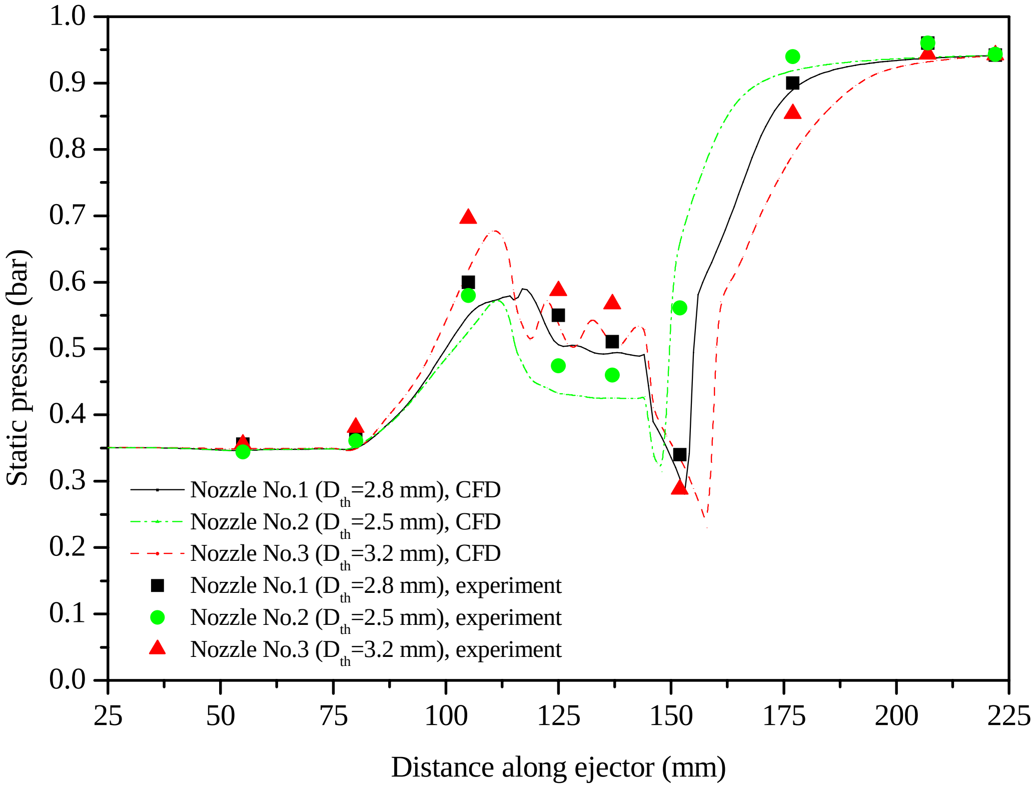

Figure 5.4 Static pressure profile along the ejector at T_P = 110^oC, T_S = 5^oC , and
P_C = 0.94 bar, effect of the primary nozzle throat diameter.

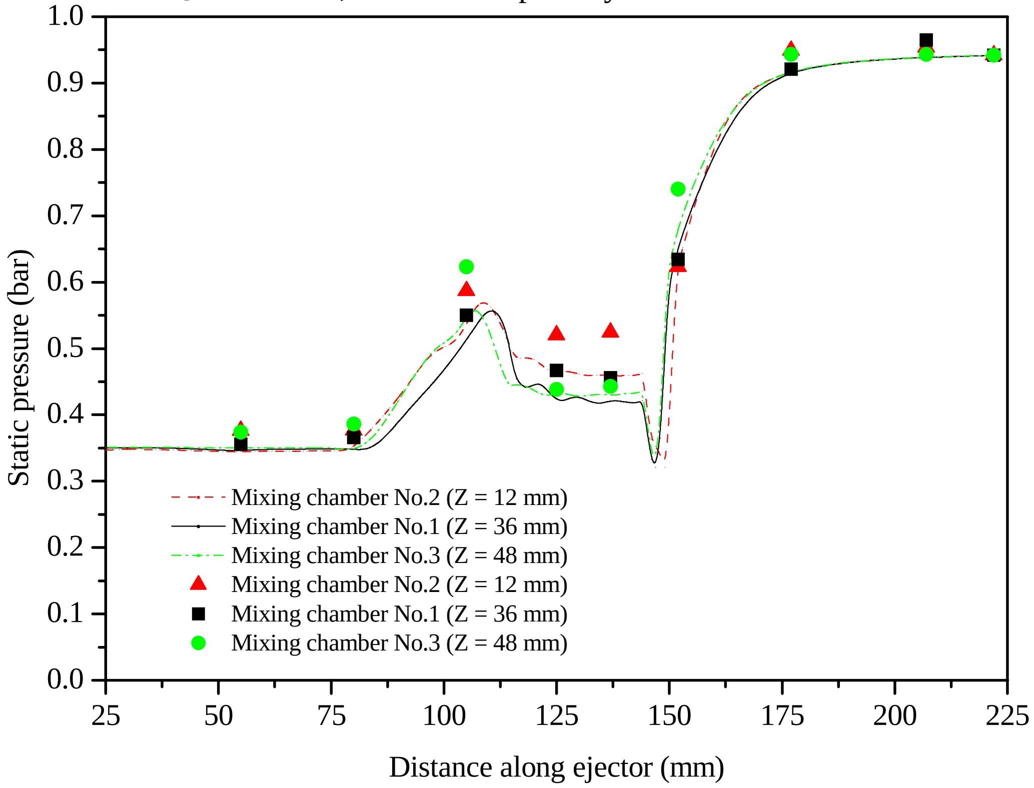

Figure 5.5 Static pressure profile along the ejector at T_P = 100^oC, T_S = 5^oC, and P_C = 0.94 bar, effect of the mixing chamber inlet diameter.

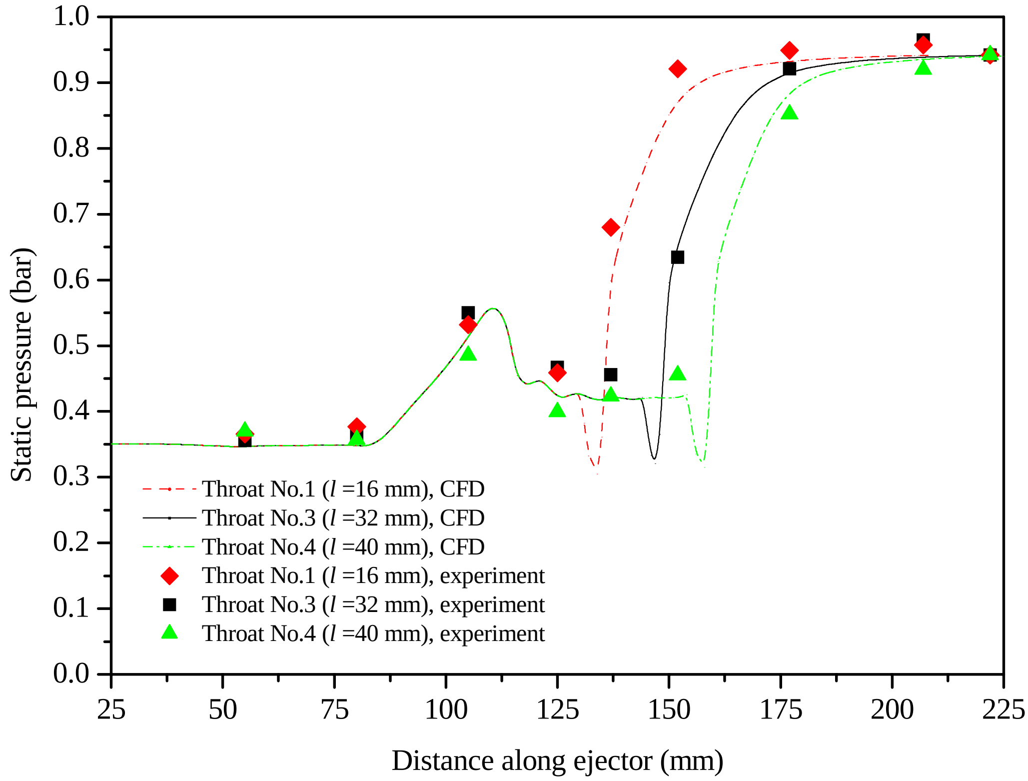

Figure 5.6 Static pressure profile along the ejector at $T_P = 100^oC$, $T_S = 5^oC$, and $P_C = 0.94$ bar, effect of the throat length.

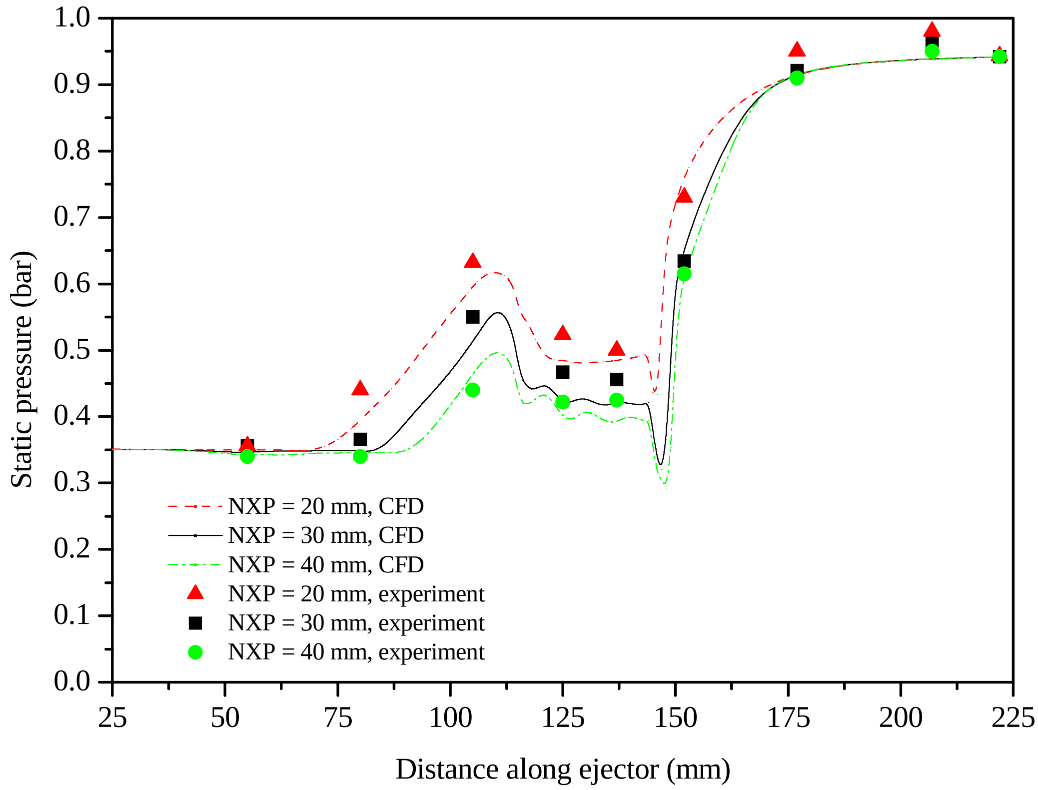

Figure 5.7 Validation of Static pressure profile along the ejector at $T_P = 100^oC$, $T_S = 5^oC$, and $P_C = 0.94$ bar, effect of the nozzle exit position (NXP).

5.3 Validation of the Entrainment Ratio and Critical Back Pressure

Regarding the calculated entrainment ratio, it was found to have good agreement with the results obtained from the experiments. Figure 5.8 and Table B.1 in Appendix B shows the similarity in the ejector performance characteristic between the calculated and the actual values, when the upstream and downstream operating conditions of the R141b ejector were varied. It is obvious that the predicted entrainment ratios are offset slightly lower than those of the experimental values. This error may come from the fact that the predicted values of the primary mass flow rates were found at higher rates compared to the actual values as discussed previously in section 5.1. Figures 5.9 to 5.12 also show the similarities in the ejector performance characteristic, when the ejector's operating geometries were varied, from the two different approaches, the experiment and the CFD method.

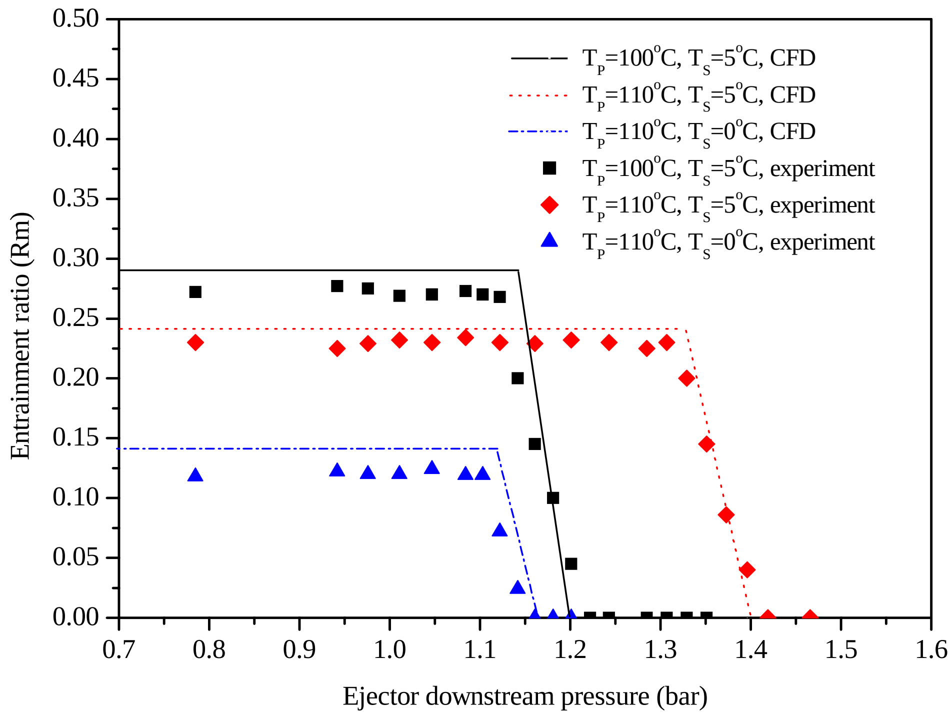

Figure 5.8 Validation of entrainment ratio, effect of operating conditions.

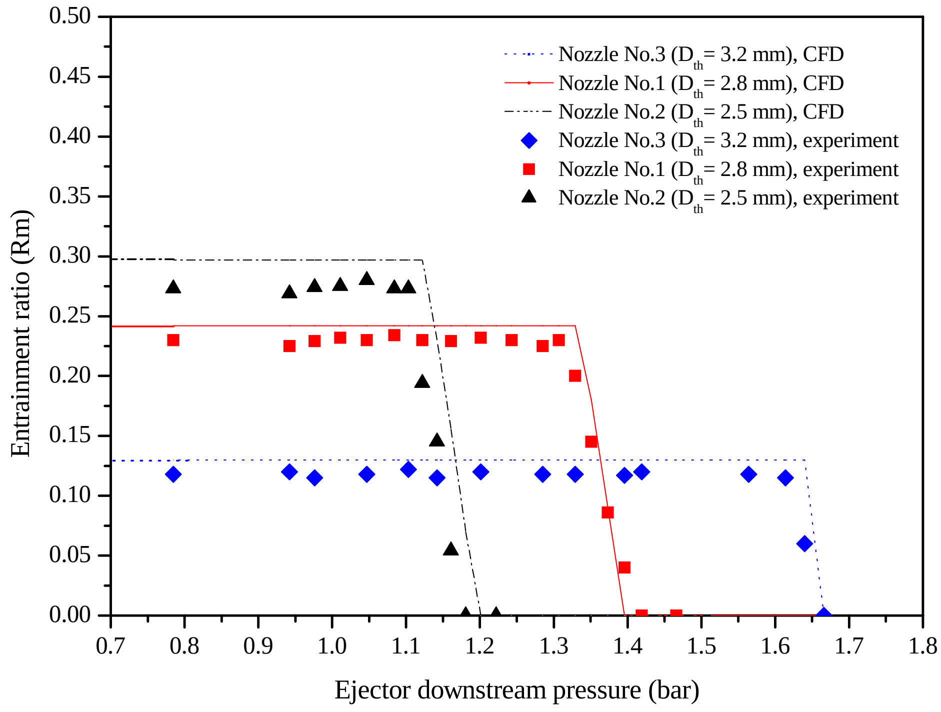

Figure 5.9 Validation of entrainment ratio, effect of primary nozzle throat diameter.

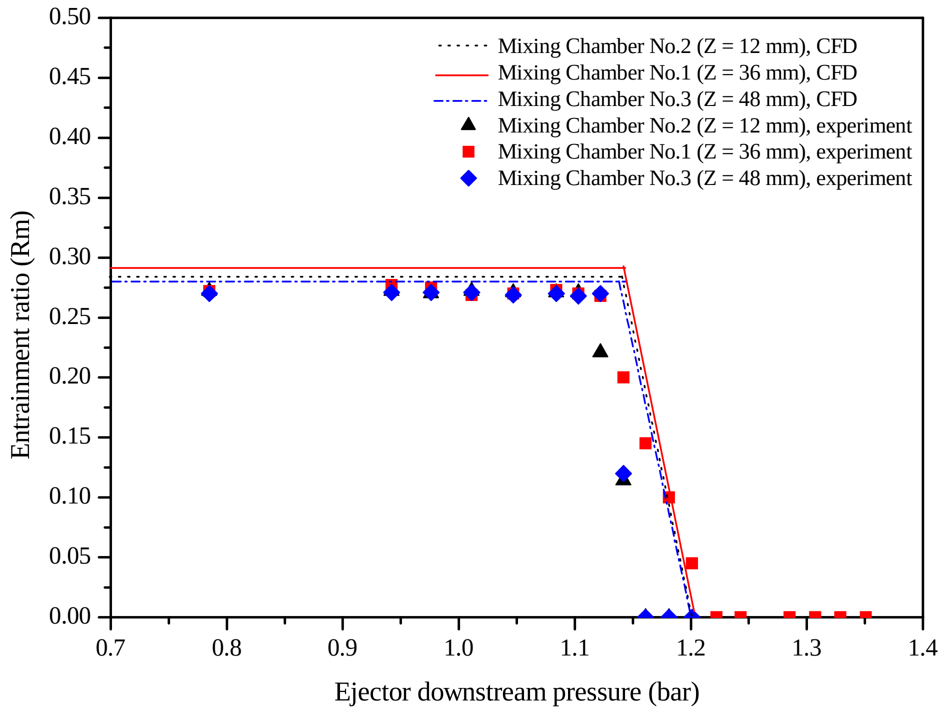

Figure 5.10 Validation of entrainment ratio, effect of mixing chamber inlet diameter.

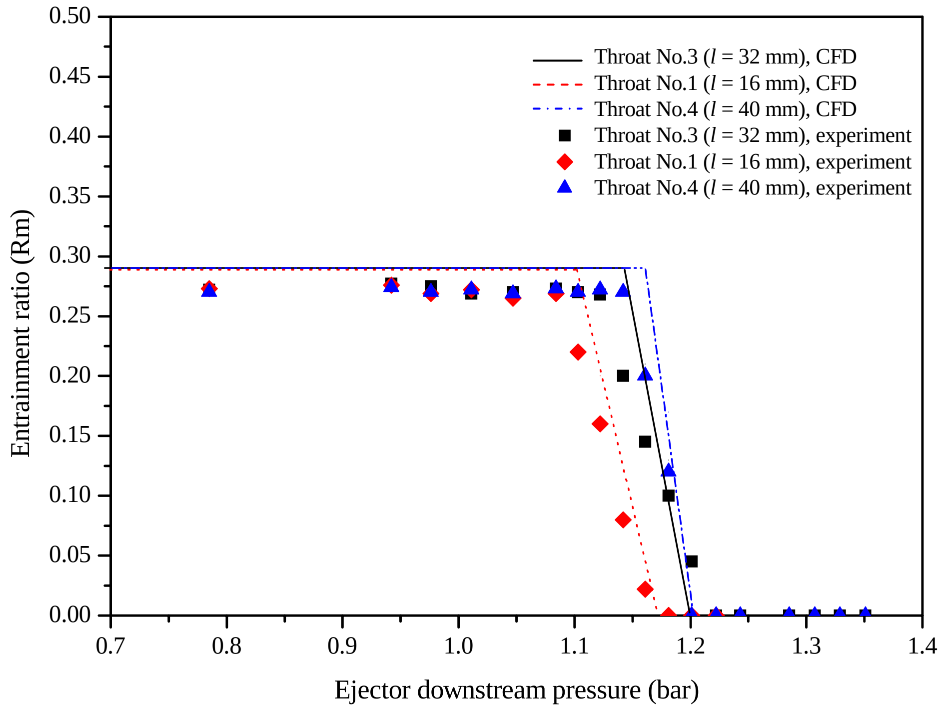

Figure 5.11 Validation of entrainment ratio, effect of throat length.

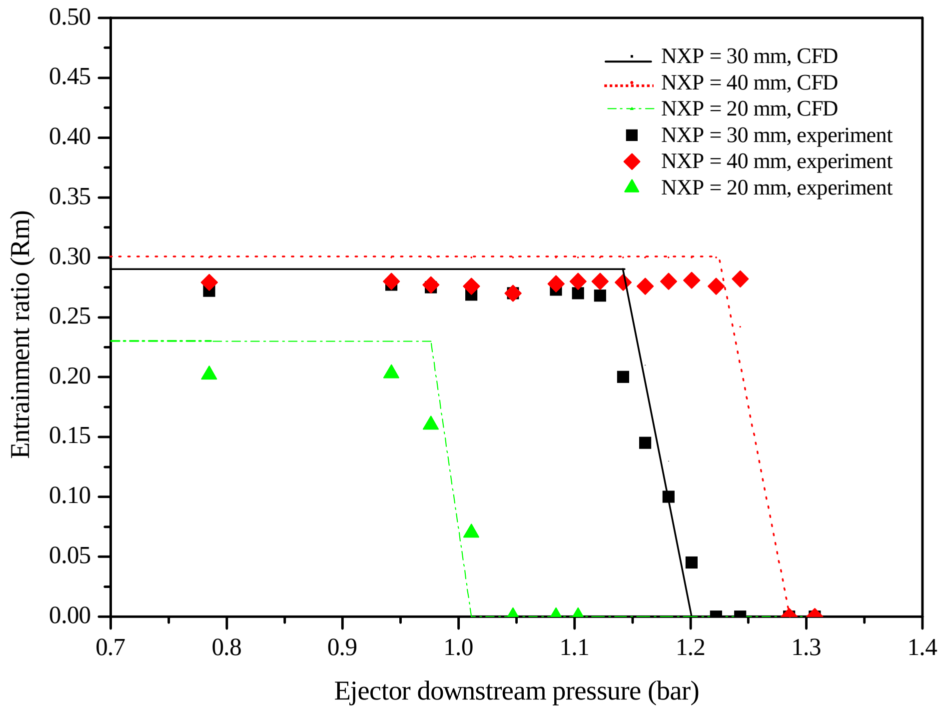

Figure 5.12 Validation of entrainment ratio, effect of nozzle exit position.

The comparison between the CFD analysis and the experimental results of the ejector's performance at the critical point and critical back pressure of the experiment R141b ejector are also illustrated in Table B.2. Figure 5.13 shows the comparison between the CFD and the experimental results of the entrainment ratio in the choked and the unchoked flow region. At the unchoked flow region, Figure 5.13 b), the distribution of the error in predicted values of the entrainment ratio to the experimental ones is wider than the ones at the choked flow region, Figure 5.13 a). Possible reasons for this error may come from, firstly, the difficulty of calibrating the absolute pressure transducer. In the unchoked flow region, the entrainment ratio is subjected to change sensitively to the change of downstream pressure. A slight change in the downstream pressure causes more effect to the entrainment ratio than was found in the choke flow region. Hence, a small error in calibrating the absolute pressure transducer may result in an error in reading the entrainment ratio. Secondly, a very complicated flow at the unchoked flow region, due to shocking behavior, probably gives unexpected results in the experiment.

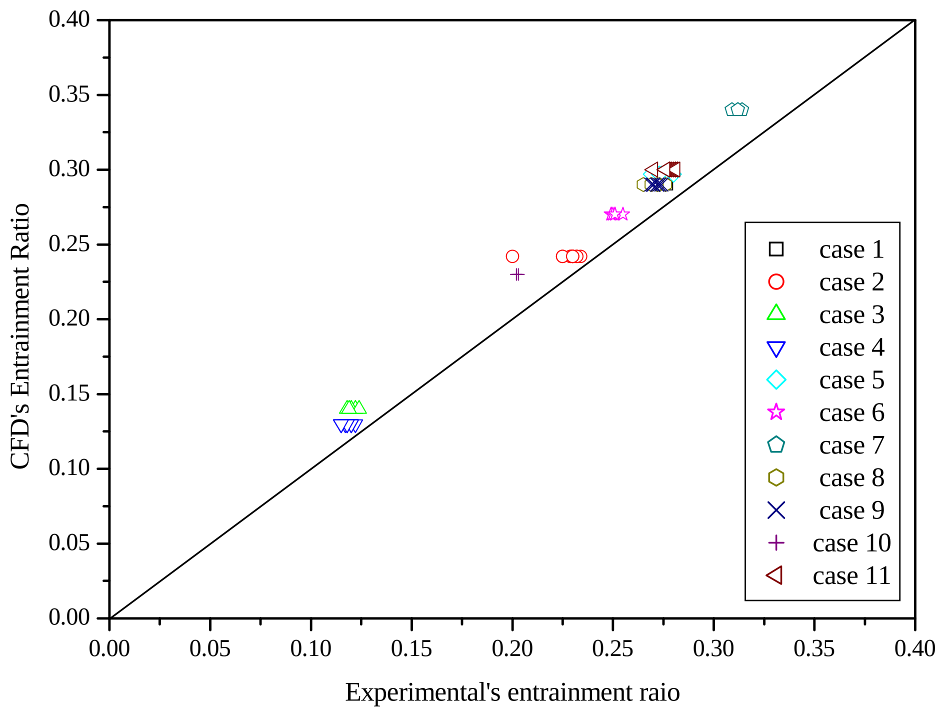

a) Choked flow region

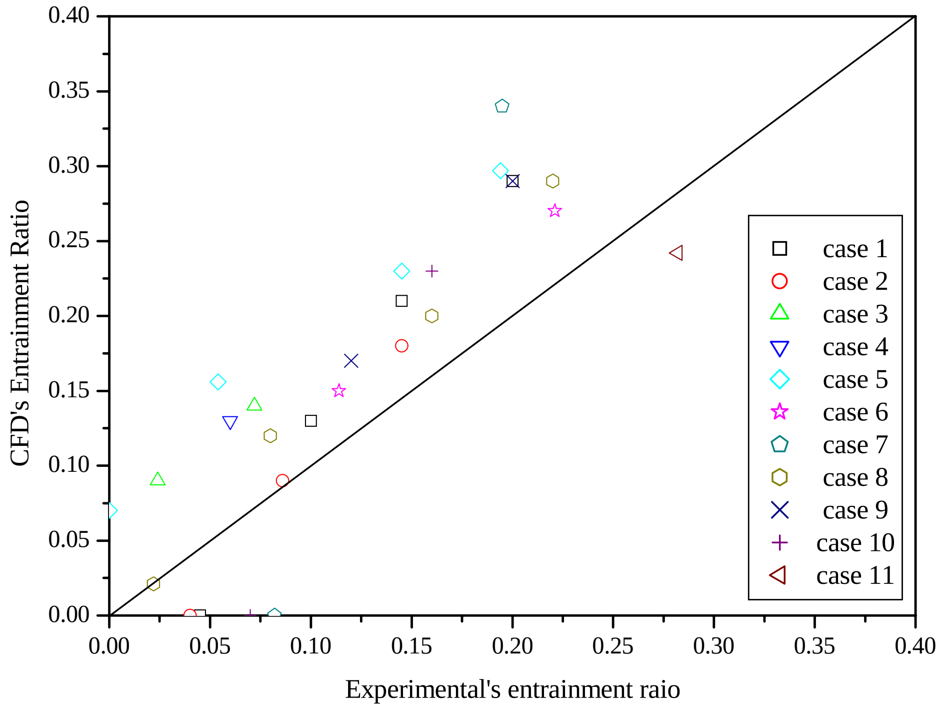

b) Unchoked flow region

Figure 5.13 Comparison between the CFD and the experimental results of the entrainment ratio in the choked flow and the unchoked flow region for various operating conditions and geometries (case 1 to case 11 correspond to the experimental cases in Table B.1).

Comparison between the CFD and the experimental results of the critical back pressure (the highest possible condenser pressure) is shown in Figure 5.14. It is obvious that the overall CFD calculated results agree well with actual values.

Overall, it may be concluded that, the comparison demonstrates the proficiency of the CFD model in predicting an accurate performance for both entrainment ratio and critical back pressure of a typical designed ejector. Average errors of the predicted entrainment ratio and the critical back pressure were both found to be less than 9% and 2%, respectively.

.

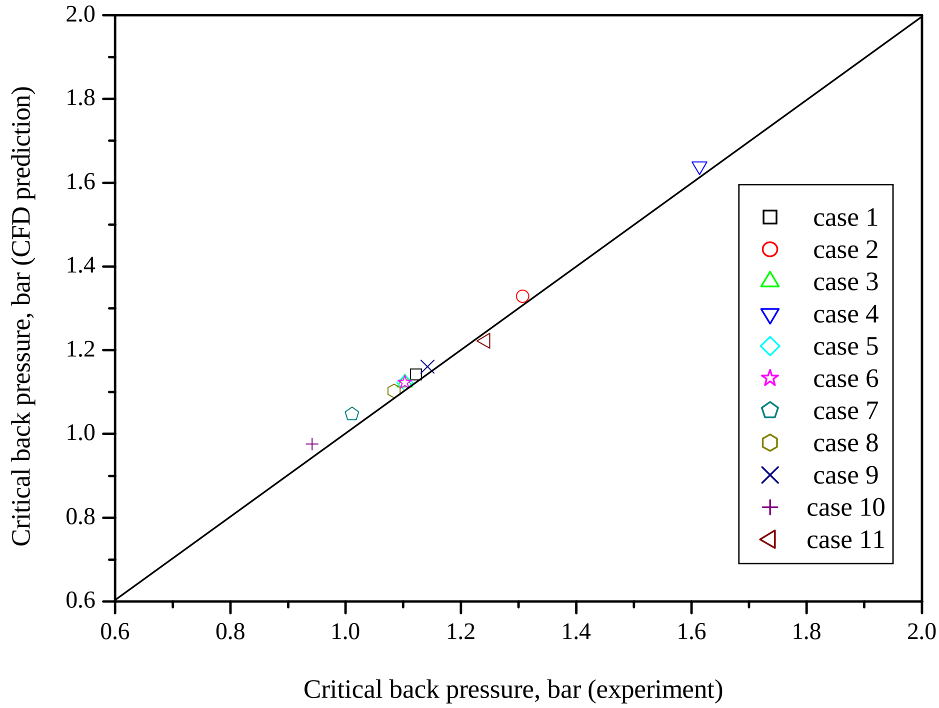

Figure 5.14 Comparison between the CFD and the experimental results of the critical back pressure for various operating conditions and geometries (case 1 to case 11 correspond to the experimental cases in Table B.1).

5.4 Conclusions

This chapter demonstrates the validation of the CFD results and the experimental data obtained from the constructed experimental R141b ejector refrigerator. Three types of the following information were used to validate the simulated model:

- The primary fluid's mass flow rate
- The static pressure distribution at the wall of the ejector
- The entrainment ratio including its critical back pressure

It was verified that the CFD method is an efficient tool to predict the entrainment ratio and critical back pressure of the ejector. The tabulated ejector performances from the experiment and the calculations show the accuracy of the model. Even though no correction factors were added as was done in one-dimensional theories, it was found that the CFD method provides reliable results compared to the actual values from the experiment. Unlike one-dimensional theories, a constant mass flow which is a typical characteristic of an ejector was shown. Even though the errors of calculations were found to be quite large at some points, they could be clarified.

It can be said that the CFD study in this research was just one of the very first studies in the field of the ejector in refrigeration application. In order to utilize this method more efficiently, further studies are needed. From the study, it was shown that the constructed CFD model may not represent the experiment ejector perfectly; therefore, some improvements on the model setup and the calculation domain are needed. For instance, the real gas equations should be applied as the properties of the working fluid rather than using the perfect gas assumption. Moreover, the heat transfer function at the wall surfaces, that allows not only the investigation of heat transfer, but also of condensation during the process, should be turned on so that the model could be more realistic.

After the achievement in validating the simulated results with the experimental values as presented in this chapter, the flow and mixing process within the R141b ejector is explained utilizing other useful information available from the simulated solutions.

CHAPTER VI

FLOW CHARACTERISTICS AND MIXING PROCESS

The successful validation as was done in the previous chapter and in the past studies [26, 39, and 40] have brought to the conclusion that the CFD model can efficiently predict the performance of ejectors and provide valuable information that can represent the flow inside the ejectors. In this chapter, a basic knowledge of the flow and the mixing process of an ejector used in a jet refrigerator is provided. The details concentrate on the use of CFD in visualizing the flow phenomena inside the R141b ejector. The differences in the flow structure of the R141b ejector and the steam ejector based on the data obtained from Sriveerakul et al. [39 and 40] are discussed.

As described in the previous chapters, the study of the R141b ejector was conducted by two parallel methods which were 1) the experimental investigation and 2) the simulation of the flow within the ejector using a CFD software package. Regarding the experimental measurement, the wall static pressure curves obtained form the experiment were used to validate the results obtained from the simulation. It was fascinated that both results were agree well. However, the nature of the flow and the mixing process in an ejector are complicated, using the information of the wall pressure distribution only can not explain them clearly. Therefore, other information obtained from the simulation; for example, the Mach contour plot and the static pressure distribution along the axis of the ejector, which is a better representative of the flow, could be fairly used to explain the flow and the mixing process in the ejector. Please note that the knowledge provided in this chapter will later be applied and compared to the changes in the flow structure and the mixing process inside the R141b ejector (Chapter VII) as affected to the ejector's performance when its operating conditions and its geometry were varied.

6.1 Flow and Mixing Process of the R141b Ejector under its Choked Flow Condition

Figure 6.1 illustrates the contour lines of Mach number and static pressure distribution of the R141b ejector when it operates in the choked flow mode (the primary fluid saturated temperature (T_P) of 100°C, the secondary fluid saturated temperature (T_S) of 5°C and the back pressure (P_C) of 0.94 bar). Detailed explanation of the simulated flow structure is provided as follows.

As the high-temperature and high-pressure primary fluid exiting from the vapour-generator enters the convergent section of the primary nozzle, the subsonic motive flow accelerates to sonic value and chokes at the nozzle throat (1). In the divergent portion of the nozzle, the primary fluid accelerates and expands further to achieve a supersonic speed. At the nozzle exit plane (2), it is found that the supersonic stream could leave the nozzle with its static pressure lower or higher than the surrounding pressure in the mixing chamber (P_S = 0.35 bar). To preserve the static pressure across the free boundary between the primary jet core (3) and the surrounded fluid, the first series of oblique shock and expansion waves, called the *"diamond wave"* pattern (4), is induced. This phenomenon can be investigated from the fluctuation of static pressure at the center line of the ejector while the flow passes through a mixing chamber (Figure 6.1). In the theory of supersonic flow through a convergent-divergent nozzle as was used as the primary nozzle of the ejector, the change in the flow state at the nozzle's exit is subjected to change with the change of the exit pressure ratio [52]. This exit pressure ratio is the ratio between the pressure which exists immediately upstream of the shock wave standing at the exit of the nozzle and the pressure downstream of the shock.

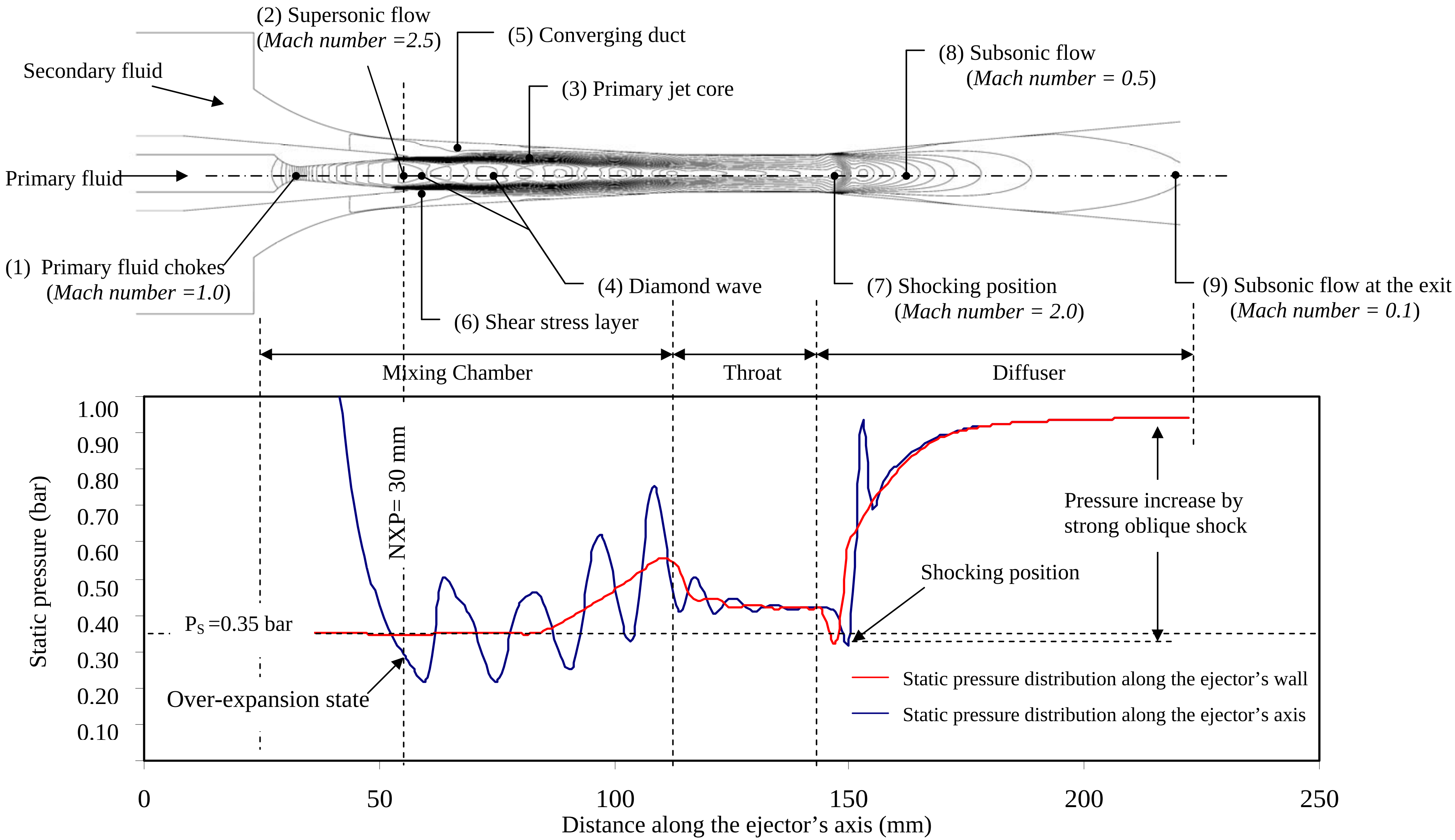

Figure 6.1 Filled contours of Mach number and static pressure distribution of the R141b ejector.

For the flow in an ejector, the pressure downstream of the shock is referred as the surrounding pressure (this pressure is assumed to be equal to the secondary fluid saturated pressure). The state of the flow immediately after leaving the primary nozzle can be called the "*primary flow state*".

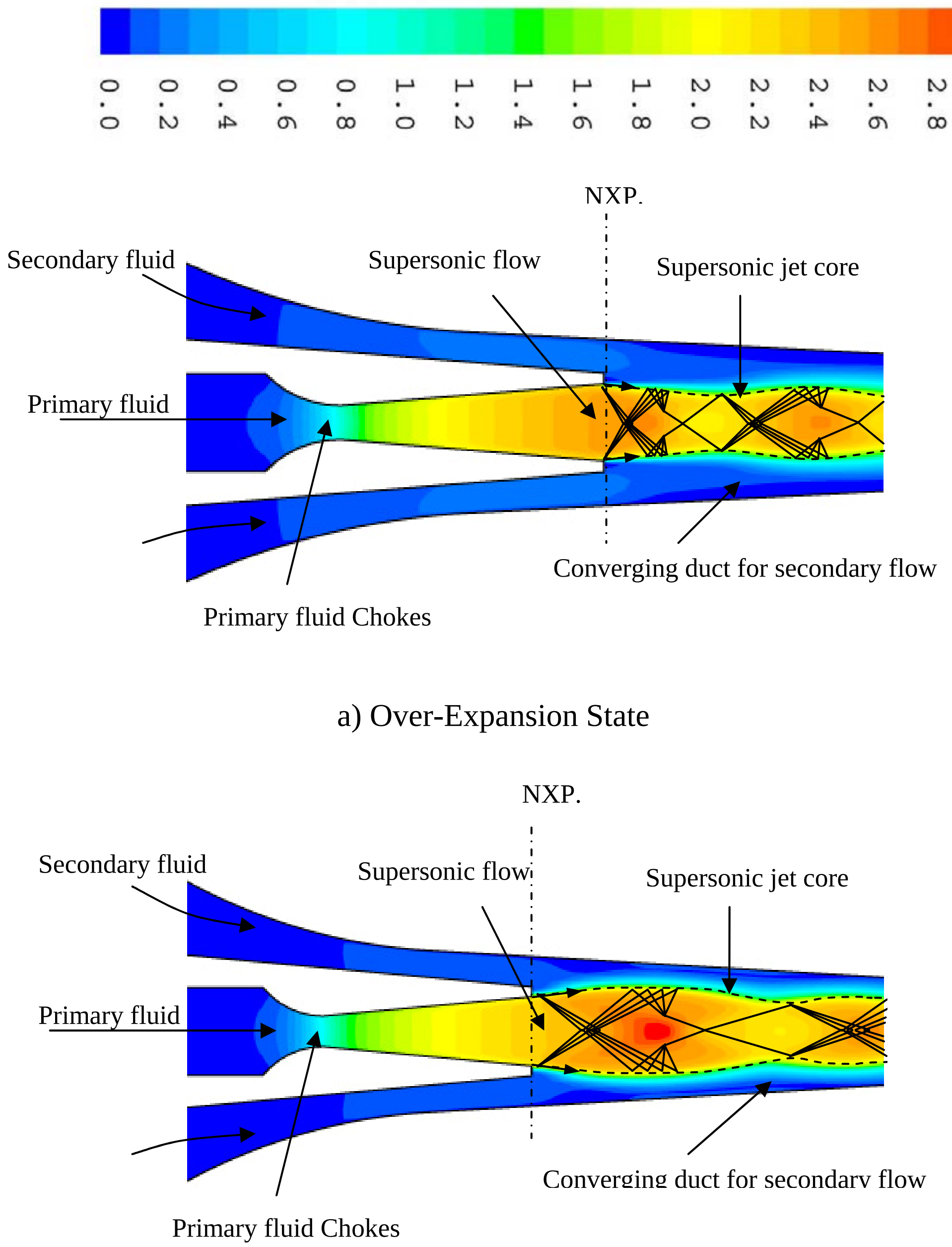

a) Over-Expansion State

b) Under-Expansion State

Figure 6.2 Primary flow states of the flow in the ejector colored by contours of Mach number.

The primary flow state can be classified into two states which are the "*Over-expansion state*" and the "*Under-expansion state*". In the case of the supersonic stream leaving the nozzle with its static pressure already expanded below the surrounding pressure, the primary fluid immediately leaves the primary nozzle as an "over-expansion state" with the expansion wave angle converged into the axis line of the ejector and accelerates as an over-expanded wave as shown in Figure 6.2a. If the primary fluid stream leaves the nozzle with its static pressure greater than the surrounding pressure, the flow is said to be in an "under-expansion state". In this case, the flow is capable of additional expansion after leaving the nozzle. The diamond wave pattern at the nozzle exit is at a diverged angle to the centerline of the ejector as shown in Figure 6.2b. The difference in the states of the primary flow could affect the flow field of the ejector and, hence, alter the ejector's performance which will be discussed in the next chapter.

The occurrence of a diamond wave jet core in the mixing chamber indicates the semi-separation between the high speed primary flow and the surrounded secondary fluid. Thus, the converging duct (5) for entraining a secondary fluid into the mixing chamber, similar to that proposed by Munday and Bagster [30], is formed. Moreover, according to the large velocity difference between these two streams, the shear stress layer (6) interfacing between them is presented. The shear mixing of two streams begins as the secondary fluid from the evaporator is entrained and interfaces with the expanded wave. Flowing through the converging duct, the shear mixing process causes the secondary fluid to accelerate, conversely, the shear mixing and the viscosity of the fluid cause the diamond wave to decay. As investigated in Figure 6.1, the static pressure of the flow steadily decreases at the beginning of the flow process and the violence of the diamond wave reduces, respectively.

At the throat of the mixing chamber, most of the entrained secondary fluid accelerates and reaches the sonic velocity. Very small amounts move slightly faster than the sonic value when it flows close to the shear stress layer attached to the primary jet core, but slower when it flows close to the wall boundary layer (mixing chamber's wall). Moreover, it is seen that the violence of the diamond wave reduces as the primary jet core travels with lower supersonic speed, consequently, a relatively smooth jet core results. Therefore, the secondary flow can be considered as choked. The choke area or "*effective area*" [42] of the secondary fluid can be estimated from the annulus area between the wall of an ejector throat and the primary fluid jet core. Despite using the CFD visualization, it is difficult to locate the exact position of the effective area within the ejector. During the choke flow mode, the entrainment ratios remained constant, the effective area, hence, can be estimated at anywhere within the constant area ejector's throat.

At a certain distance into the ejector throat or in the beginning of the diffuser section, called the *"shocking position"* (7), a non-uniform mixed stream produces the second series of oblique shock waves (8). Therefore, when the flow is dominated by a series of oblique shocks, the static pressure gradually recovers to discharge value and the flow speed gradually decreases to subsonic level, while it passes through the diffuser. In addition, across this process, the mixed stream loses most of its total pressure. However, in concept, a series of oblique shock should provide smaller pressure loss in total pressure than a single normal shock.

6.2 Comparison of the Flow Structures: the R141b Ejector and a Steam Ejector

This section provides an explanation of significant differences between the flow structures of the current R141b ejector and the steam ejector based on the work done by Sriveerakul et al. [39 and 40]. Figure 6.3 illustrates the flow structure of a steam ejector that was evaluated at vapour-generator temperature of 120^{o}C, evaporator temperature of 10^{o}C and condenser pressure of 30 mBar.

At some conditions, the flows at the exit plane of the primary nozzle of both the ejectors were found to be distinct. For the steam ejector, it normally experienced the state of under-expansion flow, since there were large pressure differences between the primary fluid and secondary fluid inlets. Consequently, the nozzle exit pressure (the pressure upstream of the shock) is usually higher than the back pressure. The flow is also capable of additional expansion after leaving the nozzle. Whereas the R141b ejector usually experienced less difference between the primary fluid and secondary fluid inlets pressures compared to the steam ejector. The state of the flow at the exit of the nozzle, hence, can be found both over-expanded and under-expanded.

Due to the high molecular weight of the HCFC refrigerants, where their momentums are large compared to that of steam, the second series of oblique shock in the recovery process is strong and likely to be a normal shock (Figure 6.1). Whereas in the steam ejector (Figure 6.3), the weak shock called oblique shock is presented. The pressure recovery zones of both ejectors were different. The shock that occurred in the R141b ejector is a combination of a bifurcated shock and a series of shocks downstream of the bifurcated shock. As indicated in Figure 6.1, there was only a small number of the repeated strong shock downstream of the bifurcated shock before all the shock disappeared. Unlike the R141b ejector, the shock found in the steam ejector was usually an oblique shock that formed a bifurcated shock with significant amount of repeated shock.

This implies that for the R141b ejector, the diffuser plays a less important role in recovering the ejector's total pressure than that in the steam ejector. The diffuser of the R141b ejector can then be designed into a short length diffuser necessary to cover the pressure recovery zone.

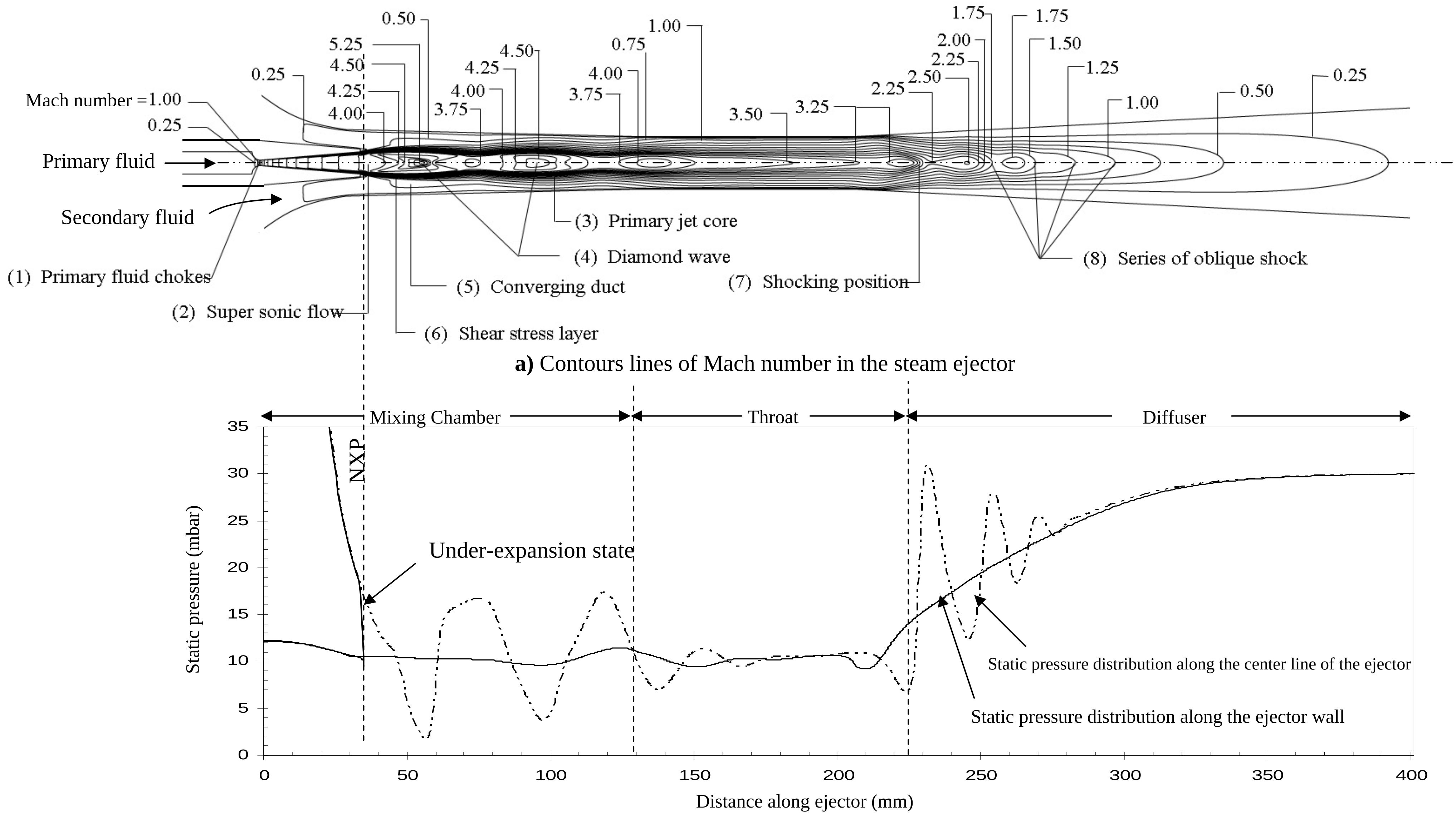

a) Contours lines of Mach number in the steam ejector

b) Static pressure distribution of the steam ejector

Figure 6.3 Mach number and static pressure distribution in the steam ejector based on the work of Sriveerakul et al. [39 and 40].

This implies that for the R141b ejector, the diffuser plays a less important role in recovering the ejector's total pressure than that in the steam ejector. The diffuser of the R141b ejector can then be designed into a short length diffuser necessary to cover the pressure recovery zone.

The series of oblique shocks, verified in the models, is definitely in contrast to the single normal shock which was proposed by Keenan's theory [24 and 27]. Actually, the effect of oblique shocks in an ejector has been investigated experimentally by few researchers [31, 42, 44 and 47]. Unfortunately, without the flow visualization, the collected data was discussed as a normal shock. Moreover, its pressure sudden rising behavior of a normal shock was thought to weaken by the viscous flow or it was even thought to be swallowed by the oversized diffuser of an ejector.

6.3 Conclusions

In this chapter, the theory describing the flow and mixing process in the R141b ejector using the CFD's visualization was proposed. It is summarized that the nature of flow structure of the R141b ejector used in refrigeration purposes is complicated. The primary nozzle was found to be always operated with chokes. At the nozzle exit, the primary fluid leaves the nozzle as the supersonic *"diamond wave"* jet core, with different flow states either the over-expansion or under-expansion states. The difference in the flow states is caused by the nozzle's exit pressure ratio which is mainly dependent on the upstream conditions of the ejector. According to the large velocity difference, the secondary fluid is entrained, accelerated and mixed with the primary jet core by the shear stress layer interfaces between two streams. Therefore, it is thought that the shear mixing of two streams starts as the secondary fluid is entrained into the mixing chamber.

With help of the CFD, the flow phenomena in the R141b ejector are summarized as follows.

- The CFD visualization shows that the effective area as proposed by Huang [42] does exist; however, it is difficult to locate the exact position of the effective area within the ejector. In the choke flow mode, the entrainment ratios remained constant, the effective area, hence, can be estimated at anywhere within the constant area ejector's throat.
- Two series of oblique shocks were found in the simulation. The first series was found immediately after the primary fluid stream leaves the primary nozzle and begins to mix with the secondary fluid stream. The second series of oblique shock was found at the beginning of the diffuser section as a result of a non-uniform mixed stream. A major compression effect is caused by this second series of oblique shock. This latter shock is definitely contrary to a single normal shock which was proposed by Keenan's theory [24 and 27]. This is probably because this study utilized relatively lower pressure of the primary fluid (vapour-generator saturated temperature of 120-140^{o}C), while others used larger industrial vapour-generator to produce the higher pressure primary fluid (vapour-generator saturated temperature of 160-220^{o}C).

The differences in the flow structures between the R141b ejector and the steam ejector were investigated and reported according to the differences found in:

- the flow states after the primary fluid leaves the primary nozzle
- the shock phenomena occurs before the pressure recovery region
- the pressure recovery process

In the next chapter, there will be the study of the interested parameters, which are thought to affect the performance of the ejector. The performance characteristics and the contours of Mach number of the experiment ejectors will be evaluated. The proposed flow and mixing theory in this chapter will be applied to explain the flow structures of the ejector which cause the changes of its performance characteristic.

CHAPTER VII

PERFORMANCE OF THE EJECTOR:

EFFECTS OF OPERATING CONDITIONS

This chapter provides the investigation's results of the influences of operating conditions on the performance characteristics of the R141b ejector. From Chapter V, the validations of the CFD results of the R141b ejector model with the actual values obtained from the experiment were satisfied. This chapter, therefore, will only present the CFD investigation's results of the influences of interested parameters on the performance characteristic of the ejector. The performances of the experimental R141b ejector were evaluated in terms of the mass entrainment ratio (Rm) and the critical back pressure (P_C). The other flow information such as, the change in the static pressure distribution along the axis of the ejector and the change in contours of mach number, regarding the change of the operating conditions and the variation in the ejector's geometry, were used to explain how the performance of the ejector was altered.

The parameters of the ejector's operating conditions including the variation of the upstream and the downstream operating conditions are listed below.

- Vapour-generator saturation temperature (the primary fluid)
- Evaporator saturation temperature (the secondary fluid)
- Condenser saturation pressure (the back pressure)

In addition, it is expected that using the simulated Computational Fluid Dynamics (CFD) ejector models, the detail analyses of the results leads to a better understanding and the flow and mixing behavior which cause the change in ejector performance can be described clearly.

The investigations of the effects of operating pressures were carried out over a variety of upstream and downstream operating conditions. During the simulation, vapour-generator saturation temperature or the “upstream of the primary fluid” was ranged from 90 to 120^{o}C. The evaporator saturation temperature was considered as the “upstream of the secondary fluid”, and it was varied in the range of 0 to 10^{o}C. Lastly, the condenser saturation temperature, the “downstream of the ejector”, was varied from 25 to 45^{o}C. To avoid any unwanted influences from other parameters, the studies were done with a fixed geometry model as shown in Figure 4.2. The modeled ejector was constructed from primary nozzle no.1, mixing chamber no.1, throat section no.3 and the subsonic diffuser The primary nozzle exit plane was fixed at NXP = 30 mm.

7.1 Effect of Downstream Conditions (the condenser saturation pressure)

Figure 7.1 represents the calculated entrainment ratio when upstream and downstream conditions of the ejector were varied. Similar to the performance characteristics curve of typical steam ejector as shown in Chapter I, Figure 2.5, at each setting of vapour-generator and evaporator condition, the operation of the R141b ejector can be categorized into 3 regions, the choked flow, the un-choked flow and the reversed flow of secondary fluid. The ejector entrains the same amount of secondary fluid when it operates under critical condenser pressure. If the ejector operates beyond the critical point, the entrainment rate drops with an increasing of downstream pressure. If the condenser saturation pressure is further increased to the point called breakdown pressure, the secondary fluid cannot be induced into the ejector.

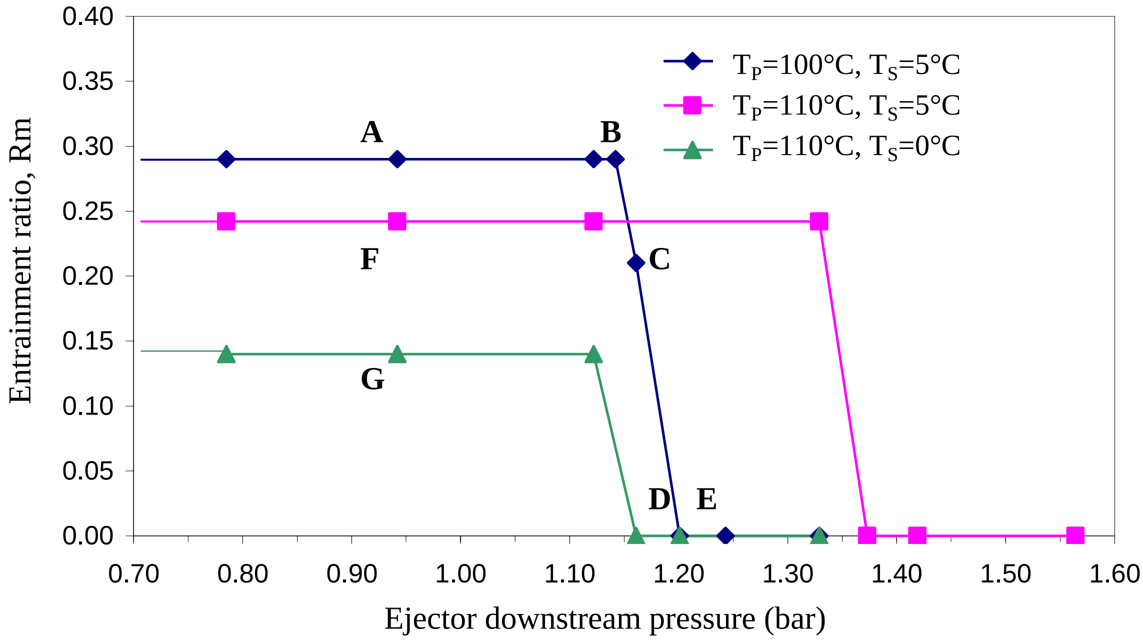

Figure 7.1 Performance characteristics of an R141b ejector, effect of operating conditions.

Considering filled contours of Mach number and path lines display simultaneously with static pressure profiles along the centerline of the R141b ejector, as shown in Figure 7.2a and 7.2b, it was found that, increasing downstream pressure from point **A** to **E** caused the shocking position to move upstream into the ejector throat. However, when back pressure does not exceed the critical point or within the choked flow region (**A** and **B**), the shock will not affect the mixing behavior of the two streams. Flow structures in front of a shocking position are shown unchanged and the size of the primary jet core remained constant and independent from downstream conditions. It was thought, that during this choke flow region, the effective areas were always forced to appear within the constant area throat section, since, the entrainment ratio remained constant. This proved the existence of the choking phenomenon.

When a downstream pressure increased higher than the critical point (**C**, **D** and **E**), the second series of oblique shocks, as given the description in Chapter VI, was forced to move further upstream and combine with the first series of oblique shocks to form a single

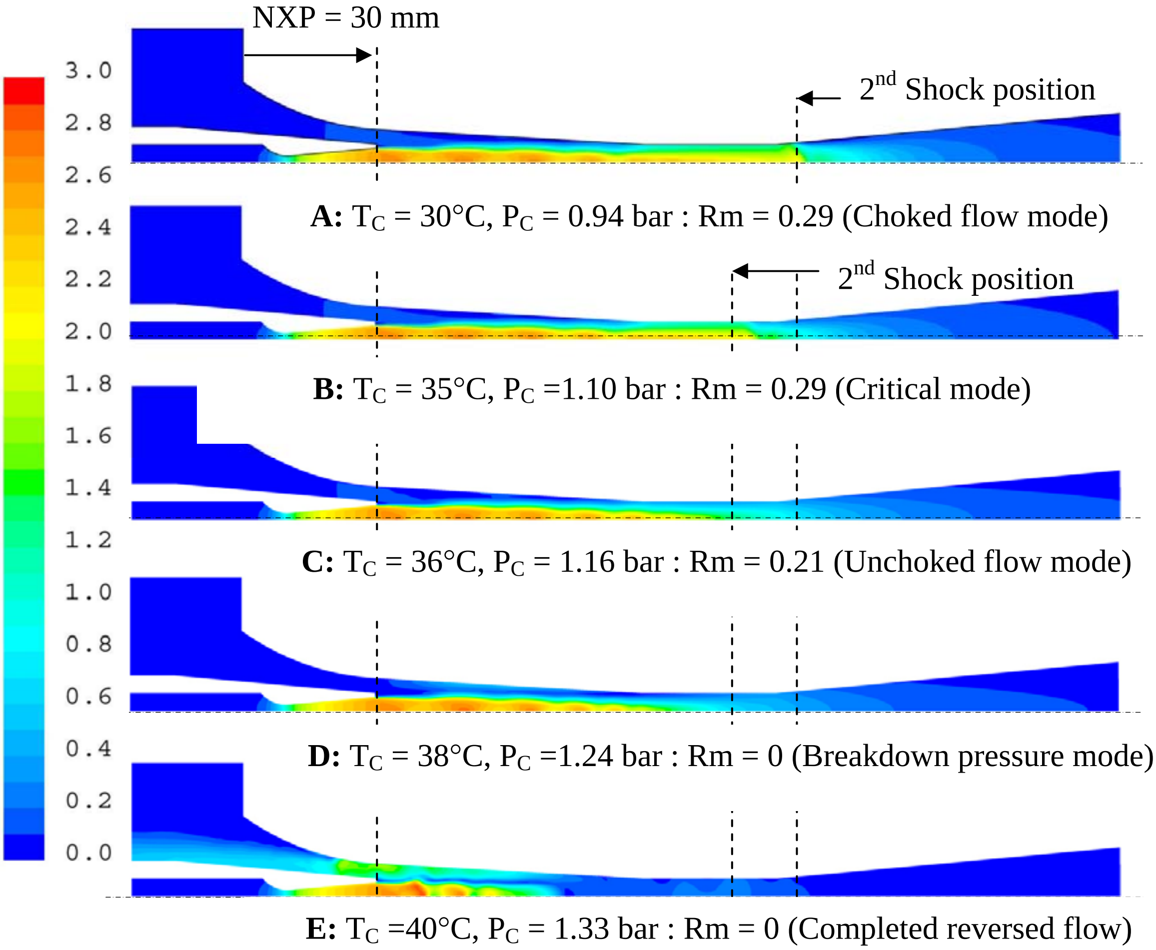

(a) Filled contours of Mach number (Axisymretic view)

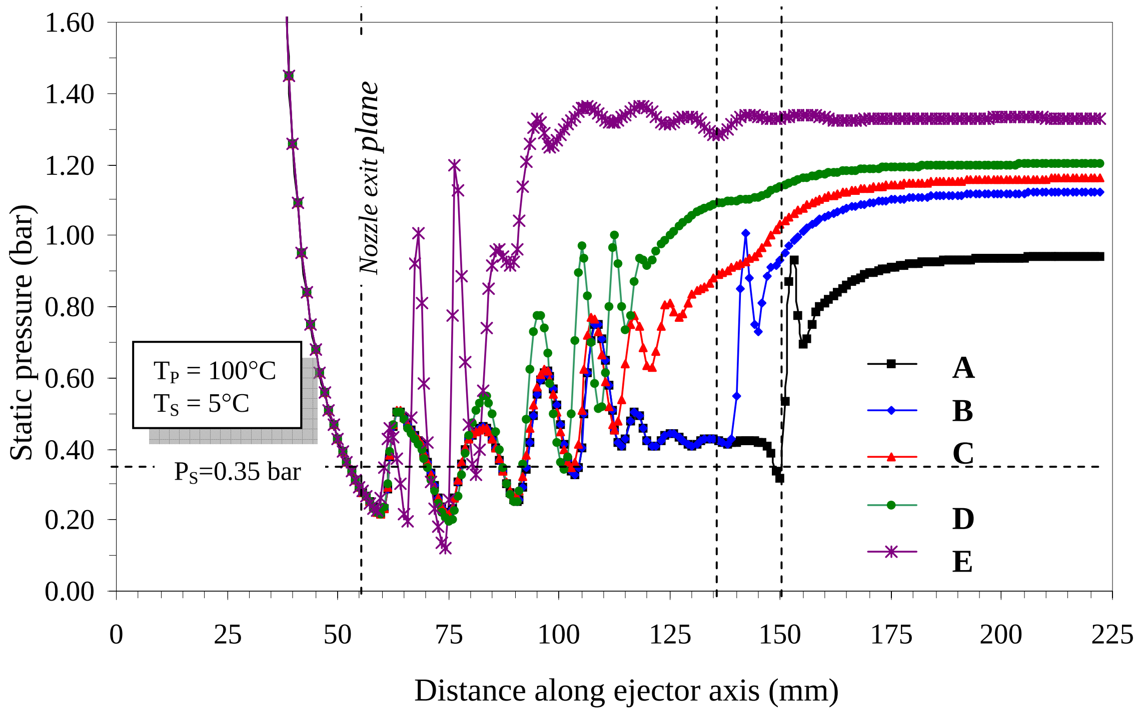

(b) Static pressure distribution along the centerline of the ejector

Figure 7.2 Effect of downstream operating conditions on the flow in the R141b ejector (All operating points, **A**, **B**, **C**, **D** and **E**, correspond to those shown in Figure 7.1).

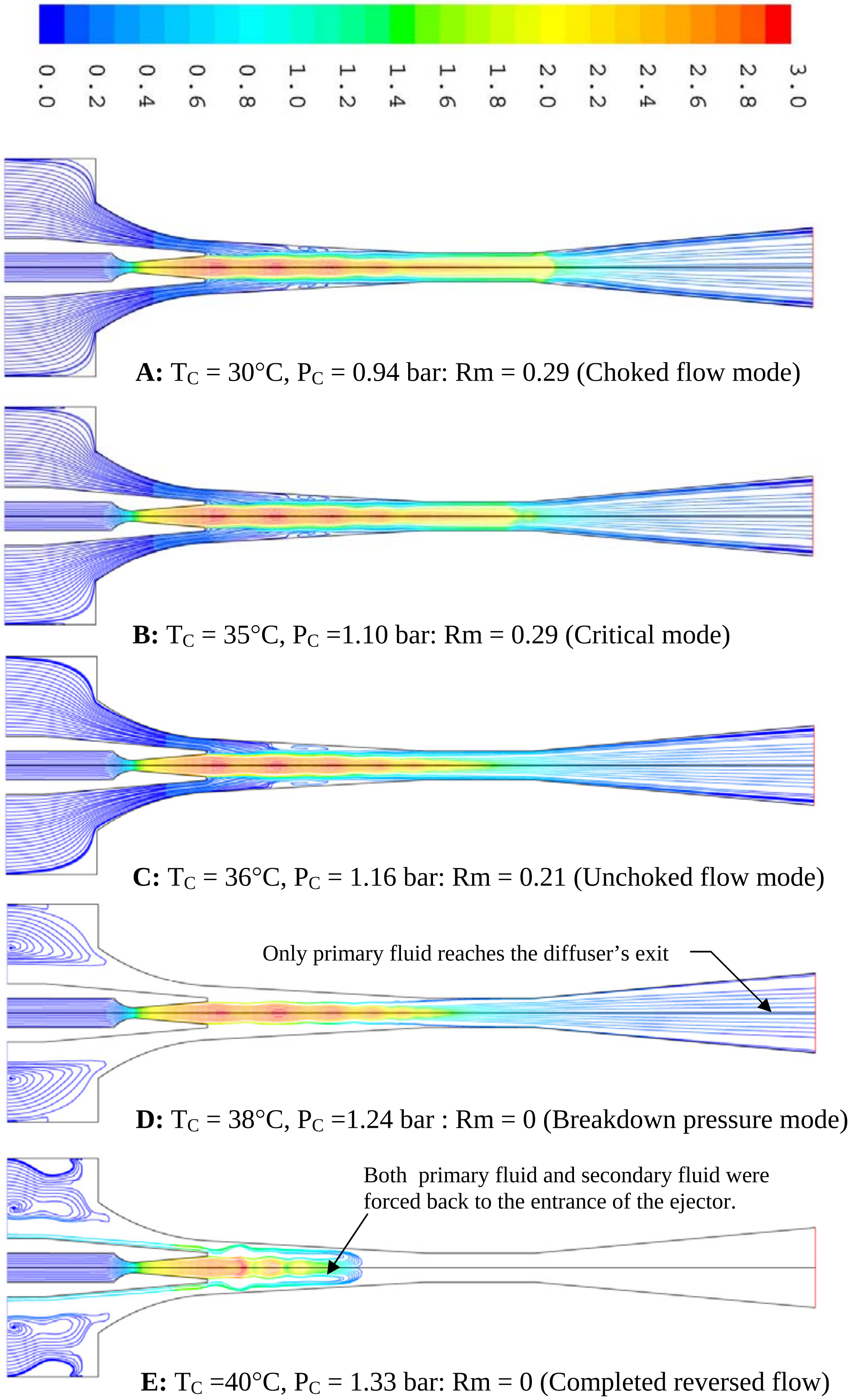

Figure 7.3 Path lines colored by Mach number of the flow in R141b ejector (corresponding to Figure 7.2).

series of oblique shocks. This movement of the second series of oblique shocks caused the secondary fluid to be no longer choked in the constant throat section, and hence, disturbed the entrainment process. The variation in the entrainment ratio under the unchoked flow region resulted from the variation in position of the effective area happening in the convergent mixing chamber. This can be investigated from the lowering of an entrained fluid speed and hence, the increasing of static pressure before shock. It should be noted that the size and the momentum of the jet core was independent from the variation of the downstream pressure.

Figure 7.3 illustrates path line displays colored by Mach number in which the flow directions of both the primary fluid and secondary fluid can be visualized (corresponding to the contours of Mach number in Figure 7.2). It was shown that, when back pressure does not exceed the critical point (**A** and **B**), the flow direction upstream of the shock position is the same. At the unchoked flow mode (**C**), the flow direction upstream of the shocking position was disturbed, hence, caused difficulties in entraining the secondary fluid. If the back pressure was increased to reach the breakdown pressure at point **D**, only the primary fluid was allowed to flow to the diffuser's end of the ejector. Thus, the entrainment ratio is zero at point **D**. At point **E**, where the back pressure exceeds the breakdown pressure, the flow direction shows that both the primary fluid and secondary fluid were forced to reverse to the entrance of the ejector.

7.2 Effect of the Primary Fluid's Upstream Conditions (the vapour-generator saturation pressure)

Figure 7.4 (**A** and **F**) shows that increasing the primary fluid pressure, the Mach number of motive fluid leaving a primary nozzle remains unchanged. This obeys the principle of supersonic compressible flow; the supersonic flow leaves the different converging-diverging nozzles at the same speed when those nozzles are modeled with the identical area ratios. However, the mass flow through the primary nozzle and the momentum of the flow were increased. The increasing of momentum allowed the primary fluid to leave and further under-expand and accelerate with a larger expansion angle. This causes the diamond flow to shock at a higher Mach number at the first oblique shock. The increased expansion angle causes the enlarging of a jet core, therefore, the annulus effective area is reduced and less secondary fluid can be entrained and accelerated through the steeper converging duct. Thus the lower entrainment ratio was obtained as can be seen from the performance curves at point **A** and **F** in Figure 7.1. However, with higher momentum of the jet core, the shocking position moves downstream, and the ejector can be operated at a higher discharged pressure.

7.3 Effect of the Secondary Fluid's Upstream Conditions (the evaporator saturation pressure)

When secondary fluid pressure is increased, it can be seen from the Mach number contours, Figure 7.4 (**F** and **G**), that the expansion angle of the under-expanded wave was influenced by an increasing of the secondary fluid pressure. The pressurized condition causes the decreasing in an expansion angle, thus a smaller jet core and a larger effective area resulted. The expanded wave was further accelerated at a lower Mach number. Therefore, momentum of the jet core was reduced. However, an enlarged effective area allows a larger amount of secondary fluid to be entrained and passed through the converging duct (Figure 6.2). Total momentum of the mixed stream which was decreased by the jet core is compensated by the higher secondary fluid pressure.

So, it can be concluded that the total momentum of the mixed stream becomes higher, and the shocking position moves downstream as the secondary fluid saturated pressure rises. This enables the ejector to be operated with a higher entrainment ratio and at higher critical back pressure (Figure 7.1).

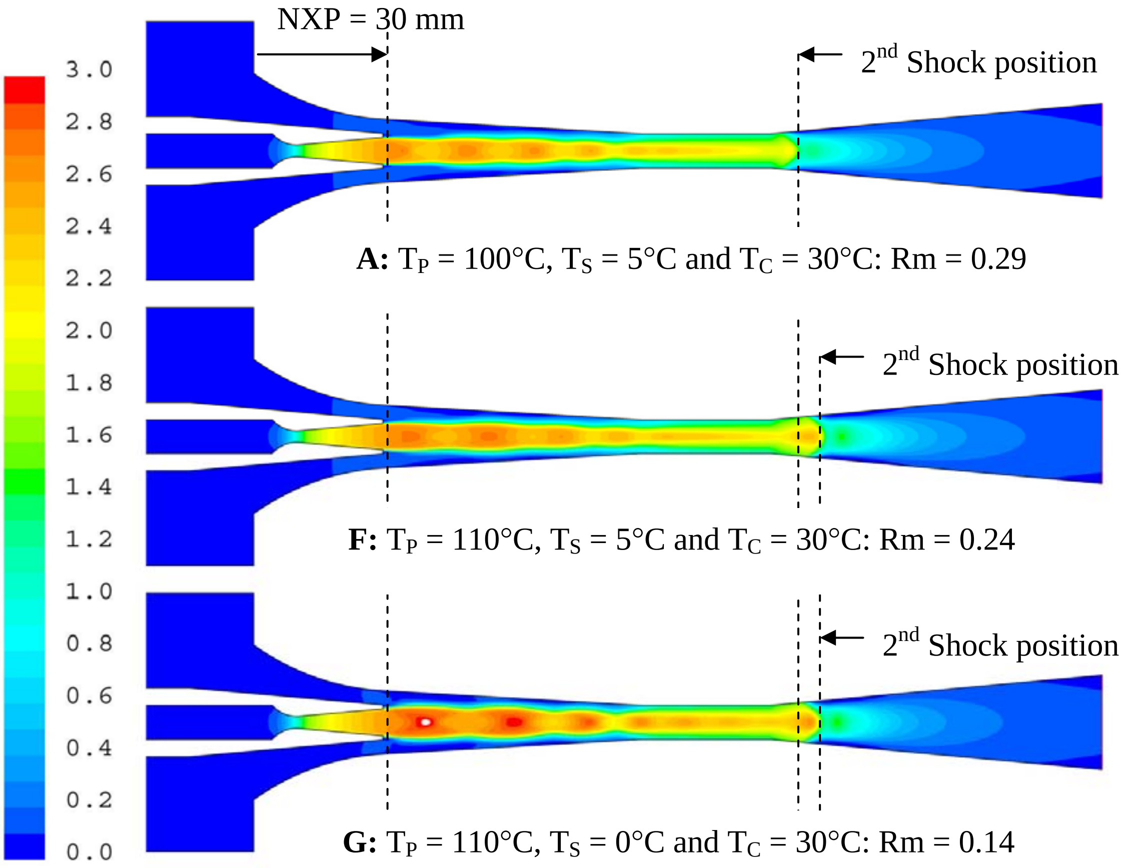

a) Filled contours of Mach number

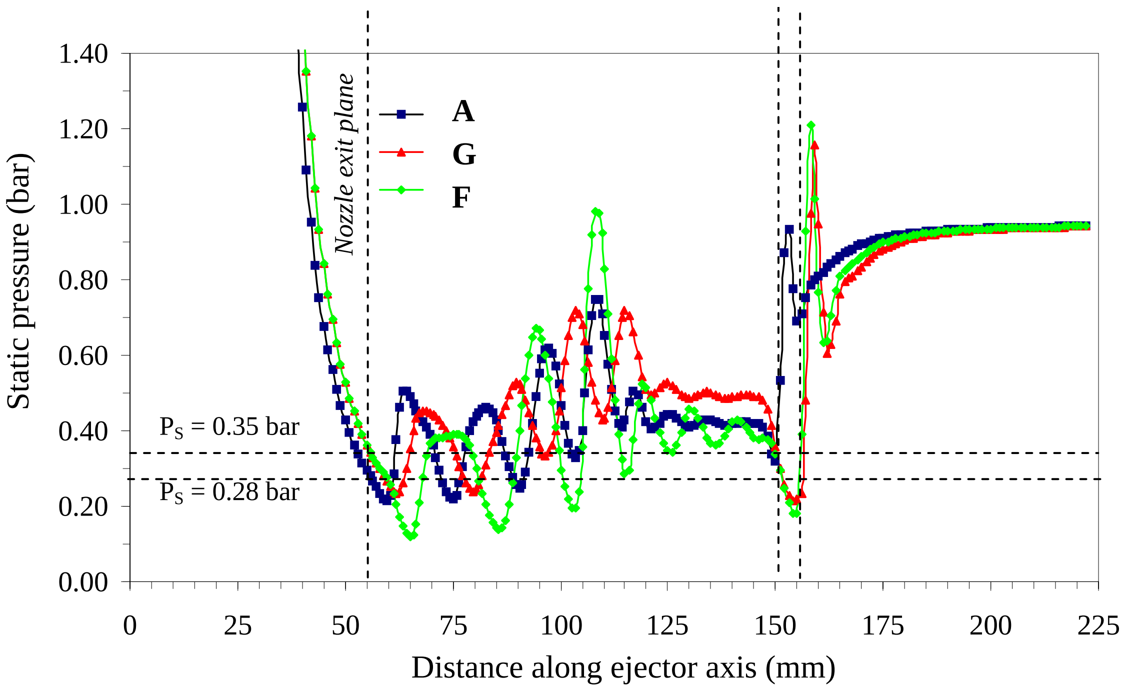

b) Static pressure distribution along the centerline of the ejector

Figure 7.4 Effect of upstream operating conditions on the flow in the R141b ejector (All operating points, **A**, **G,** and **F**, correspond to those shown in Figure 7.1).

In addition to the cases of various operating conditions, the parameters of upstream operating conditions could be combined into a single parameter called the upstream pressure ratio (P_S/P_P) which altered the primary flow state at the primary nozzle exit's plane. At different upstream pressure ratios, it was found that the primary fluid could leave the primary nozzle's exit with different nozzle exit pressure ratios and different primary flow states, either an over-expansion state or an under-expansion state as described in the previous chapter. Hence, it could be useful to consider the effect of the primary flow states, as a result of various operating conditions, on the performance and flow characteristics of the ejector. In this investigation, the primary fluid saturation temperature was ranged from 80°C to 130°C, whilst the secondary fluid saturation temperature and the ejector's exit pressure were fixed at 5°C and 30°C, respectively. Table 7.1 and Figure 7.5 summarize the ejector's flow information when the upstream pressure ratio was varied.

It can be seen from Table 7.1 and Figure 7.5 that increasing the upstream pressure ratio to the value of 0.04644 corresponding to the primary fluid saturation temperature of 105°C and the secondary fluid saturation temperature of 5°C, there was a transition of the primary flow state from an under-expansion state to an over-expansion state.

Table 7.1 Results of CFD simulation for the R141b ejector operated with various upstream pressure ratios.

T_P (°C)	P_S/P_P	$\dot{m}_P$ (kg/s)	$\dot{m}_S$ (kg/s)	Rm	Primary flow state
80	0.08315	0.0103	0	0	Over-expansion
85	0.07347	0.0116	0.0030	0.256	Over-expansion
90	0.06516	0.0130	0.0048	0.365	Over-expansion
95	0.05801	0.0146	0.0053	0.370	Over-expansion
100	0.05182	0.0162	0.0049	0.303	Over-expansion
105	0.04644	0.0179	0.0045	0.251	-
110	0.04175	0.0198	0.0044	0.220	Under-expansion
120	0.03405	0.0240	0.0040	0.170	Under-expansion
130	0.02806	0.0290	0.0033	0.114	Under-expansion

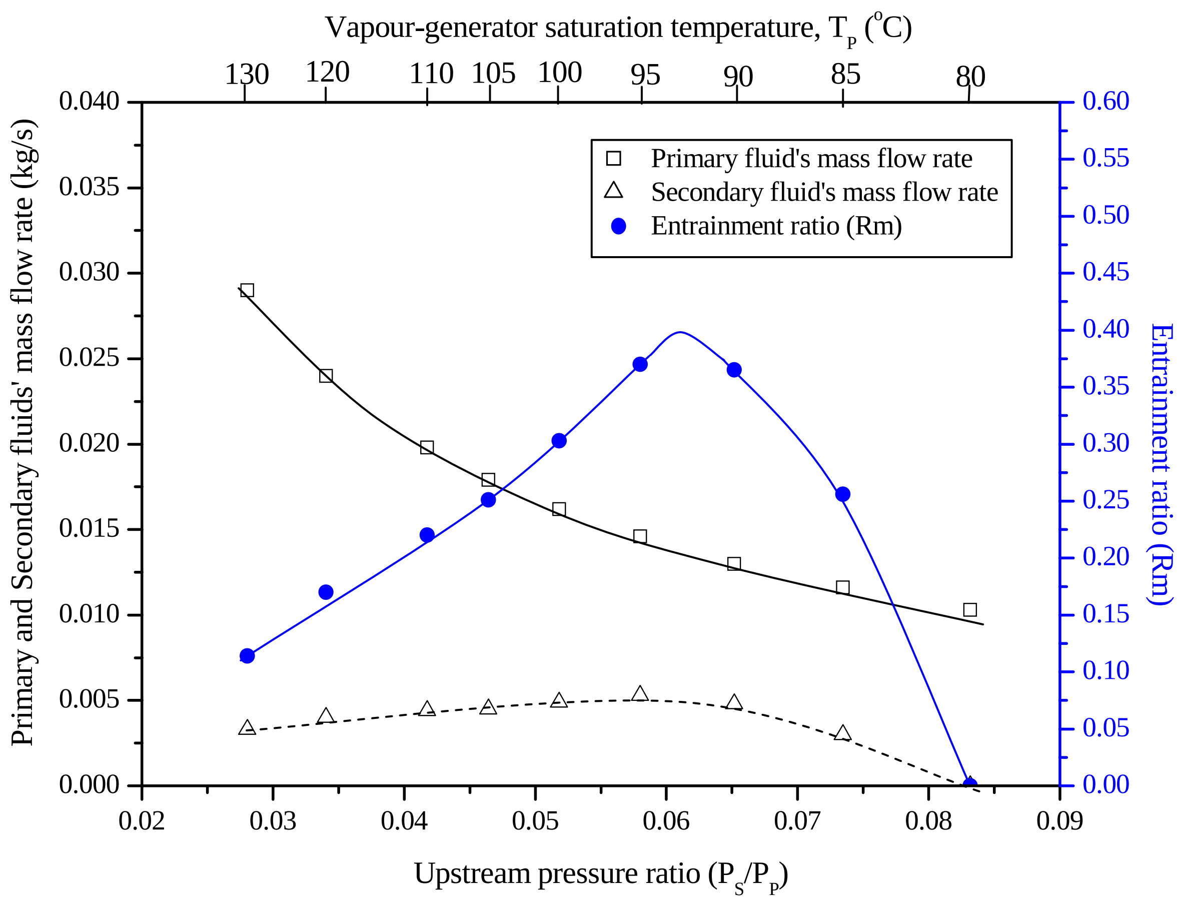

Figure 7.5 Simulated Entrainment ratio and mass flow rates of the two streams at different upstream pressure ratio.

The difference in the state of the primary flow at the primary nozzle exit causes the variation in entrainment ratio. If the primary flow state was in an under-expansion state, increasing the upstream pressure ratio caused the entrainment ratio to be increased. This is because at higher upstream pressure ratio (lower in primary fluid saturation pressure), the primary flow leaves the primary nozzle with a smaller expansion angle; therefore, a smaller jet core with larger effective area resulted. If the upstream pressure ratio was further increased, a maximum entrainment ratio existed. After the primary flow state was turned to an over-expansion state, even though the primary flow leaved the primary nozzle with a smaller expansion angle, the rate of the entrained secondary fluid dropped due to the drop in capability of the lower momentum primary fluid. In conclusion to this section, the pressure difference between the ejector primary inlet and the secondary inlet governs the amplitude of the secondary flow entrainment as reflected in the state of nozzle exit flow.

According to the investigation on the effect of the upstream pressure ratio, it was shown that the maximum secondary flow and, hence, the maximum entrainment ratio of 0.37 were produced at the primary fluid temperature at 90-95°C where the primary flow is in an over-expansion state. At the primary fluid temperature of 90°C, the upstream pressure ratio, P_S/P_P is equal to 0.065.

If we consider that in order to obtain the state of over-expanded primary flow in which the maximum entrainment ratio is achieved, the pressure ratio between the secondary fluid and the primary fluid should be at a proper value.

Let us recall the value of $P_S/P_P = 0.065$, and use this value for other test conditions where the primary fluid and the secondary fluid temperature were varied. The results of the investigation on effect of increasing the primary fluid temperature with a fixed $P_S/P_P = 0.065$ are shown in the following table.

Table 7.2 Results of CFD simulation for the R141b ejector operated with a fixed upstream pressure ratio.

T_P (°C)	T_S (°C)	$\dot{m}_P$ (kg/s)	$\dot{m}_S$ (kg/s)	Rm	Primary flow state
85	2	0.0103	0	0	Over-expansion
90	5	0.0130	0.0048	0.365	Over-expansion
100	10	0.0162	0.0062	0.383	Over-expansion
130	26	0.0290	0.0113	0.390	Over-expansion
150	36	0.0402	0.0155	0.386	Over-expansion

It can be said that, if the same P_S/P_P is applied, the following situations resulted.

- The entrainment ratio remains almost the same value when operated with the downstream pressure less than the critical back pressure.
- Properties of the flow upstream of the throat remain the same.

- The primary flow state is in an over-expansion state.
- At the primary fluid temperature of 85°C and P_S/P_P = 0.065, there is no entrained secondary flow into the ejector. This does not mean this pressure ratio is not applied to this temperature range, but, the zero-entrained fluid was influenced by the back pressure. If the back pressure is reduced, i.e. to the pressure corresponding to saturated temperature of 25°C, the entrainment ratio was found to be 0.37.

In conclusion, during operation, the proper P_S/P_P could be controlled in order to ensure the flow will leave the nozzle in an over-expanded state and to obtain maximum entrainment ratio. The disadvantage of keeping the same upstream pressure ratio is that the desired secondary fluid saturation temperature (evaporator saturation temperature) may be sacrificed.

7.4 Conclusions

This chapter proposes the theory explaining the flow characteristics reflecting the performance of the R141b ejector, when the operating conditions of the ejector were varied. With help of the CFD, the change in the flow structure, influenced by interested parameters, in the R141b ejector could be visualized. It was found that, the size of the primary jet core and the effective area (between the wall of an ejector throat and the primary fluid jet core), as can be visualized from the contours of Mach number, was directly related to the amount of the entrained secondary fluid and thus the entrainment ratio. The critical back pressure (the highest possible condenser pressure) was affected by the shocking position at some point between the constant area throat and the entrance of the diffuser. The shocking positions can be investigated from the simulated static pressure profiles along the axis of the ejector.

Table 7.3 Summarized table for the effect of operating conditions on the R141b ejector.

Effect Parameters	**action**	**Primary flow state**	**Performance Characteristic**	
			Entrainment ratio **(Rm)**	Critical back pressure **(P_C)**
Effect of Operating Conditions				
Primary fluid saturation pressure	(-)→ (+)	Over-expansion	↑	↑
		Under-expansion	↓	↑
Secondary fluid saturation pressure	(-)→ (+)	Over-expansion / Under-expansion	↑	↑
Downstream saturation pressure	(-)→ (+)	Choked flow	**Unchanged**	
		Unchoked flow	↓	

During the simulation, it was discovered that the primary flow state at the nozzle exit plane play a significant role in the performance of the ejector at various operating conditions. The influences of the studied parameters associated with the primary flow state on the performance characteristic of the R141b ejector are presented in Table 7.3.

From Table 7.3, it can be seen that the performance of the R141b ejector, both the entrainment ratio and the critical back pressure, can be improved by the following:

- Increasing of the primary fluid saturation pressure when the primary flow state was in the over-expansion state.
- Increasing of the secondary fluid saturation pressure when the primary flow state was either the over-expansion state or under-expansion state.

Changing the downstream condition or the back pressure in the choked flow region, caused the entrainment ratio to remain constant. In the unchoked flow region, if the back pressure was increased, the entrainment ratio is reduced.

The enhancement of the critical back pressure, but with the decrease in the entrainment ratio could be found, when adjusting the following:

- Increasing of the primary fluid saturation pressure when the primary flow state was at the under-expansion state.

In conclusion, this chapter shows the advantage of CFD in investigating the flow mechanisms and the performance of the R141b ejector when operating with various operating conditions. Using the information provided in this chapter leads to the development in the design and the operation of the ejector for refrigeration purposes.

CHAPTER VIII

PERFORMANCE OF THE EJECTOR:

EFFECTS OF GEOMETRY'S VARIATION

Form the literature review, it was seen that not only the operating conditions, but the geometries of the ejector also affects the performance of the ejector. In this chapter, in order to study the effect of ejector geometries on the performance of the ejector, 4 interested parameters concerning the geometries are as follows:

- the primary nozzle's throat diameter,
- the mixing chamber inlet diameter,
- the length ejector's throat section, and
- the nozzle exit position.

To investigate the influences of each parameter, the ejector was modeled with the different pieces of components. Variations in shape of the ejector were modeled with respect to the dimension of the experimental ejector given in Table 3.2. During the simulation, for each geometry cases, the upstream operating conditions were fixed. Please also note that, the flow structures in this chapter were analyzed when the ejector models were operated in the choke flow mode at the downstream pressure of 0.94 bar (corresponding to the condenser saturation temperature of around 30°C). Similar to the previous chapter, the detail analyses and discussion on the effect of ejector geometries to the flow characteristics and the performance of the R141b ejector are provided in this chapter.

8.1 Effect of Primary Nozzle Throat Diameter

In the simulation, the primary nozzle throat diameter was varied from 2.5 mm. (Nozzle no.2), 2.8 mm. (Nozzle no.1), and 3.2 mm. (Nozzle no.3). Since the ejector's throat diameter was fixed at 8 mm, changing the size of the primary nozzle diameter caused the variation in the area ratio (AR) from 6.25 to 10.24. The primary fluid pressure and the secondary fluid pressure were fixed at the corresponding saturated temperature of 110°C and 5°C, respectively. Once again, referring to Table 3.2, other significant parts of the ejector were modeled from mixing chamber no.1, throat section no.3 and the subsonic diffuser. The primary nozzle exit plane was fixed at a positive NXP of 30 mm. The results are shown in Figure 8.1.

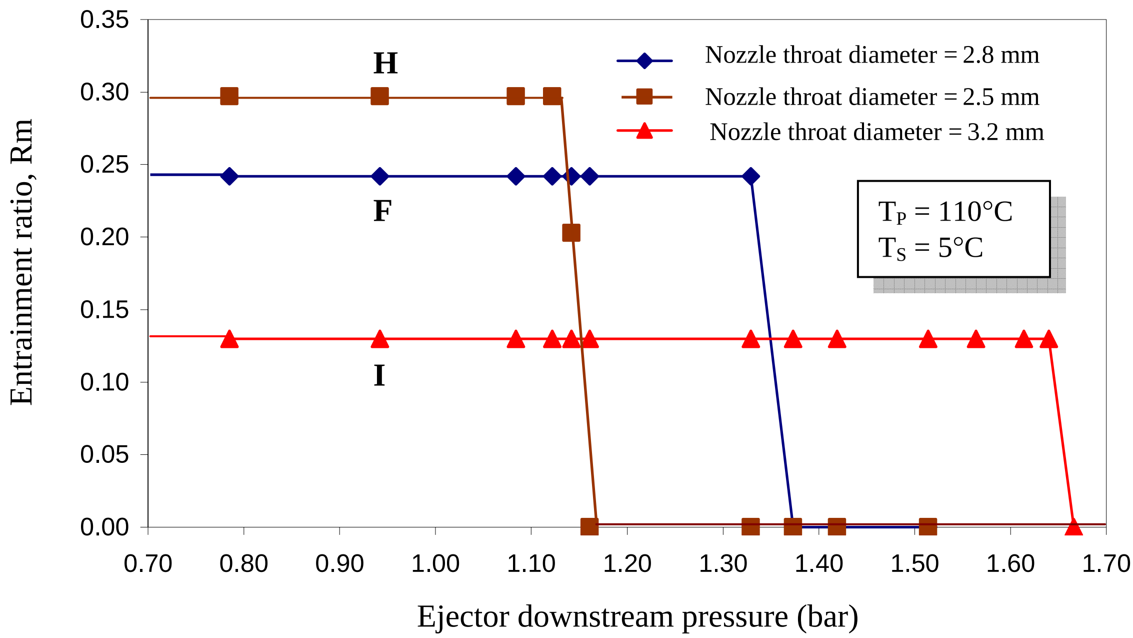

Figure 8.1 Performance characteristics of the R141b ejector, effect of primary nozzle throat diameter.

From Figure 8.1, point H and I, it is seen that when the ejector is equipped with a smaller primary nozzle (H), the entrainment ratio of the ejector can be increased. However, the ejector has to be operated at a lower critical back pressure.

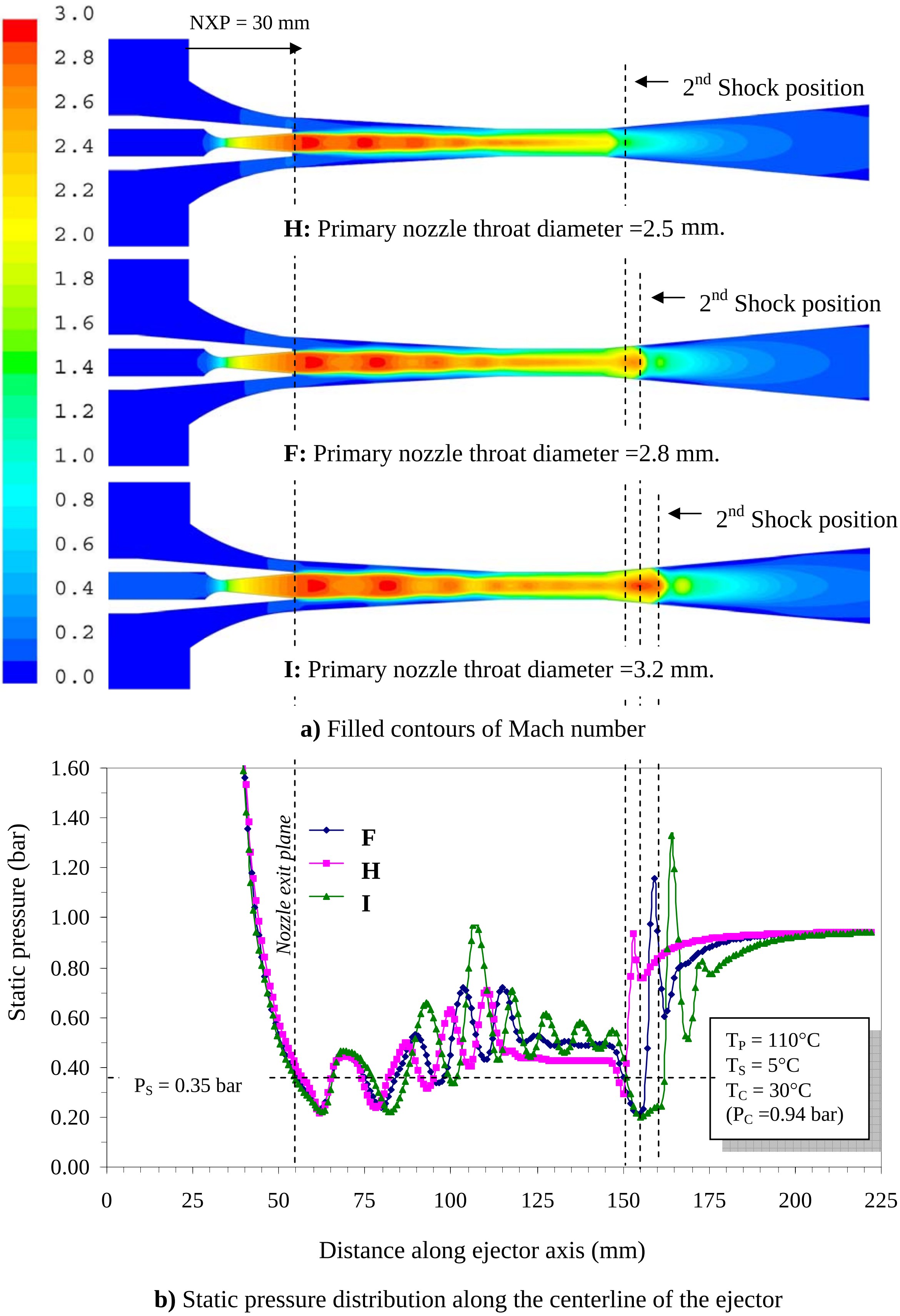

Figure 8.2 Effect of the primary nozzle throat diameter on the flow in the R141b ejector (All operating points, **F**, **H,** and **I**, correspond to those shown in Figure 8.1).

Figure 8.2 shows the contours of Mach number of the ejector simultaneously with the static pressure distributions along the ejector's axis, when its primary nozzle geometry is varied. When the ejector is equipped with a larger primary nozzle, a larger jet core which has higher momentum is produced. Therefore a smaller amount of the secondary fluid is allowed to be entrained through the resultant smaller effective area. On the other hand, the total momentum of the mixed stream increases and a stronger second series of oblique shock can be induced as seen in Figure 8.2b. Consequently, less compression process from the divergent diffuser is needed, and the shocking position moves forward closer to the ejector exit. In conclusion, these flow structures cause a decrease of the entrainment ratio. However, an ejector can be operated at a higher critical back pressure.

8.2 Effect of Mixing Chamber Inlet Diameter

In this case, the simulated domains were modeled with various mixing chamber inlet diameters which were mixing chamber no.1 (inlet diameter = 36 mm.), mixing chamber no.2 (inlet diameter = 12 mm.), and mixing chamber no.3 (inlet diameter = 48 mm.). Other significant parts of the ejector were modeled from, primary nozzle no.1, throat section no.3 and the subsonic diffuser. The primary fluid pressure and the secondary fluid pressure were fixed at the corresponding saturation temperatures of 100°C and 5°C, respectively. The primary nozzle exit plane was fixed at a positive NXP of 30mm. The simulated performance characteristics curves are shown in Figure 8.3.

Figure 8.4a demonstrates the contours of Mach number of the R141b ejector, when its mixing chamber inlet diameter is varied. Obviously, the graphic flow visualization indicates that there is not much effect from the shear mixing and the viscosity of the fluid on the expanded wave.

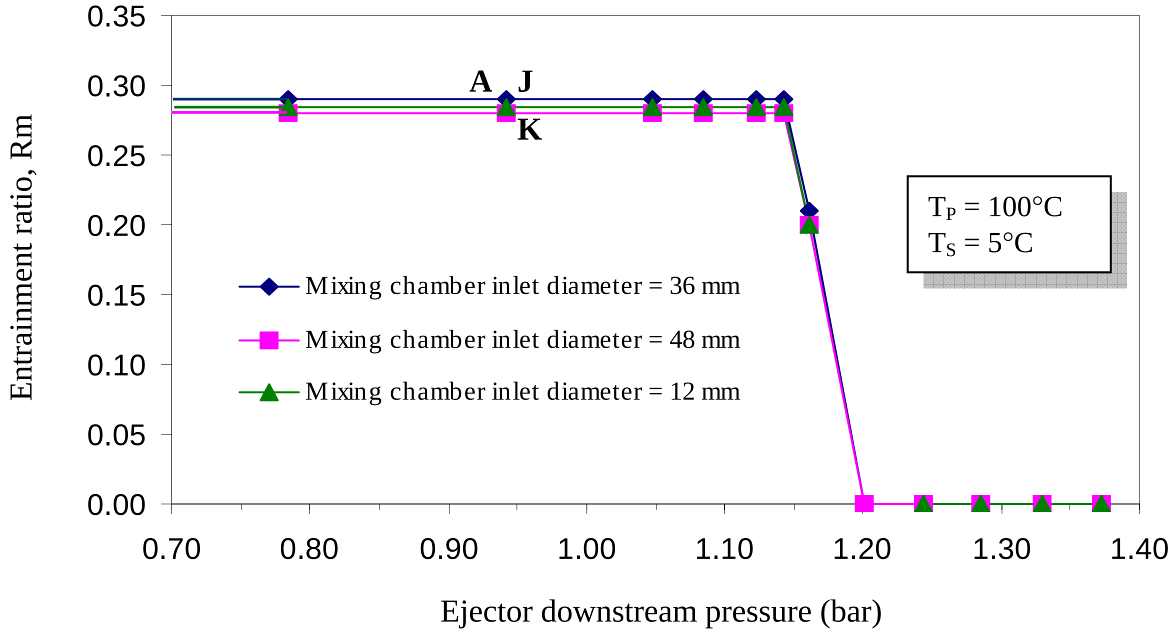

Figure 8.3 Performance characteristics of the R141b ejector, effect of mixing chamber inlet diameter.

The primary jet core of the smaller mixing chamber inlet diameter moves with slightly greater speed and hence higher momentum. On the other hand, entraining the secondary fluid under a slightly higher effect of the shear mixing and the viscosity of the fluid on the expanded wave introduces the higher total pressure loss to the mixed stream. However, as seen from Figure 8.4b, the static pressure profiles along the ejector's axis upstream of the shocking position were almost the same and the shocking position and the critical back pressure of the ejectors were almost unchanged. Moreover, it is seen that the size of jet core and the effective area of the ejectors are similar. Therefore, they can draw the identical amount of secondary fluid, and their entrainment ratios remain the same (Figure 8.3).

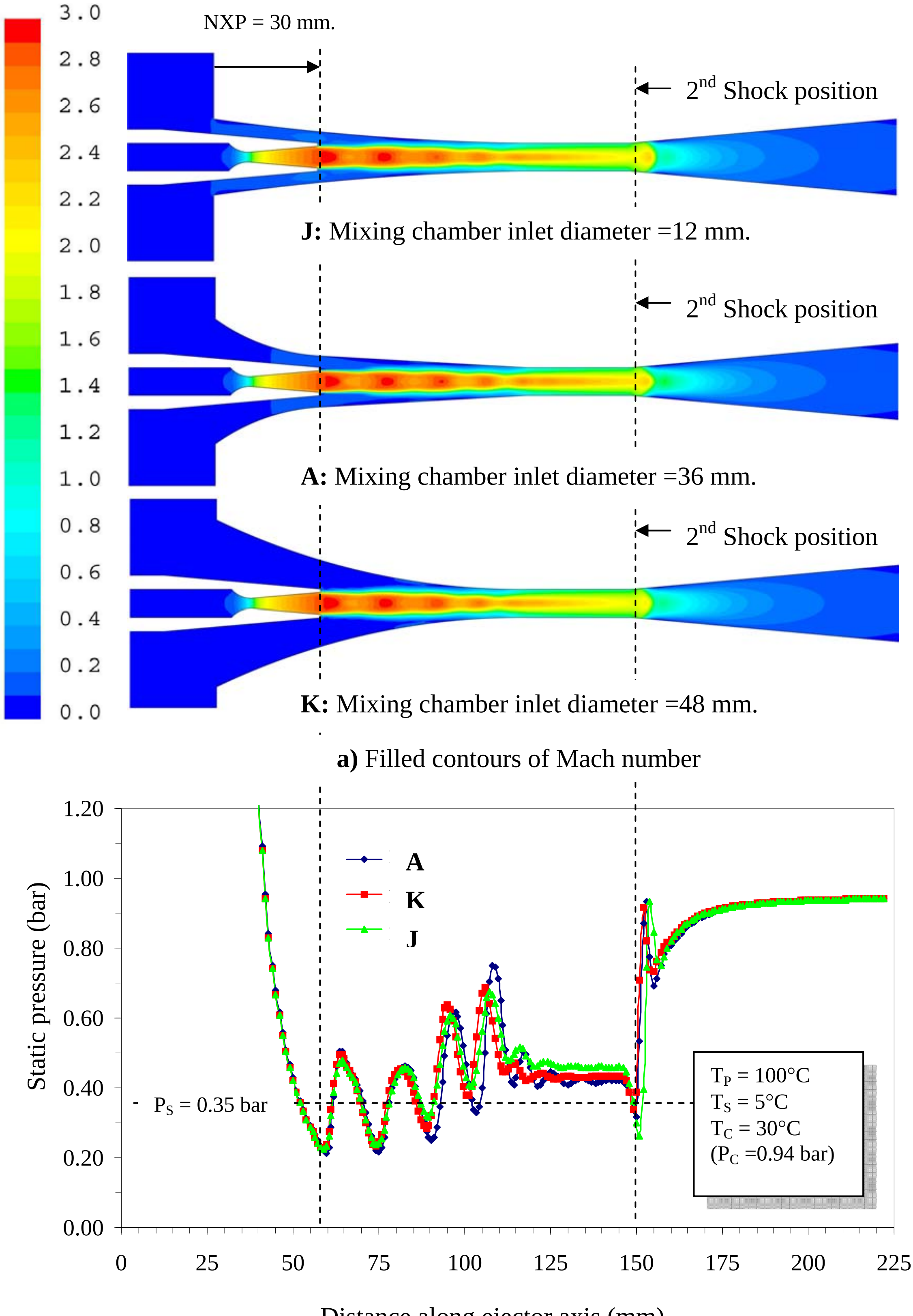

a) Filled contours of Mach number

b) Static pressure distribution along the centerline of the ejector

Figure 8.4 Effect of the mixing chamber inlet diameter on the flow in the R141b ejector (All operating points, **A**, **J,** and **K**, correspond to those shown in Figure 8.3).

8.3 Effect of Throat Length

In the simulation, the throat length of the ejector was varied from 16, 32, and 40 mm. The primary fluid pressure and the secondary fluid pressure were fixed at the corresponding saturated temperatures of 100°C and 5°C, respectively. Other significant shapes of the ejector were, for example, the primary nozzle diameter = 2.8 mm, and the NXP = +30 mm. The results of simulated performance are shown in Figure 8.5.

Referring to Figure 8.5, point A, L and M illustrate the performance characteristics of the R141b ejector when its throat length was varied. It is clear that the length of the ejector throat section has almost no influence on the entrainment ratio of the ejector. However, when the ejector is assembled with a longer throat (**M**), the ejector can be operated at a higher critical back pressure.

Figure 8.6 illustrates the graphic flow visualization inside the R141b ejector, when the length of the ejector's throat section is varied.

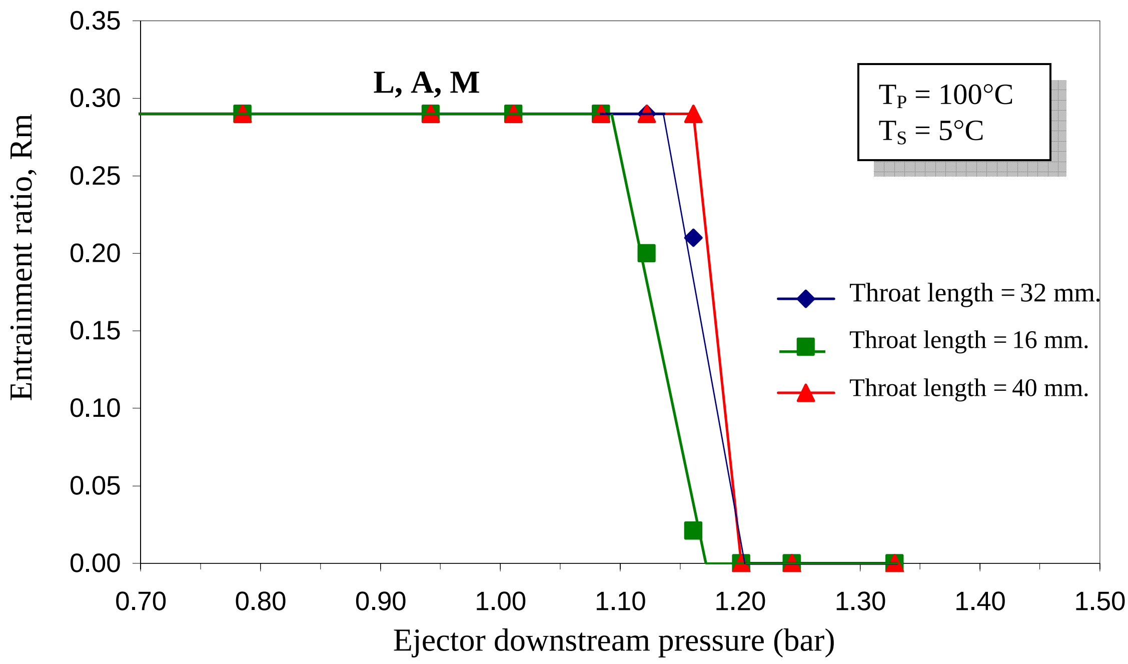

Figure 8.5 Performance characteristics of the R141b ejector, effect of throat length.

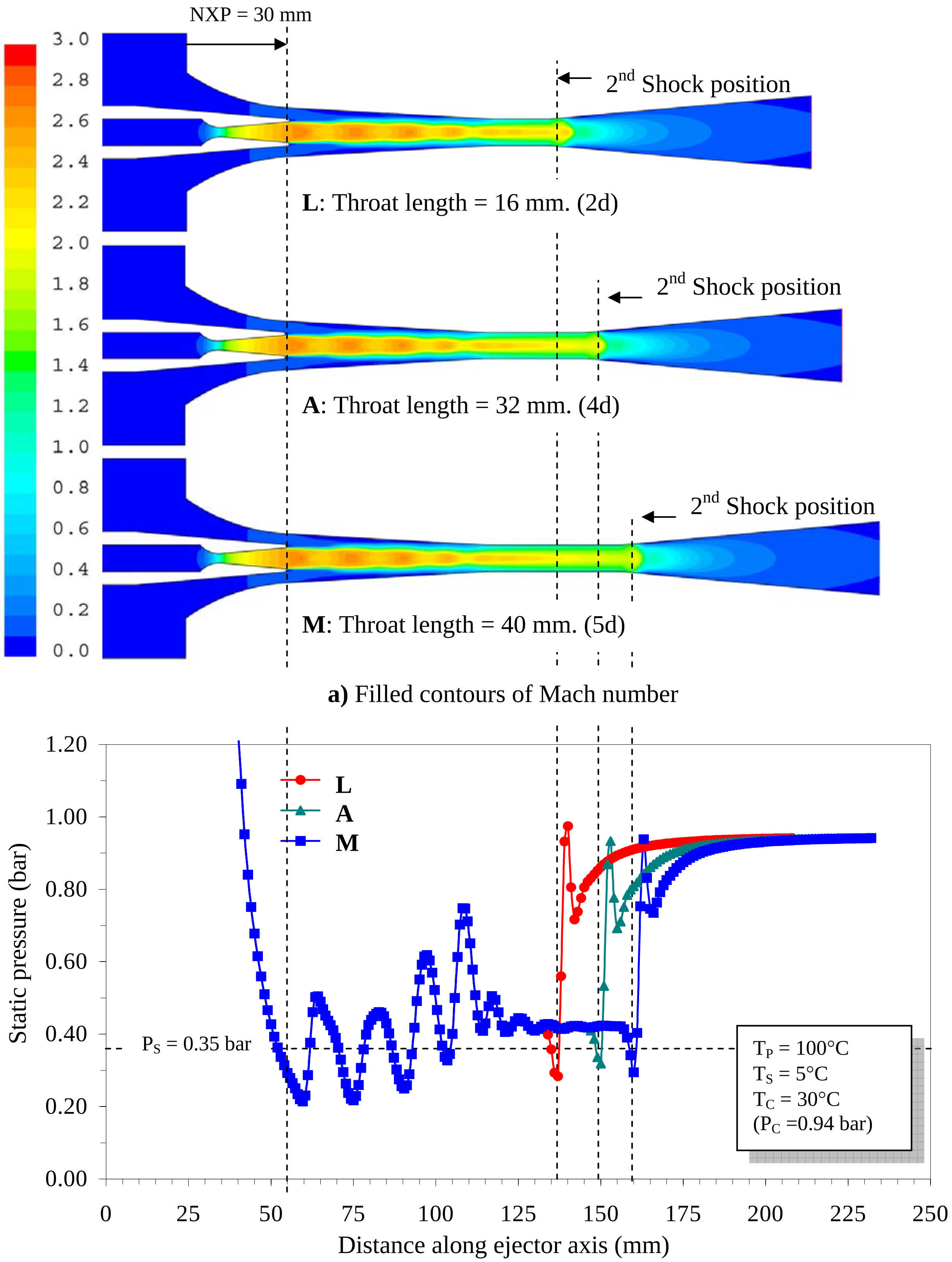

a) Filled contours of Mach number

b) Static pressure distribution along the centerline of the ejector

Figure 8.6 Effect of the throat length on the flow in the R141b ejector (All operating points, **A**, **L,** and **M**, correspond to those shown in Figure 8.5).

It is seen that the length of the ejector throat has almost no influence on the flow structure inside the R141b ejector. These modeled ejectors show the identical sizes of the primary jet core and the expansion angle, thus, resulted in the same size of the effective area. Therefore, the same amount of the secondary fluid can be drawn into the ejector, and consequently the entrainment ratio remains constant.

One interesting point is that the shape of the second series of oblique shock can vary with the length of ejector throat. It is thought that better mixing between the primary jet core and the entrained fluid can be achieved when the longer contact time is provided, as the ejector is fitted with a longer throat section. The better mixing causes the smaller difference between the speed of the primary jet core and the surrounding secondary fluid. Thus the mixed stream becomes more uniform. The induced oblique shock is flattened and a higher compression effect across the shock wave can be achieved, as can be seen in Figure 8.6b.

It can be seen that less compression effect from the divergent portion of a subsonic diffuser is required, and the shocking position moves closer to the diffuser exit. In conclusion, the extended length of the throat section, plus the moving downstream of the shocking position provide a longer distance between the shocking position and the effective area. Therefore, the ejector can be operated at a higher critical back pressure.

However, please note that the elongation of the ejector throat introduces the pressure loss from the interaction of the flow with the viscous boundary layer on the ejector wall. In addition, the reduction of total pressure of the mixed stream is also a result of the induced stronger shock wave. Even though these losses are believed to be small, the accumulated losses from a very long throat and the very strong shock can mitigate the advantage of ejector throat length on the critical point of an ejector.

From the study, it is found that the location of the second shock wave can be varied between the ejector throat and the beginning of the divergent portion of the diffuser. It is determined by the ejector operating conditions which affect the increase of static pressure across the shocking process, plus that in the divergent portion of the subsonic diffuser behind the process. Therefore, in some situation when the shocking position is created in the subsonic diffuser, the supersonic stream is first further accelerated, and its static pressure decreases. However, right after the first shock, its static pressure rebounds and rises to the discharge value.

8.4 Effect of Nozzle Exit Position

In the simulation, only the ejector model constructed with the primary nozzle no.1 was investigated for the effect of various nozzle exit positions. The nozzle exit position (NXP) was varied from positive 20, 30 and 40 mm. The NXP is defined as the distance between the primary nozzle exit plane and the mixing chamber inlet planes. The primary fluid pressure and the secondary fluid pressure were fixed at the corresponding saturated temperatures of 100°C and 5°C, respectively. Other significant shapes of the ejector were, for example, the throat length = 32 mm. (throat no.3), and the mixing chamber inlet diameter = 36 mm. (mixing chamber no.1). The performance curves of the ejector affected by the nozzle exit position are shown in Figure 8.7.

Concerning Figure 8.7, for a given primary fluid and secondary fluid upstream conditions, an entrainment ratio of ejector can be varied when the primary nozzle exit position was placed at the different position. Moving the primary nozzle into the mixing chamber causes the enhancement of both the entrainment ratio and the critical back pressure. Figure 8.8 shows the contours of Mach number of the modeled ejectors, simultaneously with the axis's static pressure distribution, as influenced by the primary nozzle position. For all cases of different NXP, the primary fluid leaved the primary nozzle's exit in an over-expansion state.

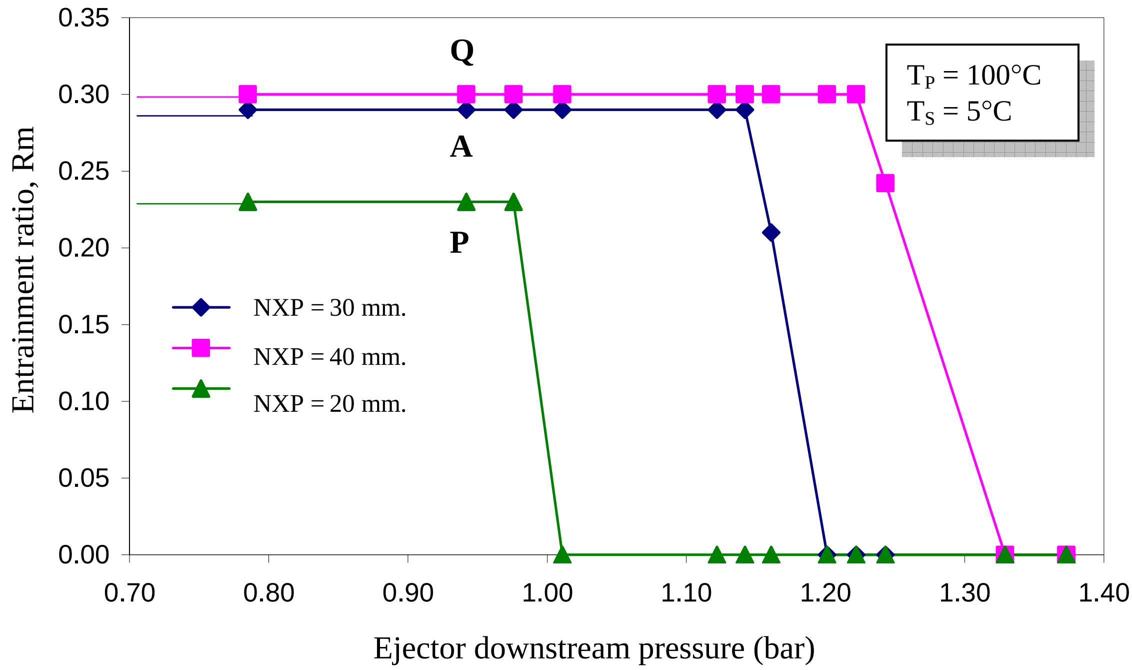

Figure 8.7 Performance characteristics of the R141b ejector, effect of nozzle exit position.

Figure 8.8a shows the contours of Mach number of the modeled ejectors for different primary nozzle positions. The comparison is made at constant condenser pressure of 0.94 bar. At a glance, it can be seen that moving the primary nozzle into the mixing chamber causes a motive fluid to leave the primary nozzle with a smaller expansion angle. According to these changes, the smaller jet core which moves with slightly lower speed and momentum was the result. Thus, there was the larger effective area for the secondary fluid to be entrained through.

From Figure 8.8b, the static pressure profiles along the axis of the ejector, there was an increase of static pressure profiles in the throat section in front of the shocking position, as the primary nozzle was placed closer to the throat section of the ejector. Moreover, moving the nozzle to a higher positive NXP caused the shocking position to slightly move upward closer to the diffuser's end.

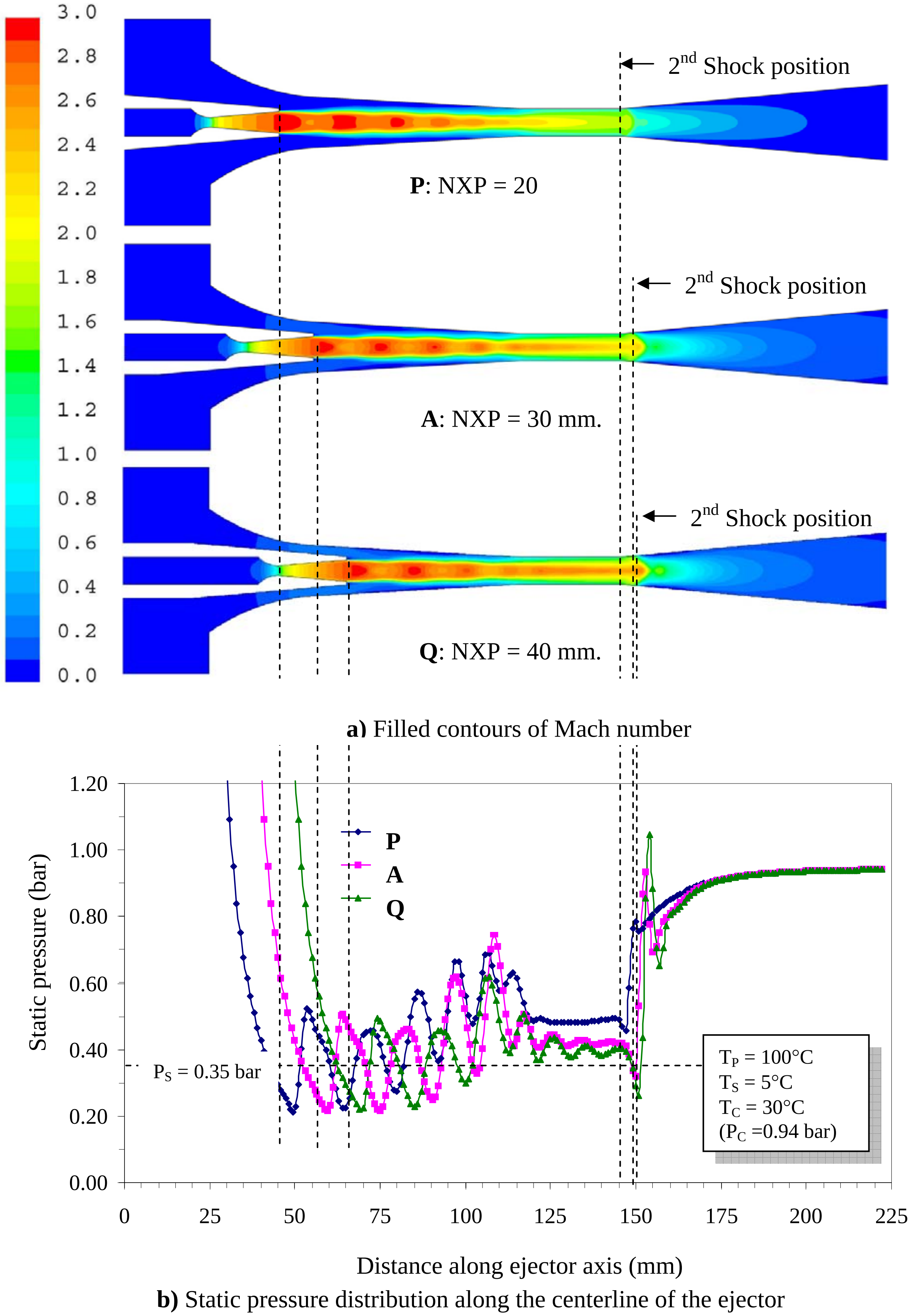

Figure 8.8 Effect of the nozzle exit position (NXP) on the flow in the R141b ejector (All operating points, **A**, **P,** and **Q**, correspond to those shown in Figure 8.7).

In conclusion, when the primary nozzle was placed downstream into the mixing chamber, the resultant larger effective area allows the primary fluid to entrain a higher rate of secondary fluid into the ejector, thus the higher entrainment ratio is achieved. Moreover, the higher static pressure of the mixed stream in the throat section causes the major increase of its total momentum. Therefore the shocking position moves forward closer to the diffuser's end, and the ejector could be operated at a higher critical condenser pressure.

On the contrary, when the primary fluid leaved the nozzle's exit in an under-expanded state, as normally happened in the case of the steam ejector [39, 40 and 47], retracing out the primary nozzle position off the mixing chamber resulted in a higher entrainment ratio but a lower in the critical back pressure.

8.5 Conclusions

This chapter proposes the theory explaining the flow characteristics reflected the performance of the R141b ejector, when the geometries of the ejector were varied. The change in the flow structure according to the change of the geometries, as visualized using the CFD post-functions, altered the performance of the ejector. It was found that, the change in the performance when the geometries were changed also depended on the primary flow state. At the different primary flow states, the change in the ejector's geometries could affect the change in the flow and the performance of the R141b ejector in different ways as can be concluded in Table 8.1

From Table 8.1, it can be seen that the performance of the R141b ejector, both the entrainment ratio and the critical back pressure, can be improved by moving the nozzle exit position downstream into the mixing chamber when the primary flow state was in an over-expansion state.

Table 8.1 Summarized table for the effect of geometries on the R141b ejector.

Effect Parameters	action	Primary flow state	Performance Characteristic	
			Entrainment ratio **(Rm)**	Critical back pressure **(P_C)**
<u>**Effect of Geometry Variations**</u>				
Primary nozzle throat diameter	(-)→ (+)	Over-expansion / Under-expansion	↓	↑
Mixing chamber inlet diameter	(-)→ (+)	Over-expansion / Under-expansion	**unchanged**	**unchanged**
Throat Length	(-)→ (+)	Over-expansion / Under-expansion	**unchanged**	↑
NXP	(-)→ (+)	Over-expansion	↑	↑
		Under-expansion	↓	↑

The enhancement of the critical back pressure, but with the decrease in the entrainment ratio could be found, when adjusting the following:

- Increasing the primary nozzle throat diameter.
- Moving the nozzle exit position downstream into the mixing chamber when the primary flow state was at the under-expansion state.

The critical back pressure of an R141b ejector can also be increased by using an ejector with a longer throat section, without the interruption in the amount of the entrained secondary fluid. However, if the throat section is too long, the loss in total pressure may mitigate its advantage on the back pressure which the mixed stream can emit.

Both the entrainment ratio and the critical back pressure were found unchanged, when adjusting the mixing chamber inlet diameter.

In conclusion, this chapter shows the advantage of CFD in investigating the flow mechanisms and the performance of the R141b ejector when operating with various geometries.

CHAPTER IX

CONCLUSIONS AND RECOMMENDATIONS

9.1 Conclusions

An ejector is the most critical component in the jet refrigeration cycle. In order to improve the design and the operation of jet refrigerator, a clear understanding of the flow characteristics reflecting the performance of the ejector should be obtained.

From literature surveys on the past researches of ejectors, the flow behavior and the mixing process within the ejectors were complicated. The use of 1-D assumption only may not be adequate to improve the design and the operation of the ejector. Very few studies were made to reveal the flow characteristics in ejectors by various methods, i.e., the flow visualization and the CFD (Computational Fluid Dynamics). Moreover, their analytical results were not completed. Some of them were out of experimental ranges and some were unable to be applied for refrigeration applications.

In this study, the investigations on the performance and flow characteristics of the R141b ejector (in refrigeration application) at various operating conditions and various geometries were performed experimentally and theoretically. A small scale R141b ejector refrigerator was constructed and tested. The experimental ejectors were modeled and investigated theoretically using the Computational Fluid Dynamics (CFD) method. It was shown that the CFD results were successfully validated with the experimental results. Average errors of the predicted entrainment ratio and the critical back pressure were both found to be less than 9% and 2% respectively. Three types of the following information: the primary fluid’s mass flow rate, the static pressure distribution at the wall of the ejector, and the entrainment ratio including its critical back pressure, were used to validate the simulated model. It was verified that the CFD method is an efficient tool to predict the entrainment ratio and critical back pressure of the ejector.

After the correctness of the model was guaranteed, then other calculated information, which were the static pressure distribution along the ejector's axis, and the contours of Mach number, were used to represent the flow phenomena and the mixing behaviors in the R141b ejector. Hence, a new theory describing the flow and mixing process in the R141b ejector using the CFD's visualization was proposed.

Unlike past research on CFD investigation of the ejector, the advantage of using the static pressure distribution along the ejector's axis instead of the static pressure distribution at the wall was discussed. It was shown that the exact shocking positions and the fluctuations on the shock pattern could be better represented. With this advantage, the two series of oblique shocks were found in the simulation. The first series of oblique shock was found immediately after the primary nozzle exit attached to the jet core of the primary fluid. In the distance between the constant area throat and the diffuser, the second series of oblique shock, which is the shock of the mixed stream fluid, was investigated. Moreover, the differences in the flow structures between the R141b ejector and the steam ejector were investigated and reported according to the differences found in the flow states after the primary fluid leave the primary nozzle, the shock phenomena occurs before the pressure recovery region, and the pressure recovery process.

In Chapter VII and Chapter VIII, the influences of the operating conditions and the ejector's geometries on the flow characteristics reflecting the ejector performance were reported, respectively. With help of the CFD solution and visualization, a better understanding of the flow characteristics and the performance of the R141b ejector as impacted by various operating conditions and geometries were obtained.

It was proved that the CFD's prediction provided similar results of performance characteristics curves compared to the experimental investigation and the typical performance curves of the ejector as discussed in the literature. At each setting of vapour-generator and evaporator condition, increasing the downstream pressure caused the operation of the R141b ejector to be categorized into 3 regions, the choked flow, the un-choked flow and the reversed flow of secondary fluid with respect to the change in the entrainment ratio. Within the choked flow region where the entrainment ratio remained constant, the effective area was always forced to occur somewhere in the constant-area throat section. For the ejector operated in the unchoked flow condition, the increase in the downstream pressure caused the second series of oblique shock to move upstream and disturb the entrainment process. The effective area was also pushed back into the convergent mixing chamber part where the cross sectional area of the effective area and, hence, the entrainment ratio can be varied according to the shape of the mixing chamber.

When the ejector was operated with various upstream operating conditions including the upstream conditions of the primary fluid (vapour-generator saturation pressure) and secondary fluid (evaporator saturation pressure), the parameters of upstream operating conditions could be combined into a single parameter called the upstream pressure ratio (P_S/P_P). This upstream pressure ratio altered the primary flow state at the primary nozzle exit's plane. The primary flow state can be classified into two states which are the "Over-expansion state" and the "Under-expansion state". The difference in the states of the primary flow was found to affect the flow field of the ejector and, hence, alter the ejector's performance. In an over-expansion state, the expansion wave angle of the primary fluid jet core converged into the axis line of the ejector. Thus, a smaller primary fluid jet core and a larger effective area were produced. It can be said that in order to obtain a better performance ejector, the ejector should be designed and operated so that the primary flow state is in an over-expansion state.

At the different primary flow states, the change in the ejector's operating conditions and geometries could affect the flow and the performance of the R141b ejector in different ways, as can be concluded in Table 9.1.

Table 9.1 Effect of operating conditions and geometries on the R141b ejector.

Primary flow state	**Effect Parameters**	**action**	**Performance Characteristic**	
			Entrainment ratio **(Rm)**	Critical back pressure **(P_C)**
Effect of Operating Conditions				
Over-expansion	Primary fluid saturation pressure	(-)→ (+)	↑	↑
	Secondary fluid saturation pressure	(-)→ (+)	↑	↑
	Primary nozzle throat diameter	(-)→ (+)	↓	↑
	Mixing chamber inlet diameter	(-)→ (+)	**unchanged**	**unchanged**
	Throat Length	(-)→ (+)	**unchanged**	↑
	NXP	(-)→ (+)	↑	↑
Effect of Geometry Variations				
Under-expansion	Primary fluid saturation pressure	(-)→ (+)	↓	↑
	Secondary fluid saturation pressure	(-)→ (+)	↑	↑
	Primary nozzle throat diameter	(-)→ (+)	↓	↑
	Mixing chamber inlet diameter	(-)→ (+)	**unchanged**	**unchanged**
	Throat Length	(-)→ (+)	**unchanged**	↑
	NXP	(-)→ (+)	↓	↑

According to the results, the design and operation of the ejector should be as following:

- The ejector should be designed and operated so that the primary flow state is always in an over-expansion state.
- In order to produce a small jet core or a large effective area, the throat diameter of the primary nozzle should be designed as small as possible. But the total momentum of the mixed stream should still be enough for the ejector to operate as close as the critical downstream pressure.
- The ejector with a longer throat section can be operated at a higher downstream pressure without any changes in its entrainment ratio. However, if the ejector is equipped with too long throat section, the loss in total pressure may mitigate its advantage on the downstream pressure which the mixed stream can emit.
- The diffuser of the R141b ejector and all halocarbon refrigerant driven ejectors can be designed into a very short length diffuser necessary to cover a narrow pressure recovery zone (effect of strong oblique shock).
- The enhancement of both the entrainment ratio and the critical back pressure can be obtained by moving the nozzle exit position (NXP) downstream into the mixing chamber when the primary flow state is in the over-expansion state.

The conclusion drawn from this research is that the CFD method is an efficient tool to predict the performance of the ejector including the entrainment ratio and the critical back pressure. The validation of the CFD results of the simulated model compared to the experimental results was fascinated. The flow characteristics reflected the performance of the ejector at various operating conditions and geometries were revealed. Finally, it is expected that the information provided in this thesis will lead to the improvement in the design and the operation of the ejector used in refrigeration applications, thus, increase the performance of the overall system.

9.2 Recommendations

It can be said that the CFD study of the ejector in this research was one of the first studies in the field of refrigeration purpose. In order to utilize this method more efficiently in modeling a flow in any ejectors, the followings are needed.

- The exit of the CFD domain should be extended to include the section connected to the condenser. From the validation of static pressure distribution, the simulated static pressure recovering process at the diffuser part was occurring within a shorter distance than the actual distance in the experiment. At the exit of the diffuser the static pressure recovering process seemed to be incomplete. If the calculation domain is extended to the end of the connecting pipe, the model would become more realistic. Hence, the prediction of the critical back pressure will become more accurate.
- The real gas equations should be applied to the calculation model as the properties of the working fluid rather than using the perfect gas assumption.
- The heat transfer function at the wall surfaces that allows not only the investigation of heat transfer, but also of condensation during the process, should be turned on so that the model could be more realistic.
- Other substitute refrigerants such as R123 and R245fa could be used in the simulation and also in the experiment. The properties of R123 and R245fa are similar to R141b. Moreover, in practice, R123 and R245fa are more compatible to most sealing materials.

APPENDIX A

PRIMARY DESIGN OF EJECTOR USING 1-DIMENSIONAL THEORY

The design method based on 1-dimensional analysis for compressible-gas flow in ejector using the models of stream mixing at constant pressure was first proposed by Keenan and Neumann [1]which was later become a classical theory. Eames et al. [2] proposed a set of the 1-D equation in designing the ejector based on Keenan and Neumann's theory [1]. The loss coefficient at the primary nozzle, the mixing chamber and the diffuser were accounted. In this thesis, the 1-D theory of Eames et al. [2] was selected to use for the design of the ejector.

A.1 Theoretical assumptions

List of simplified assumptions used in Aphornratana's theory is given:

1) Friction Losses are accounted to the base equations of Keenan by applying appropriate loss efficiencies to the primary nozzle (η_N), the diffuser (η_d) and the mixing process (η_m).
2) Kinetic energies of both the primary fluid and secondary fluid at the ejector inlet and the diffuser outlet are negligible (zero velocity).
3) The static pressure at the primary nozzle exit plane where the two fluid streams first met is assumed to be uniform
4) The two streams completely mix before a normal shock wave occurs at the end of the mixing chamber.

A.2 Governing Equations

The analysis of 1-D theory of Keenan [xx] was based on the ideal gas assumption combined with the principles of mass, momentum, and energy conservation. For a study flow process, the equations are given as follows:

Energy Equation for Adiabatic Process:

$$\sum \dot{m}_i \left(h_i + \frac{V_i^{\,2}}{2} \right) = \sum \dot{m}_e \left(h_e + \frac{V_e^{\,2}}{2} \right) \tag{A.1}$$

Momentum Equation:

$$F + P_i A_i + \sum \dot{m}_i V_i = P_e A_e + \sum \dot{m}_e V_e \tag{A.2}$$

Continuity Equation:

$$\sum \rho_i V_i A_i = \sum \rho_e V_e A_e \tag{A.3}$$

Referring to Figure 2.2, applying energy equation and introducing an assumed isentropic efficiency (η_N) of the primary nozzle between state P_0 and $2'$, the speed of the primary fluid leaving the primary nozzle exit is:

$$V_{2'}^{\,2} = 2\eta_N \left(h_{P_0} - h_{2'} \right) \tag{A.4}$$

The Mach number of the primary fluid at the nozzle exit plane, therefore, can be calculated using:

$$M_{2'} = \sqrt{\frac{2\eta_N}{k-1} \left[\left(\frac{P_{P_0}}{P_2} \right)^{\frac{k-1}{k}} - 1 \right]} \tag{A.5}$$

Similar to equation (A.5), between state S_0 and $2''$, the Mach number of the secondary fluid at the nozzle exit plane is determined by:

$$M_{2''} = \sqrt{\frac{2}{k-1} \left[\left(\frac{P_{S_0}}{P_2} \right)^{\frac{k-1}{k}} - 1 \right]} \tag{A.6}$$

Introducing the isentropic efficiency (η_m) during the mixing process of the two streams, between state 2 and 5, the momentum equation can be written in the following form:

$$\eta_m \left(P_2.A_2 + \dot{m}_P.V_{2'} + \dot{m}_S.V_{2''} \right) = P_5.A_5 + V_5 \left(\dot{m}_p + \dot{m}_s \right) \quad \text{(A.7)}$$

The speed of the mixed stream at state 5 can then be given as:

$$V_5 = \eta_m \left(\frac{\dot{m}_p.V_{2'} + \dot{m}_s.V_{2''}}{\dot{m}_p + \dot{m}_s} \right) \quad \text{(A.8)}$$

Introducing the relation between M and M*

$$M^* = \sqrt{\frac{(k+1).\left(\frac{M^2}{2} \right)}{1 + (k-1).\left(\frac{M^2}{2} \right)}} \quad \text{(A.9)}$$

Equation (A.8) can be written in term of Mach number as:

$$M_5^* = \frac{M_{2'}^* + Rm.M_{2''}^*.\sqrt{\frac{T_S}{T_P}}}{\sqrt{(1+Rm).\left(1 + Rm.\sqrt{\frac{T_S}{T_P}} \right)}} \quad \text{(A.10)}$$

Assuming that the normal shock wave occur between state 5 and 6, the Mach number of the mixed fluid immediately after the normal shock wave is determined from:

$$M_6 = \sqrt{\frac{M_5^2 + \frac{2}{(k+1)}}{\left(\frac{2.k}{(k-1)}.M_5^2 \right) - 1}} \quad \text{(A.11)}$$

The pressure ratio across the normal shock wave is calculated from:

$$\frac{P_6}{P_5} = \frac{1 + k.M_5^2}{1 + k.M_6^2} \quad \text{(A.12)}$$

If assumed that the flow speed is brought to stagnation state at the end of the diffuser and a loss coefficient of the diffuser (η_d) is applied, the pressure ratio across the subsonic diffuser can be written as:

$$\frac{P_b}{P_6} = \left[\left(\frac{\eta_d.(k-1)}{2}.M_6{}^2\right)+1\right]^{\left(\frac{k}{k-1}\right)} \tag{A.13}$$

From equation (A.1) to (A.13), if the isentropic efficiencies are initially given and the entrainment ratio is first assumed, the Mach number of each position and the pressure ratios across the ejector can be iteratively calculated.

After the pressure ratios are obtained, the cross sectional areas at each location of ejector can be determined using equation (A.14) to (A.19) with a given diameter of the primary nozzle throat.

The mass flow rate of the primary fluid ($\dot{m}_p$) is calculated using theory of compressible gas flow through convergent-divergent nozzle which is the critical mass flow rate or maximum mass flow rate for a given throat diameter of the nozzle.

$$\dot{m}_p = A_1.P_{P_0}\sqrt{\frac{k}{RT_{P_0}}\left(\frac{2}{k+1}\right)^{(k+1)/(2(k-1))}} \tag{A.14}$$

Thus, the cross sectional area at the throat of the primary nozzle can be written as:

$$A_1 = \frac{\dot{m}_p}{P_{P_0}}\sqrt{\frac{T_{P_0}.R}{k}\left(\frac{k+1}{2}\right)^{\frac{k+1}{k-1}}} \tag{A.15}$$

Applying continuity equation of an ideal gas between state 1 and 2′, the cross sectional area at the primary nozzle exit can be calculated using the following equation:

$$\frac{A_{2'}}{A_1} = \frac{\left(\frac{2}{k+1}\right)^{\frac{1}{k-1}}\left(\frac{P_{P_0}}{P_2}\right)^{\frac{1}{k}}}{\sqrt{\frac{k+1}{k-1}\left(1-\left(\frac{P_2}{P_{P_0}}\right)^{\frac{k-1}{k}}\right)}} \tag{A.16}$$

Where as the annular cross sectional area of the secondary fluid at the inlet of mixing chamber (primary nozzle exit plane) can be evaluated as:

$$\frac{A_{2''}}{A_1}=\frac{Rm.\sqrt{\frac{T_{S_0}}{T_{P_0}}}.\left(\frac{2}{k+1}\right)^{\frac{1}{k-1}}.\left(\frac{P_{P_0}}{P_{S_0}}\right).\left(\frac{P_{S_0}}{P_2}\right)^{\frac{1}{k}}}{\sqrt{\frac{k+1}{k-1}.\left(1-\left(\frac{P_2}{P_{S_0}}\right)^{\frac{k-1}{k}}\right)}} \tag{A.17}$$

If a zero thickness of the primary nozzle exit's wall is assumed, the mixing chamber inlet diameter can be expressed as:

$$A_2 = A_{2'} + A_{2''} \tag{A.18}$$

The area ratio (*AR*) between the cross sectional area of constant area's throat to the cross sectional area of the primary nozzle's throat can finally be obtained as follows:

$$\frac{A_6}{A_1}=\frac{\sqrt{(1+Rm)(1+Rm.T_s/T_p)}.\left(\frac{2}{k+1}\right)^{\frac{1}{k-1}}.\left(\frac{P_{P_0}}{P_b}\right).\left(\frac{P_b}{P_6}\right)^{\frac{1}{k}}}{\sqrt{\frac{k+1}{k-1}.\left(1-\left(\frac{P_6}{P_b}\right)^{\frac{k-1}{k}}\right)}} \tag{A.19}$$

APPENDIX B

EXPERIMENATAL AND CFD RESULTS

Table B.1 Experimental and CFD results for R141b ejector.

Operating Condition			Ejector Geometries (based on data provided in Table 3.2)				Entrainment Ratio	
Primary Fluid Saturated Temperature (T_P), °C	Secondary Fluid Saturated Temperature (T_S) , °C	Ejector downstream pressure (P_c), bar	Primary Nozzle No.	Mixing Chamber No.	Throat No.	NXP	Experiment	CFD
Case 1								
100	5	0.785	1	1	3	30	0.272	0.290
100	5	0.942	1	1	3	30	0.277	0.290
100	5	0.976	1	1	3	30	0.275	0.290
100	5	1.011	1	1	3	30	0.269	0.290
100	5	1.047	1	1	3	30	0.270	0.290
100	5	1.084	1	1	3	30	0.273	0.290
100	5	1.103	1	1	3	30	0.270	0.290
100	5	1.122	1	1	3	30	0.268*	0.290
100	5	1.142	1	1	3	30	0.200	0.290**
100	5	1.161	1	1	3	30	0.145	0.210
100	5	1.181	1	1	3	30	0.100	0.130
100	5	1.201	1	1	3	30	0.045	0
100	5	1.222	1	1	3	30	0	0
100	5	1.243	1	1	3	30	0	0
100	5	1.285	1	1	3	30	0	0
100	5	1.307	1	1	3	30	0	0
100	5	1.329	1	1	3	30	0	0
100	5	1.351	1	1	3	30	0	0
Case 2								
110	5	0.785	1	1	3	30	0.230	0.242
110	5	0.942	1	1	3	30	0.225	0.242
110	5	0.976	1	1	3	30	0.229	0.242
110	5	1.011	1	1	3	30	0.232	0.242
110	5	1.047	1	1	3	30	0.230	0.242
110	5	1.084	1	1	3	30	0.234	0.242
110	5	1.122	1	1	3	30	0.230	0.242
110	5	1.161	1	1	3	30	0.229	0.242
110	5	1.201	1	1	3	30	0.232	0.242
110	5	1.243	1	1	3	30	0.230	0.242
110	5	1.285	1	1	3	30	0.225	0.242
110	5	1.307	1	1	3	30	0.230*	0.242
110	5	1.329	1	1	3	30	0.200	0.242**
110	5	1.351	1	1	3	30	0.145	0.180
110	5	1.373	1	1	3	30	0.086	0.090
110	5	1.396	1	1	3	30	0.040	0
110	5	1.419	1	1	3	30	0	0

Table B.1 Experimental and CFD results for R141b ejector (continue).

Operating Condition (°C)			Ejector Geometries (based on data provided in Table 3.2)				Entrainment Ratio	
Primary Fluid Saturated Temperature (T_P), °C	Secondary Fluid Saturated Temperature (T_S) , °C	Ejector downstream pressure (P_c), bar	Primary Nozzle No.	Mixing Chamber No.	Throat No.	NXP	Experiment	CFD
Case 3								
110	0	0.785	1	1	3	30	0.118	0.140
110	0	0.942	1	1	3	30	0.122	0.140
110	0	0.976	1	1	3	30	0.120	0.140
110	0	1.011	1	1	3	30	0.120	0.140
110	0	1.047	1	1	3	30	0.124	0.140
110	0	1.084	1	1	3	30	0.119	0.140
110	0	1.103	1	1	3	30	0.119*	0.140
110	0	1.122	1	1	3	30	0.072	0.140**
110	0	1.142	1	1	3	30	0.024	0.090
110	0	1.161	1	1	3	30	0	0
110	0	1.181	1	1	3	30	0	0
110	0	1.201	1	1	3	30	0	0
Case 4								
110	5	0.785	3	1	3	30	0.118	0.130
110	5	0.942	3	1	3	30	0.120	0.130
110	5	0.976	3	1	3	30	0.115	0.130
110	5	1.047	3	1	3	30	0.118	0.130
110	5	1.103	3	1	3	30	0.122	0.130
110	5	1.142	3	1	3	30	0.115	0.130
110	5	1.201	3	1	3	30	0.120	0.130
110	5	1.285	3	1	3	30	0.118	0.130
110	5	1.329	3	1	3	30	0.118	0.130
110	5	1.396	3	1	3	30	0.117	0.130
110	5	1.419	3	1	3	30	0.120	0.130
110	5	1.564	3	1	3	30	0.118	0.130
110	5	1.614	3	1	3	30	0.115*	0.130
110	5	1.64	3	1	3	30	0.060	0.130**
110	5	1.666	3	1	3	30	0	0
Case 5								
110	5	0.785	2	1	3	30	0.273	0.297
110	5	0.942	2	1	3	30	0.269	0.297
110	5	0.976	2	1	3	30	0.274	0.297
110	5	1.011	2	1	3	30	0.275	0.297
110	5	1.047	2	1	3	30	0.28	0.297
110	5	1.084	2	1	3	30	0.273	0.297
110	5	1.103	2	1	3	30	0.273*	0.297
110	5	1.122	2	1	3	30	0.194	0.297**
110	5	1.142	2	1	3	30	0.145	0.230
110	5	1.161	2	1	3	30	0.054	0.156
110	5	1.181	2	1	3	30	0	0.07
110	5	1.201	2	1	3	30	0	0

Table B.1 Experimental and CFD results for R141b ejector (continue).

Operating Condition (°C)			**Ejector Geometries (based on data provided in Table 3.2)**				**Entrainment Ratio**	
Primary Fluid Saturated Temperature (T_P), °C	Secondary Fluid Saturated Temperature (T_S) , °C	Ejector downstream pressure (P_c), bar	Primary Nozzle No.	Mixing Chamber No.	Throat No.	NXP	Experiment	CFD
Case 6								
100	5	0.785	1	3	3	30	0.272	0.285
100	5	0.942	1	3	3	30	0.272	0.285
100	5	0.976	1	3	3	30	0.270	0.285
100	5	1.011	1	3	3	30	0.272	0.285
100	5	1.047	1	3	3	30	0.271	0.285
100	5	1.084	1	3	3	30	0.271	0.285
100	5	1.103	1	3	3	30	0.271*	0.285
100	5	1.122	1	3	3	30	0.221	0.285**
100	5	1.142	1	3	3	30	0.114	0.2
100	5	1.161	1	3	3	30	0	0
100	5	1.181	1	3	3	30	0	0
Case 7								
100	5	0.785	1	2	3	30	0.269	0.280
100	5	0.942	1	2	3	30	0.270	0.280
100	5	1.103	1	2	3	30	0.268	0.280
100	5	1.122	1	2	3	30	0270*	0.280
100	5	1.142	1	2	3	30	0.12	0.280**
100	5	1.161	1	2	3	30	0	0.200
100	5	1.181	1	2	3	30	0	0
Case 8								
100	5	0.785	1	1	1	30	0.273	0.290
100	5	0.942	1	1	1	30	0.276	0.290
100	5	0.976	1	1	1	30	0.269	0.290
100	5	1.011	1	1	1	30	0.272	0.290
100	5	1.047	1	1	1	30	0.265	0.290
100	5	1.084	1	1	1	30	0.269*	0.290
100	5	1.103	1	1	1	30	0.220	0.290**
100	5	1.122	1	1	1	30	0.160	0.200
100	5	1.142	1	1	1	30	0.080	0.120
100	5	1.161	1	1	1	30	0.022	0.021
100	5	1.181	1	1	1	30	0	0
100	5	1.201	1	1	1	30	0	0
Case 9								
100	5	0.785	1	1	4	30	0.270	0.290
100	5	0.942	1	1	4	30	0.274	0.290
100	5	0.976	1	1	4	30	0.270	0.290
100	5	1.011	1	1	4	30	0.272	0.290
100	5	1.047	1	1	4	30	0.269	0.290
100	5	1.084	1	1	4	30	0.273	0.290
100	5	1.103	1	1	4	30	0.270	0.290
100	5	1.122	1	1	4	30	0.272	0.290
100	5	1.142	1	1	4	30	0.270*	0.290
100	5	1.161	1	1	4	30	0.200	0.290**
100	5	1.181	1	1	4	30	0.120	0.170
100	5	1.201	1	1	4	30	0	0

Table B.1 Experimental and CFD results for R141b ejector (continue).

Operating Condition (°C)			**Ejector Geometries (based on data provided in Table 3.2)**				**Entrainment Ratio**	
Primary Fluid Saturated Temperature (T_P), °C	Secondary Fluid Saturated Temperature (T_S) , °C	Ejector downstream pressure (P_c), bar	Primary Nozzle No.	Mixing Chamber No.	Throat No.	NXP	Experiment	CFD
Case 10								
100	5	0.785	1	1	3	20	0.202	0.230
100	5	0.942	1	1	3	20	0.203*	0.230
100	5	0.976	1	1	3	20	0.160	0.230**
100	5	1.011	1	1	3	20	0.070	0
100	5	1.047	1	1	3	20	0	0
100	5	1.084	1	1	3	20	0	0
Case 11								
100	5	0.785	1	1	3	40	0.279	0.300
100	5	0.942	1	1	3	40	0.280	0.300
100	5	0.976	1	1	3	40	0.277	0.300
100	5	1.011	1	1	3	40	0.276	0.300
100	5	1.047	1	1	3	40	0.270	0.300
100	5	1.084	1	1	3	40	0.278	0.300
100	5	1.103	1	1	3	40	0.280	0.300
100	5	1.122	1	1	3	40	0.280	0.300
100	5	1.142	1	1	3	40	0.279	0.300
100	5	1.161	1	1	3	40	0.276	0.300
100	5	1.181	1	1	3	40	0.280	0.300
100	5	1.201	1	1	3	40	0.281	0.300
100	5	1.222	1	1	3	40	0.276	0.300**
100	5	1.243	1	1	3	40	0.282*	0.242
100	5	1.285	1	1	3	40	0	0
100	5	1.307	1	1	3	40	0	0

*Experiment's entrainment ratio at critical back pressure
**CFD's entrainment ratio at predicted critical back pressure

Table B.2 Comparison of ejector performance from experimental measurement and CFD prediction (at critical point).

Operating Condition (°C)		Ejector Geometries (based on data provided in Table 1)				Entrainment Ratio			Critical back pressure (bar)		
Primary Fluid Saturated Temperature (T_P)	Secondary Fluid Saturated Temperature (T_S)	Primary Nozzle No.	Mixing Chamber No.	Throat No.	NXP	Experiment	CFD	[a]Error (%)	Experiment	CFD	[b]Error (%)
Effect of Primary Fluid and Secondary Fluid Saturated Temperature (Saturated Vapour-Generator Temperature and Saturated Evaporator Temperature)											
100	5	1	1	3	30	0.272	0.290	6.618	1.122	1.142	1.783
110	5	1	1	3	30	0.229	0.242	5.677	1.307	1.329	1.683
110	0	1	1	3	30	0.120	0.140	16.667	1.103	1.122	1.723
Effect of Primary Nozzle Throat Diameter											
110	5	1	1	3	30	0.229	0.242	5.677	1.307	1.329	1.683
110	5	2	1	3	30	0.274	0.297	8.394	1.103	1.122	1.723
110	5	3	1	3	30	0.120	0.130	8.333	1.614	1.64	1.611
Effect of Mixing Chamber Inlet Diameter											
100	5	1	1	3	30	0.272	0.290	6.618	1.122	1.142	1.783
100	5	1	2	3	30	0.270	0.280	3.704	1.122	1.142	1.783
100	5	1	3	3	30	0.271	0.285	5.166	1.103	1.122	1.723
Effect of Throat Length											
100	5	1	1	1	30	0.271	0.290	7.011	1.084	1.103	1.753
100	5	1	1	3	30	0.272	0.290	6.618	1.122	1.142	1.783
100	5	1	1	4	30	0.269	0.290	7.807	1.142	1.161	1.664
Effect of Nozzle Exit position											
100	5	1	1	3	20	0.203	0.230	13.300	0.942	0.976	3.609
100	5	1	1	3	30	0.272	0.290	6.618	1.122	1.142	1.783
100	5	1	1	3	40	0.278	0.300	7.914	1.243	1.222	-1.689
				Average				7.741			1.626

[a]Error (%) = 100 x (CFD's entrainment ratio - Experiment's entrainment ratio) / Experiment's entrainment ratio

[b]Error (%) = 100 x (CFD's critical back pressure - Experiment's critical back pressure) / Experiment's critical back pressure

REFERENCES

[1] Chunnanond K. and Aphornratana S., 2004. Ejectors: applications in refrigeration technology. *Renewable and Sustainable Energy Reviews*, 8: 129-155.

[2] Aphornratana S., 1996. Experimental investigation of a small capacity steam-ejector refrigerator. *RERIC International Energy Journal*, 18 (2): 83-95.

[3] Aphornratana S. and Eames I.W., 1997. A Small capacity steam-ejector refrigerator: experimental investigation of a system using ejector with movable primary nozzle. *International Journal of Refrigeration*, 20 (5): 352-358.

[4] Holton W.C., 1951. Effect of molecular weight of entrained fluid on the performance of steam-jet ejectors. *ASME Transaction*, Oct., 905-910.

[5] Aphornratana S., Chungpaibulpatana S., and Srikhirin P., 2001. Experimental investigation of an ejector refrigerator: Effect of mixing chamber geometry on system performance. *International Journal of Energy Research,* 25: 397-411.

[6] Zeren F., 1982. Freon-12 vapor compression jet pump solar cooling system. *Ph.D. thesis*, Texas A&M University, U.S.A.

[7] Al-Khalidy N., 1998. An experimental study of an ejector cycle refrigeration machine operating on R113. *International Journal of Refrigeration*, 21 (8): 617-625.

[8] Sun D.W. and Eames I.W., 1996. Performance characteristics of HCFC-123 ejector refrigeration cycles. *International Journal of Energy Research* 20 (10): 871-885.

[9] Selvaraju A and Mani A., 2006. Experimental investigation on R134a vapour ejector refrigeration system**.** *International Journal of Refrigeration*, 29 (7): 1160-1166.

[10] Huang B.J, Chang J.M, Petrenko V.A, and Zhuk K.B., 1998. A solar ejector cooling system using refrigerant R141b. *Solar Energy*, 64 (4-6): 223-226.

[11] Sokolov M. and Hershgal D., 1990. Enhanced ejector refrigeration cycles powered by low grade heat, Part 2. Design procedures. *International Journal of Refrigeration*, 13: 357-363.

[12] Sokolov M. and Hershgal D., 1990. Enhanced ejector refrigeration cycles powered by low grade heat, Part 3. Experimental results. *International Journal of Refrigeration*, 14: 24-31.

[13] Chen L.T., 1978. Heat driven mobile refrigeration cycle analysis. *Energy Conversion*, 18: 25-29.

[14] Sokolov M. and Hershgal D., 1990. Enhanced ejector refrigeration cycles powered by low grade heat, Part 1. Systems characterization. *International Journal of Refrigeration*, 13: 351-356.

[15] Huang B.J., Petrenko V.A., Samofatov I.Y., and Shchetinina N.A., 2001. Collector selection for solar ejector cooling system. *Solar Energy*, 7 (4): 269-274.

[16] Sokolov M. and Hearshgal D., 1993. Solar-powered compression enhanced ejector air conditioning. *Solar Energy,* 51 (3): 183-194.

[17] Wolpert J.L. and Riffat S.B., 2002. 13kW cooling hybrid solar/gas ejector air conditioning system. *1st International Conference on Sustainable Energy Technologies*, Paper RHO11.

[18] Sun D.W., 1997. Solar powered combined ejector-vapour compression cycle for air conditioning and refrigeration. *Energy Conversion Management*, 38 (5): 479-791.

[19] Aphornratana S., 1994. Theoretical and experimental investigation of a combine ejector-absorption refrigerator. *Ph.D. Thesis,* University of Sheffield, U.K.

[20] Riffat S.B. and Holt A., 1998. A novel heat pipe/ejector cooler. *Applied Thermal Engineering*, 18 (3-4): 93-101.

[21] Nguyen V.M., Riffat S.B., and Doherty P.S., 2001. Development of a solar-powered passive ejector cooling system. *Applied Thermal Engineering*, 21: 157-168.

[22] Srisastra P. and Aphornratana S., 2005. A circulating system for a steam jet refrigeration system. *Applied Thermal Engineering* 25 (14-15): 2247-2257.

[23] Gosney W.B., 1982. Principle of refrigeration. *Cambridge University Press*, Cambridge.

[24] Keenan J.H., Neumann E.P., and Lustwerk F., 1950. An investigation of ejector design by analysis and experiment. *ASME Journal of Applied Mechanics*, *Trans*, 72: 299-309.

[25] Zhang X.J. and Wang R.Z., 2002. A new combined adsorption-ejector refrigeration and heating hybrid system powered by solar energy. *Applied Thermal Engineering*, 22: 1245-1258.

[26] Rusly E., Aye Lu, Charters W.W.S., Ooi A. and Pianthong K., 2002. Ejector CFD modeling with real gas model. *Mechanical Engineering Network of Thailand the 16th Conference*, 150-155.

[27] Keenan J.H. and Neumann E.P., 1942. A simple air ejector. *ASME Journal of Applied Mechanics*, *Tran*s., 64: 75-81.

[28] Eames I.W., Aphornratana S., and Haider H., 1995. A theoretical and experimental study of a small-scale steam jet refrigerator. *International Journal of Refrigeration*, 18 (6): 378-386.

[29] Huang B.J. and Chang J.M., 1999. Empirical correlation of ejector design. *International Journal of Refrigeration*, 22: 379-388.

[30] Munday J.T. and Bagster D.F., 1977. A new theory applied to steam jet refrigeration. *Ind. Eng. Chem. Process Des. Dev*., 16 (4): 442-449.

[31] Eames I.W., Wu S., Worall M., and Aphornratana S., 1999. An experimental investigation of steam ejectors for application in jet-pump refrigerators powered by low-grade heat. *Proc. Instn. Mech. Engrs*., 213 Part A: 351-361.

[32] Matsuo K., Sasaguchi K., Tasaki K., and Mochizuki H., 1981. Investigation of supersonic air ejectors, Part 1, Performance in the case of zero-secondary flow. *Bull JSME 1981*, 24(198):2090-7.

[33] Tamaki T., Tomita Y., Yamane R., 1970. A study of pseudo-shock, 1st Report, j-type pseudo-shock. *Bull JSME 1970*, 13(55):51-8.

[34] Talpallikar M.V.,Smith C.E., Lai M.C. and Holdeman J.D., 1992. CFD analysis of jet mixing in low Nox flame tube combustors. *Journal of Engineering Gas Turbine and Power*, 114: 416-24.

[35] Neve R.S., 1993. Computational fluid dynamics analysis of diffuser performance in gas-powered jet pumps. *International Journal of Heat and Fluid Flow*, 14 (4): 401-7.

[36] Chen F., Liu F.C. and Yang J.Y., 1994. Supersonic flow in the second-throat ejector diffuser system. *Journal of Spacecraft and Rockets*, 31(1): 123-9.

[37] Riffat S.B., Gan G., and Smith S., 1996. Computational fluid dynamics applied to ejector heat pumps. *Applied Thermal Engineering*, 16 (4): 291-297.

[38] Riffat S.B. and Omer S.A., 2001. CFD modeling and experimental investigation of an ejector refrigeration system using methanol as the working fluid. *International Journal of Energy Reservation*, 25: 115-128.

[39] Sriveerakul T., Aphornratana S., and Chunnanond K., 2007. Performance prediction of steam ejector using computational fluid dynamics: part 1. Validation of the CFD results. *International Journal of Thermal Science*, 46: 812–822.

[40] Sriveerakul T., Aphornratana S., and Chunnanond K., 2007. Performance prediction of steam ejector using computational fluid dynamics: part 2. Flow structure of a steam ejector influenced by operating pressures and geometries. *International Journal of Thermal Science*, 46: 823–833.

[41] Pianthong K., Seehanam W., Behnia M, Sriveerakul T. and Aphornratana S., 2007 Investigation and improvement of ejector refrigeration system using computational fluid dynamics technique. *Energy Conversion and Management*, 48 (9): 2556-2564.

[42] Huang B.J., Jiang C.B. and Hu F.L., 1985. Ejector performance characteristics and design analysis of jet refrigeration system. *Transactions of ASME*, 107: 792-802.

[43] Zeren F., 1982. Freon-12 Vapor compression jet pump solar cooling system. *Ph,D thesis*, Texas A&M University, U.S.A.

[44] Chen Y.M. and Sun C.Y., 1997. Experimental study of the performance characteristics of a steam–ejector refrigeration system. *Experimental and Fluid Science*, 15: 384-394.

[45] Chang Y.J. and Chen Y.M. 2000, Enhancement of a steam-jet refrigerator using a novel application of the petal nozzle. *Experimental Thermal and Fluid Science*, 22: 203-211.

[46] Eames I.W., Aphornratana S., and Sun D.W., 1995. The jet-pump cycle-a low cost refrigerator option powered by waste heat. *Heat Recovery Systems & CHP,* 15(8): 711-721.

[47] Chunnanond K. and Aphornratana S., 2003. An experimental investigation of steam-ejector refrigerator, the analysis of pressure profile along ejector. *The Asia-Pacific Conference on Sustainable Energy and Environment Technologies*, 184-188.

[48] ESDU, Ejector and jet pump, ESDU international Ltd. London, Data item 86030, 1985.

[49] Properties, Uses, Storage, and Handling (PUSH) for Suva® 123, DuPont Fluorochemicals, USA, 1998.

[50] McLinden M.O., Lemmon E.W., and Klein S.A., 1996. REFPROP – NIST Refrigerant Properties Database, Version 6.01, *National Institute of Standards and Technology*.

[51] FLUENT 6.0 User's guide, FLUENT INC. Lebanon, NH, U.S.A

[52] Anderson J.D., 2002. Modern compressible flow, with historical perspective, Third Edition, McGraw Hill.

External Examiner's Comments and Answers to the Comments

Overview

The thesis presents the results of a numerical and experimental study of a refrigeration ejector system using R141b as the working fluid. A parametric study has been carried out to cover a range of design parameters. There is also a reasonable agreement between the experimental and CFD results. This allows the CFD simulations to be used as a design tool for these types of ejectors. The findings of the study cover a gap in previous studies and advance knowledge in this field. Therefore, it is believed that the work undertaken is worthy of a PhD and should therefore be accepted as such. However, there are some comments below which require the attention of the candidate and I urge that the modifications are undertaken.

The external examiner's comment:

1. My major criticism of the thesis is that the experimental side of the project is downplayed. For instance, although an experiment rig has been built and some interesting experiments have been performed there is no mention of this in the title. Further, the experimental aspects and chapters can be made more prominent with more detailed explanation and discussions presented.

Reply from the author:

The thesis title has been changed to "CFD AND EXPERIMENTAL ANALYSIS OF AN R141b EJECTOR USED IN A JET REFRIGERATOR". Details of experimental apparatus and the experimental results have been made more prominent in Chapter III and Chapter V, respectively.

The external examiner's comment:

2. The thesis requires some serious editing to ensure that the language is correct. I do appreciate that English is not the first language of the candidate; however it is essential that the language is corrected to ensure that the explanations and discussions are comprehensible. My suggestion is that a professional technical editor reviews and modifies the thesis in consultation with the candidate.

Reply from the author:

The language of the thesis has been revised according to a professional advice from a technical English reviewer.

The external examiner's comment:

3. Some work needs to be done on the style of the thesis and presentation to ensure that there is a consistent format followed throughout the thesis. For instance, the line spacing changes in a number of places. I am not sure what the University's guidelines are but they must be exactly and correctly followed.

Reply from the author:

The format of the thesis has been modified to match the University's style guideline.

The external examiner's comment:

4. The Introduction Chapter should be perhaps shortened and rearranged to clearly state the following:
    - Motivation and background of the study
    - Scopes of work
    - Organization of the thesis

Reply from the author:

In Chapter I (Introduction Chapter), the content of the chapter has been shortened and rearranged to state the following:

- Motivation and background of the study
- Objectives of the study
- Organization of the thesis

The external examiner's comment:

5. A clearer explanation and diagram on the ejector refrigeration cycle compared to the typical vapour-compression refrigeration cycle should be added.

Reply from the author:

A clearer explanation and diagram on the ejector refrigeration cycle compared to the typical vapour-compression refrigeration cycle has been added to Chapter I.

The external examiner's comment:

6. In chapter II, the literature reviews contains some detailed information on the ejector's operation and characteristics. However, there is little information provided on the CFD studies of the ejector. Further, there is little information provided on the various refrigerant used.

Reply from the author:

More information on the CFD studies of the ejector has been added in Chapter II. The information on the various refrigerant used had already provided in Chapter III.

The external examiner's comment:

7. In chapter IV, the key parameters and numerical models used in this study should be clearly summarized in a tabulated form (perhaps in the conclusion section).

Reply from the author:

According to this comment, Table 4.2 (Setup information of the CFD model.) has been added to make a summary of the numerical models used in this study.

The external examiner's comment:

8. Conclusions and recommendations (Chapter IX) should be written to summarize the overview of the whole thesis. The current text is not doing the thesis justice and does not really "sell" the outcomes.

Reply from the author:

In Chapter IX, the conclusions have been revised as suggestion.

The external examiner's comment:

9. The study is about the application and improvement in the ejector refrigeration system. Hence, the information relevant to the performance of the refrigeration system (eg. COP of the system and the cooling capacity) should be presented and discussed concurrently to the predicted CFD flow pattern results.

Reply from the author:

This study is in fact about the analysis of the flow characteristics that affected to the performance of the ejector (entrainment ratio (Rm) and critical back pressure (P_c)) in refrigeration application. Although, an ejector refrigerator had been built, the purpose was mainly to validate the CFD results. According to the above reason, the COP of the system will not be presented and discussed. However, if one wishes to determine the

COP of this ejector refrigeration system, which is relevant to the entrainment ratio of the ejector, it may be estimated as:

$$COP = Rm \frac{(h_{g,evap} - h_{f,cond})}{(h_{g,generator} - h_{f,cond})}$$

The ratio of the heat rejection at the evaporator to the heat input at the vapour-generator $\left(\frac{(h_{g,evap} - h_{f,cond})}{(h_{g,generator} - h_{f,cond})} \right)$ is almost constant for each operating condition. Thus, the performance curve of the jet refrigerator (COP) and the performance curve of the ejector (Rm) are similar.

The external examiner's comment:

10. All figure and table captions should be carefully checked and some need to be improved to be more formative but concise. For example the caption of Figure 2.1 may be written as "Configurations of typical ejectors". Also the format of the captions should be consistent with the thesis format and the University's guidelines.

Reply from the author:

All figure and table captions have been carefully checked and some of them have been improved as suggestion.

The external examiner's comment:

11. Finally, I believe that the interesting outcomes of the thesis are not presented and "sold" well. The results can be of great interest to the designers of such systems. Therefore, it is essential that some discussion on the design and operation of these systems based on the obtained results is presented. Perhaps, this can be done in a separate chapter covering the design and optimization of the ejectors using the tools developed and the findings of the study.

Reply from the author:

Some discussion on the design and operation of the system based on the obtained results has been added in Chapter IX.